SEPTEMBER 2018   M.Sc. in Electrical and Electronics Engineering   ALI DANLADI

UNIVERSITY OF GAZİANTEP
GRADUATE SCHOOL OF
NATURAL & APPLIED SCIENCES

PRELIMINARY DESIGN AND ANALYSIS OF ELECTRICAL POWER SUBSYSTEM FOR A CONCEPTUAL 1U CUBESAT MISSION

M. Sc. THESIS
IN
ELECTRICAL AND ELECTRONICS ENGINEERING

BY
ALI DANLADI
SEPTEMBER 2018

Preliminary Design and Analysis of Electrical Power Subsystem for a Conceptual 1U CubeSat Mission

M. Sc. Thesis
in
Electrical and Electronics Engineering
University of Gaziantep

Supervisor
Assoc. Prof. Dr. Ahmet Mete VURAL

by
Ali DANLADI
September 2018

REPUBLIC OF TURKEY

UNIVERSITY OF GAZİANTEP
GRADUATE SCHOOL OF NATURAL & APPLIED SCIENCES
DEPARTMENT OFELECTRICAL AND ELECTRONICS ENGINEERING

Name of the thesis: Preliminary Design and Analysis of Electrical Power Subsystem for a Conceptual 1U CubeSat Mission

Name of the student: Ali DANLADI

Exam date: 10.09.2018

Approval of the Graduate School of Natural and Applied Sciences

Prof. Dr. A. Necmeddin YAZICI
Director

I certify that this thesis satisfies all the requirements as a thesis for the degree of Master of Science.

Prof. Dr. Ergun ERÇELEBI
Head of Department

This is to certify that we have read this thesis and that in our opinion it is fully adequate, in scope and quality, as a thesis for the degree of Master of Science.

Assoc. Prof. Dr. Ahmet Mete VURAL
Supervisor

Examining Committee Members	Signature
Prof. Dr. Ergun ERÇELEBI	…………………..
Assist. Prof. Dr. Ökkeş Fatih KEÇECİOĞLU	…………………..
Assoc. Prof. Dr. Ahmet Mete VURAL	…………………..

I hereby declare that, all information in this document has been obtained and presented in accordance with academic rules and ethical conduct. I also declare that, as required by these rules and conduct, I have fully cited and referenced all material and results that are not original to this work.

ALI DANLADI

ABSTRACT

PRELIMINARY DESIGN AND ANALYSIS OF ELECTRICAL POWER SUBSYSTEM FOR A CONCEPTUAL 1U CUBESAT MISSION

DANLADI, Ali
M. Sc. In Electrical and Electronics Engineering
Supervisor: Assoc. Prof. Dr. A. Mete VURAL
September 2018
125 Pages

An electrical power subsystem (EPS) for a conceptual 1U CubeSat mission has been designed by thorough evaluation of the performance of the building blocks of the EPS. The requirements and functionalities of the EPS had been well defined, the functionalities include; the main power generation technology feasible, the energy storage technology allowed as per the guidelines and specifications for CubeSat development, and the types of converters necessary for the regulated power supply. The photovoltaic power generation system that was selected is made up of triple-junction solar cells, and the battery charging system and the power conditioning converters selected were based on single ended primary inductance converter topology popularly abbreviated as SEPIC. The battery storage approved was a lithium technology based. A maximum power point tracking algorithm which is known as perturb and observe (P&O) was implemented. The controller designed for the converters is Proportional-Integral (PI) controller. All of these have been well analyzed, mathematically modeled and simulated in Simulation environment. The results and implementation procedures are presented in figures and tables where necessary in the report.

Key Words: 1UCubeSat, DC-DC Converter, Lithium-ion battery, Single Ended Primary Inductance (SEPIC) Converter, Triple-junction Solar Cells.

ÖZET

KAVRAMSAL 1U KÜPLEV MİSYONU İÇİN ELEKTRİK GÜCÜ ALT SİSTEMİNİN ÖNCELİK TASARIMI VE ANALİZİ

DANLADI, Ali
Yüksek Lisans Tezi, Elektrik-Elektronik Mühendisliği
Tez Yöneticisi: Doç. Dr. Ahmet Mete VURAL
Eylul 2018
125 Sayfa

Konsept 1U CubeSat mini bir uydunun elektriksel güç alt sisteminin (EGS)tasarımı, EGS'yi meydana getiren blokların performansları değerlendirilerek yapılmıştır. EGS'nin gereksinimleri ve fonksiyonelliği iyi bir şekilde tanımlanmıştır. Fonksiyonellik, ana güç üretim teknolojisini, Cubesat geliştirilmesi için izin verilen yönergeler ve şartnameler ışığında enerji depolama teknolojisini ve regüleli güç kaynağı içingerekli olan çeviricilerin tiplerini kapsamaktadır.Seçilen fotovoltaik güç üretim sistemi üçlüjonksiyon güneş hücreleri, batarya sarj sistemi ve SEPIC olarak kısaltması yapılan tek-sonlu primer endüktif çevirici topolojisi tabanlı güç koşullandırma çeviricilerinden oluşmaktadır.Onaylanan batarya depolama lityum teknolojisi tabanlıdır. Değiştir ve Gözle (D&G) olarak bilinen bir maksimum güç noktası takip algoritması gereçekleştirilmiştir. Çeviriciler için tasarlanan denetleyici Doğrusal-İntegral (PI) denetleyicisidir.Bunların tümü iyi bir şekilde analiz edilmiş, matematiksel olarak modellenmiş ve benzetim ortamında benzetim çalışmaları yapılmıştır. Sonuçlar ve gerçekleştirilen prosedürler raporda gerekli olduğu yerde şekiller ve tablolar ile sunulmuştur.

Anahtar Kelimeler:1UCubeSat, DC-DC Dönüştürücü, Lityum-iyon pil, Tek Uçlu Birincil Endüktans (SEPIC) Dönüştürücü, Üçlü birleşim Güneş Pilleri.

Dedicated to the living memory of my parents

ACKNOWLEDGEMENTS

I wish to extend my special and profound gratitude to my supervisor Associate Professor Dr. A. Mete VURAL for accepting me as his students and believing in my capacity to deliver in this research work. I must appreciate his constructive criticisms in making sure the objective of this thesis work is achieved.

I must also acknowledge the support I received from the Governor of my home State Yobe, His Excellency Alhaji Ibrahim Gaidam and my employers – National Space Research and Development Agency (NASRDA) in Nigeria.

To my wife, I say a big thank you – for her unflinching support throughout our married life and more so during my studies while I left her at home for such a long period.

I can’t forget the scholarly support of Atif Iqbal, a professor of Power Electronics and Electric Drives at the prestigious Aligarh Muslim University India, for his positive response to my email which changed the course of my understanding of the thesis thrust.

Lastly, but not the least, I wish to say thank you to my good friends and other family members for their wonderful friendships, companionship and encouragement.

TABLE OF CONTENTS

Page

LIST OF TABLES

Page

LIST OF FIGURES

Page

LIST OF ABBREVIATIONS

ADCS	Attitude Determination and Control Sub-System
ALSM	Average Large Signal Model
AM0	Air Mass Zero
BCR	Battery Charge Regulator
BJT	Bipolar Junction Transistor
BOL	Beginning Of Life
CC-CV	Constant Current Constant Voltage
CCM	Continuous Conduction Mode
CIGS	Copper Indium/Gallium Diselenide
COMMS	Communication Sub-System
COTS	Commercial off The Shelf
D	Duty Cycle
DCM	Discontinuous Conduction Mode
DOD	Depth of Discharge
EMC	Electromagnetic Compatibility
EMI	Electromagnetic Interference
EOL	End of Life
EPS	Electrical Power Supply
ESR	Equivalent Series Resistance
ESL	Equivalent Series Inductance
FF	Fill Factor
GaAs	Gallium Arsenide

GaInP	Gallium Indium Phosphide
Ge	Germanium
IC	Incremental Conductance
IGBT	Insulated Gate Bipolar Transistor
I-V	Current versus Voltage
KCL	Kirchhoff Current Law
KHTT	Know How Technology Transfer
KVL	Kirchhoff Voltage Law
LEO	Low Earth Orbit
MeV	Mega electron Volt
MOSFET	Metal Oxide Semiconductor Field Effect Transistor
Ni-Cd	Nickel-Cadmium
Ni-MH	Nickel-Metal Hydride
OBC	On-Board Computer
P&O	Perturb and Observe
PC	Parasitic Conductance
PI	Proportional - Integral
P-POD	Poly Pico Satellite Orbital Deployer
P-V	Power versus Voltage
PV	Photovoltaic
PWM	Pulse Width Modulation
RMS	Root Mean Square
SEL	Single Event Latch-up
SEPIC	Single Ended Primary Inductance Converter
SEU	Single Event Brown-out
SEU	Single Event Upset
SMPS	Switched-Mode Power Supply

TCS Thermal Control Sub-System

LIST OF SYMBOLS

E_g	Band Gap Energy
F_{sw}	Switching Frequency
H_z	Frequency in Hertz
I_{mpp}	Current at Maximum Power Point
I_{ph}	Photo-Generated Current
I_s	Reverse Saturation Current
I_{sc}	Short-Circuit Current
P_{in}	Input Power
P_{mpp}	Power at Maximum Power Point
P_{out}	Output Power
R_p	Parallel Resistance
R_s	Series Resistance
T_s	Switching Period
V_d	Diode Voltage
V_{in}	Input Voltage
V_{mpp}	Voltage at Maximum Power Point
V_{oc}	Open-Circuit Voltage
V_{out}	Output Voltage
V_{ref}	Reference Voltage
V_t	Thermal Voltage
α_i	Temperature Parameter in Kelvin
γ_i	Ideality Constant of Temperature

C	Capacitance
k	Boltzmann's Constant
KV	Reverse Saturation Current of a Diode
L	Inductance
n	Diode Ideality Factor
q	Charge of an Electron
R	Resistance
V	Voltage
I	Current
W	Watt
β	Semiconductor Temperature Parameter
i_l	Inductor Current
v_c	Capacitor Voltage

CHAPTERI

BACKGROUND

1 Introduction

The year 1957, in October to be precise, the Soviet Union now known as The Russian Federation, launched the first known unmanned satellite christened - “sputnik” in to space effectively starting the race in to space. Immediately after, the United States followed suite, and later, other Space faring nations joined. These efforts in getting in to space have made it possible to develop technologies like satellite communication, global navigation, remote sensing etc. that are benefitting mankind today. [1].

To further consolidate the successes recorded in the space endeavours and make it easier for especially students to try their hands on these technologies, a collaborative work was started in 1999 in the USA between two teams led by Prof. Jordi Puig-Suari and Prof. Bob Twiggs of California Polytechnic State University (Cal Poly) San Luis Obispo and the Stanford University respectively, a new generation of satellite tagged CubeSat (a category of Nanosatellite) was born. They also had to proposed and adopt design guidelines and specifications for the proper development of the new concept [2, 4-5].

The design standards and specifications characterize a 1U CubeSat by mass and volume - not to exceed 1.33 Kg of weight here on the earth and 10cm x 10cm x 10cm in volume. The imposed limits therefore ensures that the satellite is "tiny" and challenging to space systems design engineers. The challenges seem more pronounced when it comes to electrical power subsystem design for the satellite [2, 4-5]. According to [2, 4, 6], the restrictions and constrains have made it difficult for the CubeSat to produce power for its consumption, therefore, its capabilities are somewhat limited to carryout missions that require large amount of electrical power. In [2, 3, 5], concerns about the limited volume and mass of the CubeSat, consequences of the harsh nature of the space environment where temperatures are dangerously varying, abundance of charged particles and radiation etc. These may harm the electronic components on the surface and inside the CubeSat have been discussed in [1 and 8]. The solar panels and the batteries on the surface and inside the satellite may be grossly affected by these environmental factors mentioned above.

The space industry stakeholders may want a very ideal system that can work perfectly well under constraints, if achievable, function beyond the mission duration. So far, only solar photovoltaic system can be employed for the power generation on a CubeSat looking at specifications and design guidelines given in [4] and this is especially so if the satellite is to operate in a region of space called the low earth orbit (LEO) since there are frequent eclipses on its path as stated by [1], load regulators (power conditioning and distribution) have to be included also as in [2, 4, 5]. In [4], the main objective of the CubeSat program was to provide opportunities for especially university students to test some their designs and also to greatly trim down development and launch overheads particularly for students' experiments and for other commercial and scientific/technology demonstrations purposes.

Development of a budget-constrained electrical power subsystem (EPS) would require that the students and design engineers develop custom or use commercial-off-the-shelf (COTS) components like the solar photovoltaic cells, lithium based batteries and the other electronic components for the power supply. Appropriate design practice therefore, is expected to be the order to ensure that the design complies with the requirements in [4]. The criticality of the EPS cannot be over emphasized because if it fails, the entire satellite mission also is deemed to have failed since the payloads and other proposed experiments need power to operate [4].
Works undertaken in [1-5] on the EPS design entails the use of solar photovoltaic cells for generating power required, a series converter for maximum power point tracking and battery charging, a module for power conditioning and distribution in the CubeSat, a lithium based battery for power storage that is required eclipse period and high power load operation in the mission, and a 'housekeeping' system for management, control, monitoring, and telemetry.

Most of the EPS on CubeSats in orbit today, are having some uniqueness because of the different missions they are serving, therefore, in this thesis, a simple design to fit all for a LEO mission was attempted so that we ensure reduction in development time and establish a minimum threshold where to start our designs.

1.1 Purpose of the Study

CubeSats do not have the capacity to adequately generate their own power and store it for use during eclipse period and when required. These challenges tend to limit the acceptance and applications of CubeSat for high power demand missions. It is therefore important to study, design and develop EPS for these CubeSats capable of solving the problems mentioned. Satellite missions have been loss because of power failure - an example of which is that of Nigeria called Nigcomsat I. So, we can't afford to have power failures on our satellites, therefore, know how on the proper design of the EPS is required.

The main purpose of this research work is to design and simulate all the main building blocks of an EPS for a 1U CubeSat that can safely, effectively and continuously supply all its loads in LEO without any failure for the intended mission lifetime where it would be employed. The concept is to have a simple and cost effective EPS design that can be reused on any type of mission of its kind. The viability of the CubeSat technology necessitates this approach since it has become popular over the years among university students, scientists and other professional engineers alike. There are also growing miniaturization of battery-powered portable consumer electronic products in the market requiring efficient and cheap EPS for their functions.

In order to achieve the stated objectives above, the following efforts among others were made and these are the main tasks conducted.

1) A literature review on some CubeSat projects and how the EPS designs of these projects were implemented was conducted, the topologies, components, mathematical methods used among others were identified.

2) Design of a skeletal and simple reusable CubeSat EPS that can be used in LEO missions or other uses in portable consumer electronics like mobile phones etc. was achieved.

3) A review on the available and most viable solar photovoltaic (PV) cells and panels was also conducted and from among the bests, a choice was made based on heritage and reported performance of the cells/panels.

4) Most popular load voltage regulators and switched-mode power supplies for power conditioning and distribution were reviewed and a decision was taken on which one to employ in this research work.

5) A review with a view to considering consider the battery technologies, chemistries topologies, and associated efficiencies available for space applications especially (LEO) was also attempted and the most suitable selected.

6) The solar photovoltaic cells were modeled mathematically and simulated in a computer simulation environment.

7) 3.3V and 5.0V power supply and MPPT based battery charging converters were designed, modeled using state-space averaging technique and simulated.

1.2 Contributions

The thesis work seeks to popularise low voltage power supply design especially for Nanosatellites (CubeSat) and other portable consumer electronic devices. In addition, the thesis also shows how to implement mathematical modeling and simulation of triple-junction photovoltaic solar cells, state-space averaging of DC-DC power converters for power supplies and battery charging. The results of the simulation and designs are very important for upcoming low voltage power supply system designers because it increases the amount of information in the research domain. Another important objective is that the results from this thesis can be applied and adapted to designs of similar CubeSat missions EPS without necessarily having to conduct extensive search of the literature for how to implement such thereby considerably reducing development time of future CubeSats. Students in Nigeria, Turkey and other similar nations can access the research and apply it to their projects since this thesis would be published in the public domain.

Finally, two journal articles on Modeling and Simulation of Triple-Junctions Solar Photovoltaic Cells and Design, Modeling and Simulation of SEPIC based Power Supply would be published. The researcher has greatly benefitted from attempting to achieve the objectives of the thesis work.

1.3 Methodology

An extensive literature survey was conducted so as to explore and exploit more possible ways and techniques of undertaking the work as published by other researchers in the field and other well-known developers of CubeSat, and to foster a better understanding of the subject matter under review and identify the gaps that needed to be filled. Consequently, a preliminary design and analysis including computer simulation of the proposed electrical power subsystem of a conceptual 1U CubeSat mission was carried out. The work focuses on analytically determining the photovoltaic array and sizing requirements as the sole power generator, efficient extraction of the maximum power from the PV module (Perturb and Observe methodology),the power conditioning and distribution sub unit (types of converters required), battery capacity sizing and selection. The best EPS topology discovered is employed. Validation and comparison was made by conducting simulations of the selected EPS. The results obtained were evaluated and further discussion gave the final directions and options. A conclusion on the lessons learnt was drawn and recommendations for further studies and other alternatives were proffered.

1.4 Scope and Limitations

This thesis work is limited to designing, analyzing, modeling and simulation of the EPS of a 1U CubeSat only. The subunits of the EPS –power generator (solar), and the converters were only modeled mathematically and a computer simulation was conducted to further validate the work and comparison of the results of the models and the characteristics information contained in the datasheets of these components

CHAPTER II

LITERATURE REVIEW

2 Introduction

In this chapter, a discussion of the general concept of the CUBESAT is presented together with the constraints on the EPS imposed by the space environment where the satellite is to operate, and other mechanical and physical constraints like the size and structure of the satellite, the orientation of the CubeSat with respect to the Sun and the Earth etc. An overview of the power generation facility – the solar cells, which is generally the only viable means of generating power for CubeSat so far, the battery storage system - and it is normally lithium technology being employed. The EPS, which is manly a combination of DC-DC converters and some control switches for current limiting and so on, is also discussed in this chapter. Various types of the EPS architecture were also evaluated with a view of selecting a suitable one for this thesis work.

2.1 Overview of the 1UCubeSat Concept

A 1U CubeSat is a satellite designed to orbit in Space having a mass of not more than 1.33 kg and a size of “1 liter”, or 10cm x 10cm x 10cm in volume as specified in and documented in [4], other variants of 2U (10cm x 10cm x 20cm), and 3U (10cm x 10cm x 30cm) exist. The CubeSat concept was developed through collaboration of researchers from two institutions in the United States – The California Polytechnic State University and Stanford University’s Space Systems Laboratory. The researchers involved in the CubeSat concept development were notably Prof. Jordi Puig-Suari of Cal Poly San Luis Obispo and Prof. Bob Twiggs of Stanford University [4]. It was envisaged to have capabilities of larger satellites at a much reduced cost and development time. The reduction in cost and other attendant issues has allowed so many universities and other corporate bodies to deploy it for educational and other civilian purposes in most cases. It was reported in [8] that the CubeSat development program is giving a very serious benefits to education where students gets hands-on access to space applications and huge experience from trying things that really work. A summary of these benefits and contributions of the CubeSat concept is given in [8] as follows;

i. *Standard design guide is made available*
ii. *A deployment system P-POD (Poly Picosatellite Orbital Deployer) was developed*
iii. *Documentation and licensing issues are coordinated and easily obtainable*
iv. *Testing of finished design and inspection platforms have been developed to ensure reliability of the designed systems and for acceptance purposes during launching*
v. *Integration of flight hardware to the launch vehicle is made easy*

Each and every satellite mission has a guiding objective, all CubeSat missions are also guided by same, some of the objectives of launched CubeSat includes Know How Technology Transfer (KHTT) for especially university students and industrial interns as in [8], and [10] including testing of new innovations in technology. For example, in [9], a CubeSat was designed and launched in 2012 by students in University of Tartu Estonia; the CubeSat was to be used as a test bed for a novel space propulsion system – Electric Solar Sail. Generally, the CubeSat concept has been deployed for scientific research, technology demonstrations and above all, EDUCATION, as enumerated in [8, 9, 10, and 22]. The overall impact of these researches and technology demonstrations are validation of scientific experiments and opportunity of building larger spacecraft with more reliability and cost effectiveness [10]. The CubeSat is composed of various subsystems describing it as follows;

i. Structure – this is the main frame housing all other subsystems (EPS, payloads, Attitude Determination and Control Subsystem ADCS, Communication subsystem COMMS, Thermal Control Subsystem TCS, On-Board Computer OBC and other peripherals). Figure2.1shows typical structures of a1U CubeSat from Pumpkin and Figure2.21U CubeSat structure from Endurosat– CubeSat kit manufacturers and suppliers.

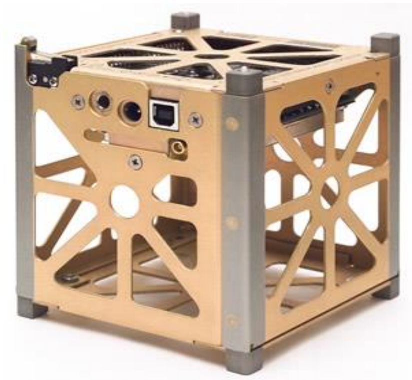

Figure 2.1 CubeSat Structure from PUMPKIN [44].

Figure 2.2 1U CubeSat Structure from ENDUROSAT [39].

ii. Electrical Power Supply (EPS) – This consists of solar cells/array, batteries, power converters and regulators, switches, sensors, etc. It is to be designed such that it generates, stores and distributes electrical power to the loads (the various subsystems), it may be regulated or unregulated voltage bus. The solar array is responsible for generating electrical power to the loads, while the batteries (in most cases lithium-ion technology is employed) stores the excess power and supply it when needed (during eclipse or high power demand operations especially when the solar array is not producing enough power required for such high power intensity operations. The power converters are employed for conditioning of the power (battery charging, regulation, and distribution), while the switches are used for control as required by [4] etc. The EPS is the main thrust of this thesis work.

iii. Communication (COMMS) – Transceiver, beacon, antenna etc. This subsystem enables communication between the satellite and the ground station for operations (data transfer both in uplink and downlink), and housekeeping i.e. (information about the "health" of the satellite).

iv. Attitude Determination and Control (ADCS) – Magnetometer, Magnetorquer, Gyroscope, and DC motor etc. the major function of this subsystem is to determine the correct orientation of the satellite in space with respect to Earth, and the Sun for pointing, communication, spinning and detumbling.

v. The Thermal Control Subsystem (TCS) – Sensors and controllers etc. This uses sensors to determine the temperature and other thermal parameters and activate the controllers (for cooling and or heating) when required.

vi. On-Board Computer and Data Handling (OBC) is the main brain of the satellite – The processor that commands and controls all the subsystems and handles the data output of the subsystems for telemetry and other control purposes. The payload is controlled by this subsystem. This subsystem must be powered throughout the life of the satellite.

vii. The Payloads (experiments/the main mission of the Satellite)-Camera etc. The payload is the main mission of the satellite, as it defines what the satellite does in space – for Earth observation missions, normally is a camera, and some CubeSat missions may be used for technology demonstrations like evaluation of solar array performance as done in [22] or Attitude Determination and Control Subsystem in the e-star CubeSat of Politecnico di Torino etc.

Table 2.1 shows a general overview of the various types of University and other Corporation's CubeSat projects with respect to the types of Power generation systems and PV cells technologies employed, the types of battery technology used and the various EPS architecture and bus voltages adapted.

From the CubeSat projects, it was understood that most of the CubeSat missions were conceived for Student's practical Hands-on experiences and novel technology demonstrations. Multi-Junction Photovoltaic cells, Lithium-ion and Lithium Polymer cells and Maximum Power Point Tracking (MPPT) Architecture mostly dominated the choices made.

Table 2.1 A Survey of some University CubeSat Projects Mostly of 1u Type

Name	Owners	Type (Size)	Purpose	Solar Cells Technology	Battery Cell Technology	Architecture	Bus Voltages
NCube1	Norwegian University of Science and Technology	1U	Research	Not Sure	Not Sure	Not Sure	3.3V & 5.0V
DICE (Dynamic IonosphericCubeSat Experiment)	Utah State University and Space Dynamics Laboratory	1.5U	Research	Triple Junction	Lithium – Polymer 1.3Ah battery	Centralized & PPT	8.2V (Unregulated), 5.0V and 3.3V
NUTS-NTNU Test Satellite	Norwegian University of Science and Technology & Norwegian Center for Space-Related Education NORAM	2U	Student Satellite Program	N/A	Lithium-ferrite-phosphate cells (LiFePO4), 1.1Ah	MPPT and Distributed	3.3V & 5.0V regulated

Name	Owners	Type (Size)	Purpose	Solar Cells Technology	Battery Cell Technology	Architecture	Bus Voltages
Aalto – 1	Aalto University School of Electrical Engineering Department of Radio Sciences and Engineering	3U	Student satellite Project- Remote sensing Technology demonstration and scientific experiments	Triple Junction GaInP/GaAs/ GeAzurSpace Solar cells 3G30C 1.2W/cell and 29.5% efficiency 2.7Voc @BOL	Lithium Polymer cells	MPPT and Centralized	3.3V, 5.0V and 12V
Aalto – 2	Aalto University EU funded project –QB50	2U	Student satellite Project- Technology demonstration and scientific experiments	Triple Junction GaInP/GaAs/ GeAzurSpace Solar cells 3G30C 1.2W/cell and 29.5% efficiency 2.7Voc @BOL	Lithium-ion and Lithium Polymer being considered	MPPT and Centralized	3.3V and 5.0V
NMTSat (New Mexico Tech Satellite)	New Mexico Tech.	3U	Educational; for Hands-On experience, and Scientific experiments	Triple Junction GaInP/GaAs/ Ge From Spectrolab- Triangular Advanced Solar Cells TASC	N/A	MPPT	3.3V and 5.0V

Name	Owners	Type (Size)	Purpose	Solar Cells Technology	Battery Cell Technology	Architecture	Bus Voltages
Conceptual Design of Nanosatellite EPS	Islamic Azad University Iran Department of Electronic Engineering	Nanosatellite, not really CubeSat	Conceptual design for Hands-on experience for Remote Sensing	Multi Junction solar cells like the triple junction	Lithium-ion battery	MPPT and Distributed	10.5V
TINYSCOPE Nanosatellite	Naval Postgraduate School Monterey, California USA	5U or 6U (Special)	Military: Tactical Earth Imaging	Advanced Triple Junction with Monolithic Diode ATJM from Emcore @27% efficiency	Lithium-ion	Not sure	3.3V, 5.0V and 12V
CubeSTAR Satellite	University of Oslo Norway Department of Physics	2U	Student's Project: Hands-On experience and scientific experiment	Multi Junction solar cells the ultra-triple junction (UTJ) solar cells from Spectrolab	LiFePO4 battery cell	MPPT and Distributed	3.3V and 5.0V Point –of-Load POL

Name	Owners	Type (Size)	Purpose	Solar Cells Technology	Battery Cell Technology	Architecture	Bus Voltages
ESTCube-1	University of Tartu Estonia	1U	Student's Satellite Project for Hands-On experience, Technology demonstration and scientific experiments	N/A	Lithium-ion	MPPT and Distributed	N/A
ECOSat	University of Victoria Canada	Size not Clear from the report	Student's Project: Hands-On experience and scientific experiment	Ultra-Triple Junction solar cells from Spectrolab@ 28% BOL	Lithium-ion	DET Direct Energy Transfer	3.3V, 5.0V and 7.0V
CubeCat-1	UniversitatPolitecnica du Catalunya UPC Barcelona Spain	1U	Student's Project: Hands-On experience and scientific experiment			MPPT and Distributed battery bus	3.3V and 5.0V

Name	Owners	Type (Size)	Purpose	Solar Cells Technology	Battery Cell Technology	Architecture	Bus Voltages
OUFTI-1	University of Liege Belgium	1U	Student's Satellite Project for Hands-On experience, Technology demonstration and scientific experiments	Triple Junction GaAs solar cells from AzurSpace @ 30% efficiency	Lithium Polymer battery cells	DET Direct Energy Transfer	3.3V, 5.0V and 7.2V
Goliath	University of Bucharest, and University Politecnica Romania with support from Romanian Space Agency and Romanian Institute for Space Sciences	1U	Student's Satellite Project for Hands-On experience, Technology demonstration and scientific experiments	N/A	N/A	DET Centralize	3.3V, 5.0V and unregulated battery voltage
Explorer 1 [PRIME] Hiscock Radiation Belt Explorer HRBE	Montana State University Physics Department Space Engineering and Laboratory	1U	Scientific experiment Monitoring of particles in the Earth's radiation belt	N/A	Lithium-ion	N/A	N/A

Name	Owners	Type (Size)	Purpose	Solar Cells Technology	Battery Cell Technology	Architecture	Bus Voltages
e-star	Politecnico di Torino Italy	1U	Student's Satellite Project for Hands-On experience, Technology demonstration and scientific experiments	N/A		N/A	N/A
AAUSAT	Aalborg University	1U	Student's Satellite Project for Hands-On experience, Technology demonstration and scientific experiments		Lithium-ion cells	MPPT	5.0 V
Kufasat	University of Kufa	1U	Student's Project: Hands-On experience and scientific experiment Remote Sensing	Hybrid AzurSpace TJ Solar Cell 3G30C and Spectrolab UTJ TASC cells	Lithium Polymer batteries	MPPT	3.3V , 5.0V and Unregulated battery voltage

Name	Owners	Type (Size)	Purpose	Solar Cells Technology	Battery Cell Technology	Architecture	Bus Voltages
NPSAT1-Solar Cell Array Tester SCAT	Naval Postgraduate School, Monterey California USA	1U	Student's Satellite Project for Hands-On experience, Technology demonstration and scientific experiments	Improved Triple junction Solar cells from Spectrolab	Lithium Polymer batteries	MPPT Centralized	3.3V , 5.0V and Unregulated battery voltage
FunCube-1	AMSAT-UK	1U	Student's Satellite Project for Hands-On experience, Technology demonstration and scientific experiments	Triple Junction GaAs solar cells 28%	Lithium-ion GOMSpace Denmark	MPPT	3.3V and 5.0V

Name	Owners	Type (Size)	Purpose	Solar Cells Technology	Battery Cell Technology	Architecture	Bus Voltages
NANOSAT C-BR1	Federal University of Santa Maria Brazil	1U	Student's Satellite Project for Hands-On experience, Technology demonstration and scientific experiments			MPPT Distributed	3.3V and 5.0V

2.2 Constraints, Requirements and Functionalities

This subsection, discusses the constraints, requirements and functionalities of the EPS which includes the dynamic and hostile nature of the Space environment consisting of high radiation and temperature, vacuum and charged particles etc. [1]. The requirements placed on the EPS to withstand these space environment characteristics and be able to continuously provide the required power for the satellite throughout its entire mission duration is also analyzed and discussed. The functionalities of the various subunits of the EPS are also evaluated from the literature available especially from similar works conducted by students of postgraduate studies and other professionals in the field. It should be noted that this thesis work is aimed at a design and analysis of an EPS for a conceptual 1U CubeSat, so, most of the expected mission requirements and constraints are coming from a prior knowledge of the CubeSats constraints and functional requirements of the EPS as expected. There are other constraints too like the variant of the CubeSat selected, and in this case - a 1U, which has limited mass, and since the thesis work is expected to dwell on such areas for students' relevant learning experiences, it is also imposing a low budget as understood from all the students' CubeSat projects surveyed. So, only Commercial-Off-The Shelf (COTS) components would be selected for this work.

2.2.1 The Space Environment

Space has been described as a place where satellites are orbiting the Earth and other planets are orbiting the Sun, while the Sun revolves about the center of our Galaxy. This environment is encountered as soon as one goes up from 130 km and further, which means, it is a place where we can place our satellite and be able to maintain it in orbit as described in [1]. From the information about Space known to us - in our solar system, the Sun is the closest star to the Earth. The Sun is undergoing nuclear fusion and this produces electromagnetic radiation and charged particles – the real source of concern for the safety of our spacecraft [1]. We can summarize the challenges our spacecraft must face as posed by the constraints in the Space environment as follows;

2.2.1.1 Radiation and Charged Particles – Unprotected satellites get severely damaged by radiation and charged particles in the radiation belts (Inner and outer called The Van Allen belts).It is expected that our CubeSat is to operate in the inner radiation belt i.e. altitude extending up to 1000 km. Solar pressure, equipment surface damage and electronic components degradation and damages due to the intensity of radiation and charged particles attack are the main problems encountered by spacecraft in this region [1, 8]. Ultraviolet radiation is among the most serious when there is a prolonged exposure, and we expect our space assets to withstand it. Solar pressure can exert force on the spacecraft and make it to lose its direction over time as reported in [1].On the other hand, charged particles are more serious a problem to our CubeSat because of its influence on especially electronic components. These charged particles could manifest as a result of solar wind, galactic cosmic rays, or from the Van Allen belts indirectly and the consequence of these affecting our satellite is so severe if unprotected. Spacecraft charging and single event phenomenon SEP are the main problems caused by these. The effect of charging and of course sputtering is to degrade surfaces of the satellite and especially solar cells generating power [1] because of the speed of the charged particles. One of the serious effects of especially single charged particle is to penetrate in to the satellite and disrupt the electronic components bringing about what is known as single event phenomenon SEP. According to [8], three types of SEPs are possible and that both single event upset(SEU) and single event brown-out(SEB) are difficult to prevent but only through proper selection of materials and shielding, while single event latch-up(SEL) can be prevented using current limiters.

1) **Single Event Upset (SEU) -** Can cause "bit flip" in the memory of processors on the CubeSat. Electronic gates may be made to close or open without being controlled locally or remotely by the operators etc.

2) **Single Event Latch-up SEL**- This directly damages a component in the CubeSat. Even though SEL problem can be corrected by the protective and control circuits in the satellite, it remains a problem. Adequate concern should be given to solve it.

3) **Single Event Brown-out SEB** is when the charged particles completely damage the electronic component or the equipment on the surface of the spacecraft. The radiation dose as estimated in [8] is expected to be up to$10^5\ rad$, and it is advised that the EPS should be designed to withstand such exposure.

2.2.1.2 Gravity -Typically, the difference between the gravitational pull on Earth and that of (LEO) is just 9% (i.e. in LEO around 300km the pull is estimated at 91% that of the Earth) according to [1], the Moon and the Sun are regarded as having no significant pull on earth orbiting spacecraft. [1, 8].

2.2.1.3 Vacuum – This presents problems to our satellite known as out-gassing, cold welding, and some heat transfer issues connected to radiation. Outgassing is a phenomenon of released gasses trapped in the materials of the spacecraft while in Space. Cold welding is the fusing of metal materials that are in close proximity on the satellite [1]. The heat transfer problems also pose a challenge to the efficiency of our solar panels, the batteries etc. being among the most sensitive components of the EPS.

2.2.1.4 Atmosphere – At LEO, the atmosphere affects our satellites in Space by presenting drag to it and atomic oxygen attack. These problems tend to shorten the life span of the Spacecraft in the mission by pulling it towards the earth, and the atomic oxygen attacks the surfaces of the materials of the satellite (sensors etc.), solar panels and other accessories are at risk of this. [1]

2.2.1.5 Debris and Micrometeoroids – The Space environment is full of objects (debris and junks)moving at very high velocities. Even though, we know that the chance of these hitting a spacecraft is remote. However, our increasing space activity is increasing the probability. Therefore, it must be considered and ways of avoiding impacts and collisions from these must be found. [1].

2.2.1.6 Temperature – Temperature variations for a LEO environment can be dramatic. The variations may range from$-40°\text{C}\, to\, +80°\text{C}$. Satellites are transported through the various atmospheric regions and the magnetosphere where these temperature gradients exist. [8]. The EPS of any CubeSat for LEO should be able to work within the determined range; for the solar panels from $(-33°\text{C}\, to\, +40°\text{C})$ and beyond up to 85°C, and for batteries within $(0°\text{C}\, to\, +45°\text{C})$ during charge and from $(-20°\text{C}\, to\, +60°\text{C})$ during discharge for Lithium-ion technologies [8]. The battery operation may necessitate some control measures as temperature rises though.

2.3 The EPS Requirements

The EPS should be able to continuously provide power to the satellite throughout the mission duration. The generation sub unit – the solar panels, must be able to withstand the harsh space environment and produce enough power for the various subsystems on the spacecraft and for charging the batteries so power is available during eclipse period.

The batteries on-board should have enough charge-discharge cycle to last the duration of the satellite mission and must have enough charge to supply the subsystems during the eclipse period. The batteries are charged when the satellite is in sunlight, and discharged when in eclipse or during a high power demand operations like command and data uplink/downlink or mission specific operations during a low irradiance period [1-9].

2.3.1 Functionalities of the EPS

2.3.1.1 Solar Cells/Panels

The power generation on CubeSat is wholly from PV solar cells/panels [2– 5, 8]. The design guidelines presented in [4] limits the CubeSat by mass and size, and as result, the PV system is the only viable generator. The solar cell has been described in [4] as a semiconductor device converting sunlight to electrical energy through what is known as the "Photovoltaic effect", and the efficiency of which depends on the semiconductor material [5]. The energy conversion from sunlight to electrical energy was described in [12] as a common knowledge.

2.3.1.2 Solar Cell Theory and Technology

The solar cell basically is made from silicon and is a P-N junction normally formed by the doping of two common surfaces N-type and a P-type semiconductor [11], characterized by its current-voltage (I-V) curve. The cell in the dark behave as a reversed-biased diode, and the effects of photons with high enough energy greater than the bang gap energy of the silicon material penetrating the cell is to increase the density of electron-hole pair which are mobile. The typical I-V and P-V characteristics curve of a PV cell is shown in Figure 2.3 and Figure 2.4respectively. There are several technologies of the PV cells today; the most common is the Silicon

Si described as the most ripe for Space applications in [13]. Other types like the III-V solar cells initially developed on Gallium-Arsenide GaAs and GaAs/Ge i.e. grown on Germanium wafers because of achieving better mechanical strength and cost reduction, dual-junction GaInP/GaAs and the very popular triple-junction GaInP/GaAs/Ge all exist today as part of the multi-junction (MJ) solar cells development, and these have been employed to power so many space vehicles and satellites with tremendous successes as reported in [13], and in [7].The GaIn/GaAs/Ge cells have been described as the only viable solar cells technology for a CubeSat type. Thin film solar cells normally based on amorphous and nano-crystalline Silicon, Cadmium Telluride CdTe, Copper-Indium/Gallium diselenide CIGS etc. with efficiencies from 8% up to 19% [11] have also been developed for space applications with some satisfying results in terms of efficiency and low weight. The conversion efficiencies of these solar cells at Air Mass zero AM0 spectrum are encouraging. Air Mass is measurement of number of atmospheres solar insolation passes before reaching an object on the earth or in space. AM0 means no atmosphere was passed before reaching the said object [1]. In addition, polymer solar cells and other types exist, but, evidence of application of such in space was not found by this researcher.

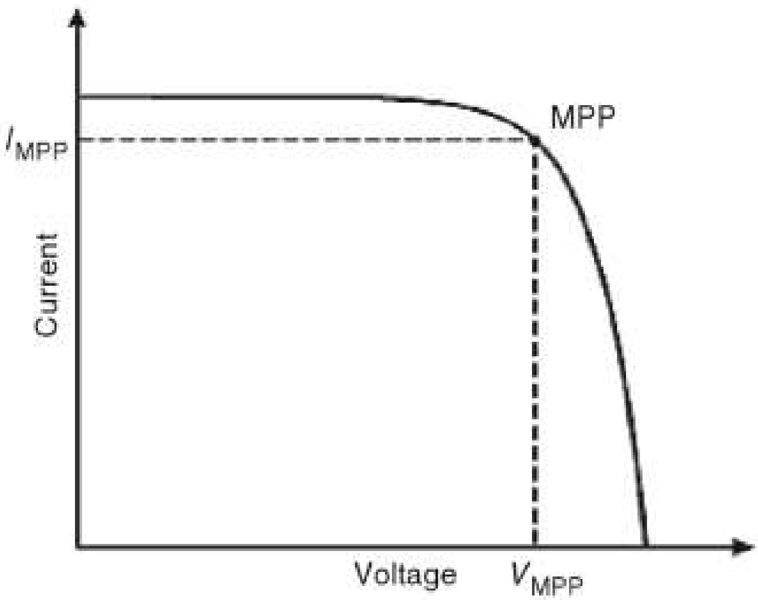

Figure 2.3 Typical I-V Characteristics Curve of a solar cell [5]

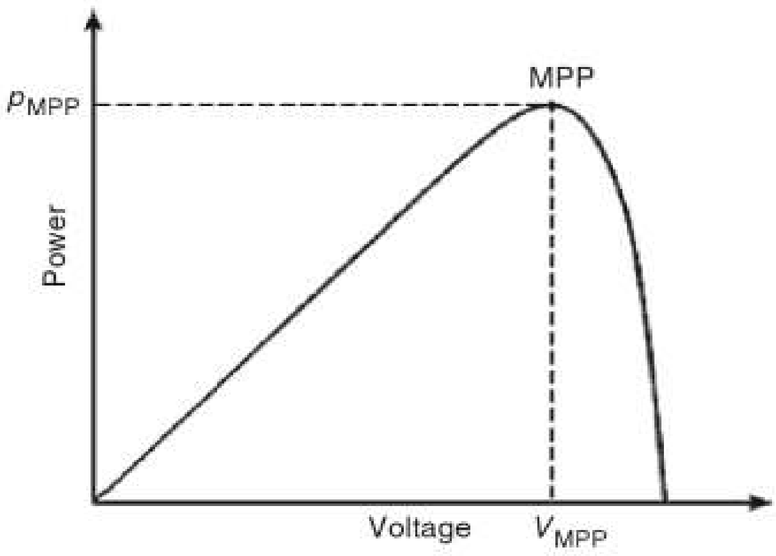

Figure 2.4 P-V Characteristics Curve of a solar cell [5]

2.4 Selection of Solar Cells for Space Applications

Several factors are guiding design engineers in selecting the types of solar cells/panels and configuration for space applications. For CubeSats, there are so many examples out there, where in [8], short circuit currentI_{sc}, open circuit voltage *Voc*, the maximum power $P_{max}$and the temperature dependencies of these on the efficiency η were considered. This is because the temperature in space is varying and to some extent extreme, also, the currents and voltages at MPPT were also observed.

Beginning of life BOL and end of life EOL efficiencies of a solar cell are related to the conversion efficiencies of the cell before and after expositing it to electron flux of 10^{15} electrons/cm^2 of space radiation at 1 MeV [45] The discussions on the BOL and EOL efficiencies of the solar cells are given appropriate consideration together with the Fill Factor (FF) which of course is tied to the efficiency η as stated explicitly in [11]. The EOL efficiencies are determined by the temperature coefficient and particle irradiation on the solar cells [15].
Designers of satellite power subsystem exploit the data sheets of cell manufacturers and suppliers like DHV technology, Spectrolab, AzurSpace, ISIS etc. [8] to extract the relevant information about the cells/panels. The cells are then modeled using single diode (in some cases double diode)equivalent circuit modeling. The diode(s) in the models are connected in parallel with a light controlled current source. A series and a parallel resistance also usually included depending on the simplicity of the

modeling chosen by the designers. In [11, 16, 27 -33], detailed modeling of photovoltaic sources ranging from the one-diode, two-diode to simplified models were presented. The modeling work considers case studies for low and high illumination environment and temperature variations. In [8], a simple one-diode model was used to study the parameters of AzurSpace solar cells. Other important factors considered are the configuration of the satellite, orientation in space, the radiation it will encounter i.e. the fluence level in mega electron-volts MeV, its mass, the intended mission duration and the size area of the cell available [15]. The characteristics curves obtained from the solar cells forms the basis of evaluation at the system selection stage. Thirion in [8] used AzurSpace solar cells of which is a triple-junction GaAs cells, and described it as having very good efficiency and also popular in space applications. The commercial version of the cell – "3G – 28%" was used in having a quoted efficiency of 28% and a size in area of 30.18cm^2 (80mm x 40mm) in dimension. A single diode modeled equivalent circuit of a solar PV cell is shown in Figure 2.5 with a series resistance $R_s$to account for metallic connection losses and a shunt resistance $R_{sh}$to account for manufacturing defects inherently possible in the cells. The current-controlled current source represents the current dependency of the cell while the diode is for the nonlinear components of the semiconductor including reverse saturation and recombination currents. The cell itself is a P-N junction.

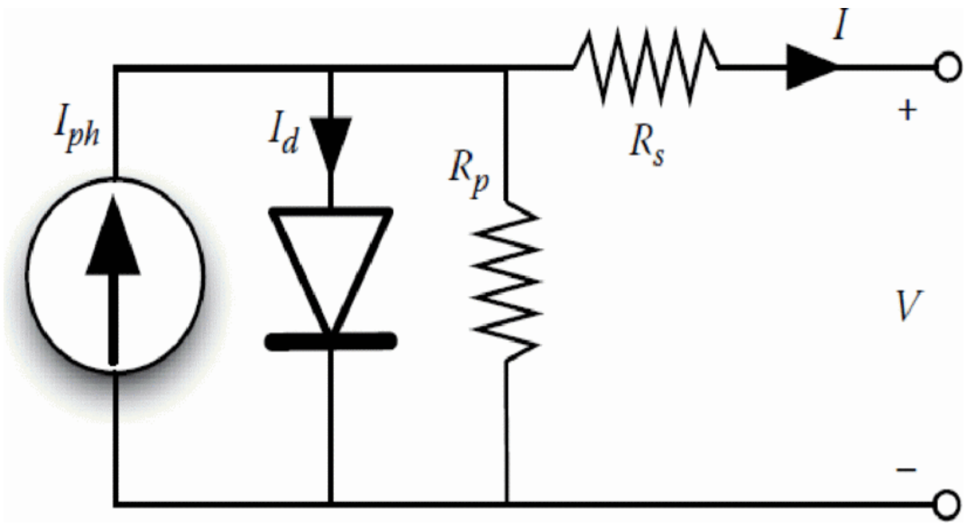

Figure 2.5 Equivalent circuit of a PV cell model taken from [16].

2.5 Power Storage Sub-Unit

The storage sub-unit has a strict requirement of supplying all loads during eclipse period. It must continue to do so if there is a peak power demand during critical operations period throughout the lifetime of the CubeSat. Peak Power demand is the scenario resulting in power demand exceeding power generation [20]. The power storage subsystem comprises mainly of batteries in a CubeSat variant of satellite, and the battery packs may or may not include; temperature sensors, a built-in protection circuit and heaters. Research in [5, 8] describes the battery storage system as "critical" component without which the satellite is completely OFF during period of eclipse which is an unwanted case. In [15],researchers explained the storage system as an electrochemical battery cell for power supply during eclipse. A connection of series and or parallel number of cells that should be able to power its load with electrical energy for a given period of time as stated in [15]. In space applications, consideration to size, cost and volume including performance are taken into account in meeting the requirements of its operations on a CubeSat. Additionally, because in most cases the solar cells on the CubeSat do not supply enough power to supply the peak loads, batteries are being employed as secondary source of power for the satellite [9]. Advises on choosing a battery was given in [8] – that is, batteries with heritage in space are preferred because of their reliable history. These should be tested to provide all the required performance under its operating conditions.

2.5.1 Battery Cell Technology

In the literature, almost all CubeSat power system designers considered Lithium-ion and Lithium-Po battery technology because of the requirements expressed in [4] of limiting the mass of the CubeSat and in [9, 15], high specific energy capacity, cost and high reliability were considered. The specific energy as quoted in [9, 18, 20] can range from 100 WH/kg to 250 WH/kg and a cell voltage of 3.7 V for Lithium-ion battery was recorded in the literature. In [20], it was reported that a Lithium-ion battery has a cut-off voltage of 2.7 V at the end of discharge, 4.2 V at end of charge, and an average discharge voltage of 3.5 V. In [15],it was concluded that the Lithium-ion batteries are preferred for European Space missions. Batteries for space applications have specific performance conditions to adhere to as provided by the

Goddard Space Flight Center (GSFC) in the General Environmental Verification Standard (GEVS) for Flight Programs and Projects as shown in [9]. The batteries should generally be able to withstand vacuum conditions and because of the sensitivity to some temperature ranges, they are expected to perform generally well within -8^0C to 37^0C according to the GEVS. The depth of discharge DOD of a battery should be kept low so as to enhance its operational capability and the capacity loss of this battery depends on it [5]. Lithium-ion batteries have some desired characteristics that makes them suitable for space applications and this should be the desired properties in any battery technology for such use as explained in [20], which includes but not limited to the following properties; very high specific energy density, high rate capability, and very long cycle life at high DOD. Additionally, it can deliver very high short time peak power without any serious effect on its life. The lithium battery also has low temperature sensitivity thereby making it a candidate for operations in a region of wide temperature variations.It has high charging efficiency of about 100%. The internal impedance is also low and it can tolerate serious abuse to some extent. The electrode corrosion is very low because lithium-ion is non-aqueous in chemistry.

Other batteries used in space applications are Nickel-Cadmium Ni-Cd and Nickel-Metal Hydride Ni-MH rechargeable batteries as stated in [15]. However, these Ni-Cd and Ni-MH have “memory effect” and are heavier for the same energy capacity when compared to Lithium based batteries. Consequently, their popularity is diminishing because of the maturity of the Lithium-ion and Lithium-Polymer technologies.

2.5.2 Battery Charge/Discharge and Protection

The battery is made from cells consisting of two electrodes. These electrodes are made of different materials, there is also an electrolyte connecting the electrodes in series. The electrode rich in negative charged ions is called anode, the other that is rich in positive charged ions is known as cathode. A potential difference between the two electrodes comes from a REDOX reaction with the electrolyte [15].

Rechargeable batteries require maintenance- charging and discharging, and protection etc. Adequate circuits for charging and discharging the battery is therefore necessary [9, 17]. In this subsection, we shall discuss the charging, discharging and protection of the battery.

2.5.2.1 Battery Discharging/Charging

Discharging battery occurs at a certain voltage resulting from a certain chemical process of reduction and oxidation. There is a release of electron at the anode as a result of oxidation, and a gain of electrons at the cathode following a reduction happens when a load is connected in between the electrodes and current flows. Charging the battery on the other hand requires a reversal of the discharging process. A voltage higher than that at the terminal of the battery is required to push the electrons in the reverse direction reversing the potential of the terminals. Several standard circuits for battery charging from Texas Instruments TI, Linear Technologies and ST Microelectronics like SPV 1040 etc. exist [9, 17], and some of these are embedded with MPPT capabilities for appropriate battery charging and protection [17].

2.5.2.2 Battery Protection

The battery should be protected both during discharging and charging so as not to degrade its capacity before its supposed usefulness. A charging circuit does well to protect the battery cells from over-charging and a possible over-current i.e. beyond the nominal voltage of say a Lithium-ion battery as pointed out in [5]. If the nominal voltage of the Lithium-ion battery is exceeded during charging, pressure may build up inside because of carbon dioxide produced, stability would be lost and an extended over-voltage charging may lead to explosion of the battery. This is taking place as a result of the plating of the Lithium material in the anode, and then, the capacity of the battery suffers. Care must be taken in implementing an appropriate charging strategy to protect the battery. Manufactures' recommendations should not be exceeded as seen in [5]. A common strategy for charging a lithium based battery is through Constant Current – Constant Voltage (CC-CV) technique. The battery voltage builds up until it nearly reaches the nominal voltage as the charging current is being reduced slowly reaching a very small value. This kind of charging ensures that the battery is not overcharged since when the nominal voltage of the battery is reached, the current becomes so insignificant. The charging circuit is fed with the battery voltage and current in order to control the charging. A typical battery charging characteristics in CC-CV mode as seen in [5] is shown in Figure 2.6. The battery is further protected by ensuring its operating temperature stays within range acceptable as stated earlier. In space applications, and especially on CubeSat, temperature sensors are connected for control; when the temperature is below a certain range, a heater is ON to heat up the battery pack, and, when it is being overdischarged, the control circuit disconnects (OFF) the load.

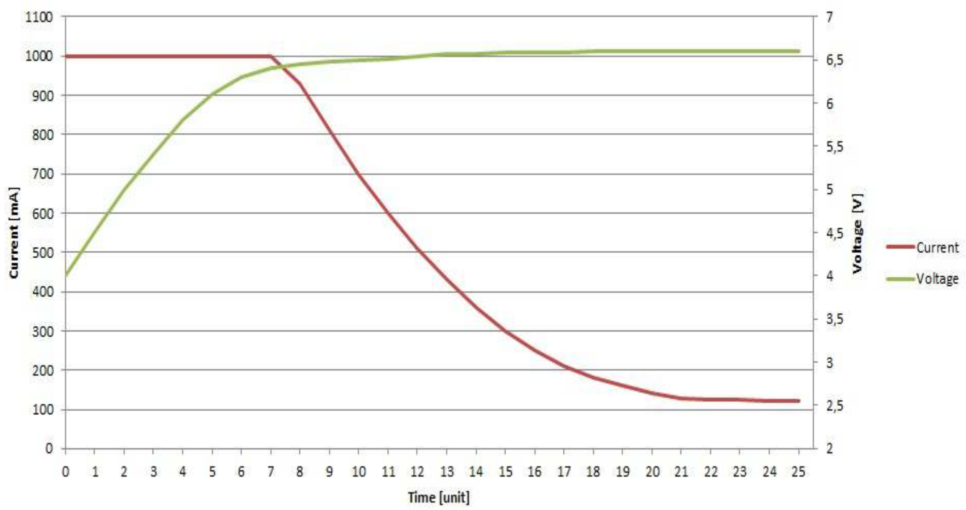

Figure 2.6 Current verses time and voltage verses time CC-CV characteristics [5]

Figure 2.7 shows an Equivalent electrical circuit of a battery with the internal voltage source and resistance, this is a simple model without the dynamics of the battery included [20].

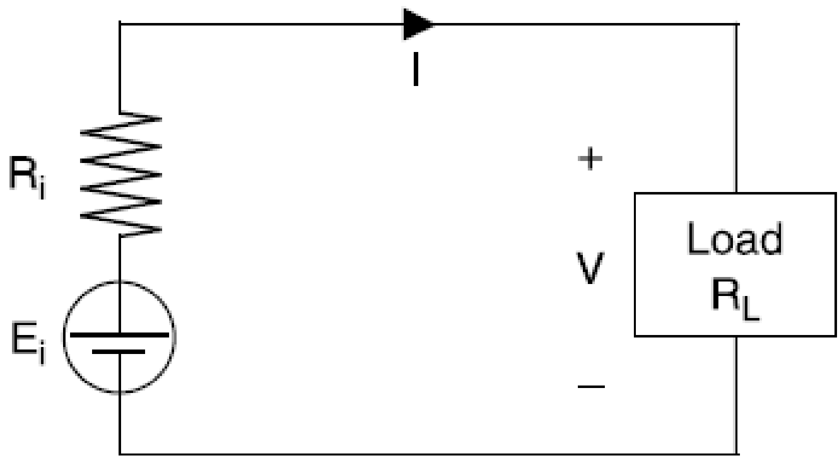

Figure 2.6 Basic equivalent circuit of battery cell [20].

2.6 Maximum Power Point Tracking Unit (MPPT)

The Maximum Power Point Tracking (MPPT) unit is a Hardware - an (DC-DC converter) implementation of algorithm to extract the maximum power available from a solar cell at any one time of instant irradiance on the solar PV module/array. This is to match the solar array with the battery bus or the voltage bus and conveniently supply the loads [17]. Literature review conducted in [7, 17] has shown that the MPPT is a very effective way of increasing efficiency of the power generation subsystem in a CubeSat by manipulation of voltage or current of the solar array through a network of switches connected between the solar cells and the loads/battery. According to [7], satellites placed in the LEO are subject to rapid variations in solar irradiance and hence, a system of extracting the maximum power from the solar cells should be connected for maximum efficiency of power generation. The MPP is a point located on the I-V and P-V curves of the solar cell as presented in [19], and the MPP depends on the total solar irradiation on the exposed area of the cells on the satellite based on the orientation with respect to the Sun, the temperature at that particular time, the cell technology used and the age of the cell as given in [7, 19]. The MPP is located at the "knee" of the characteristic curves of the PV cell. Figure 2.8 below shows a typical I-V curve of an AzurSpace solar cell under varying temperature conditions. This curve is from the results of the simulation studies performed in this thesis and is similar to what was reported in [19].

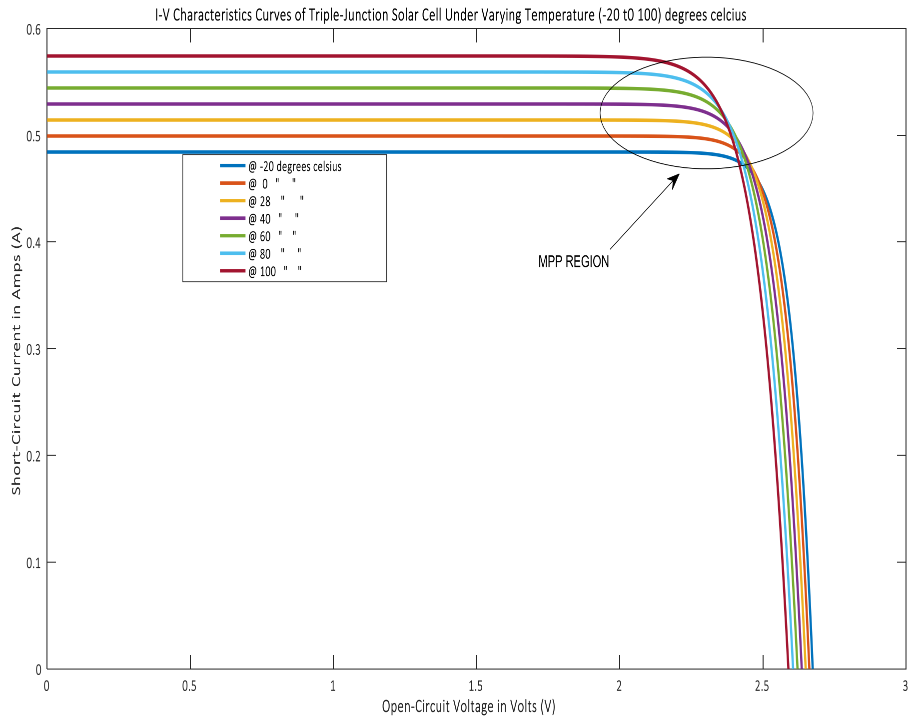

Figure 2.7 A typical I-V curve of a PV cell under varying temperature.

2.6.1 Types of MPPT Algorithm

There are several algorithms for tracking the MPP of a PV cell/array existing in the literature, however, we will discuss only the following being the most common, easily implementable, and it is worthy of note that the differences among these are on the projected and evaluated response times, the complexity in implementation and the overall efficiencies.

2.6.1.1 Perturb and Observe

The Perturb and Observe algorithm popularly written as P&O is the most popular of all the MPPT algorithms, and this is because of its higher efficiency and simplicity of implementation. As the name implies, the P&O algorithm perturbs the system and checks its operating point for maximum power, on voltage increase, if the power shoots, the operating point is near the MPP. The P&O algorithm, despite its simplicity, has some inherent output oscillation problems unless some modifications are made to it, accurate determination of the point of maximum power may not be achieved, and at the same time, it may introduce some errors if there are rapid variations of the irradiance level on the PV cells. The modifications suggested in the literature are; three points weighting of the measurements or prolonging the observation period of taking the measurements. The disadvantage of the suggestions however may lead to increased difficulty and complexity in implementation and may also severely reduce the response time of the system [19]. In the literature, most researchers explain the P&O algorithms using a flow chart like that shown in [19] as shown in Figure 2.9.

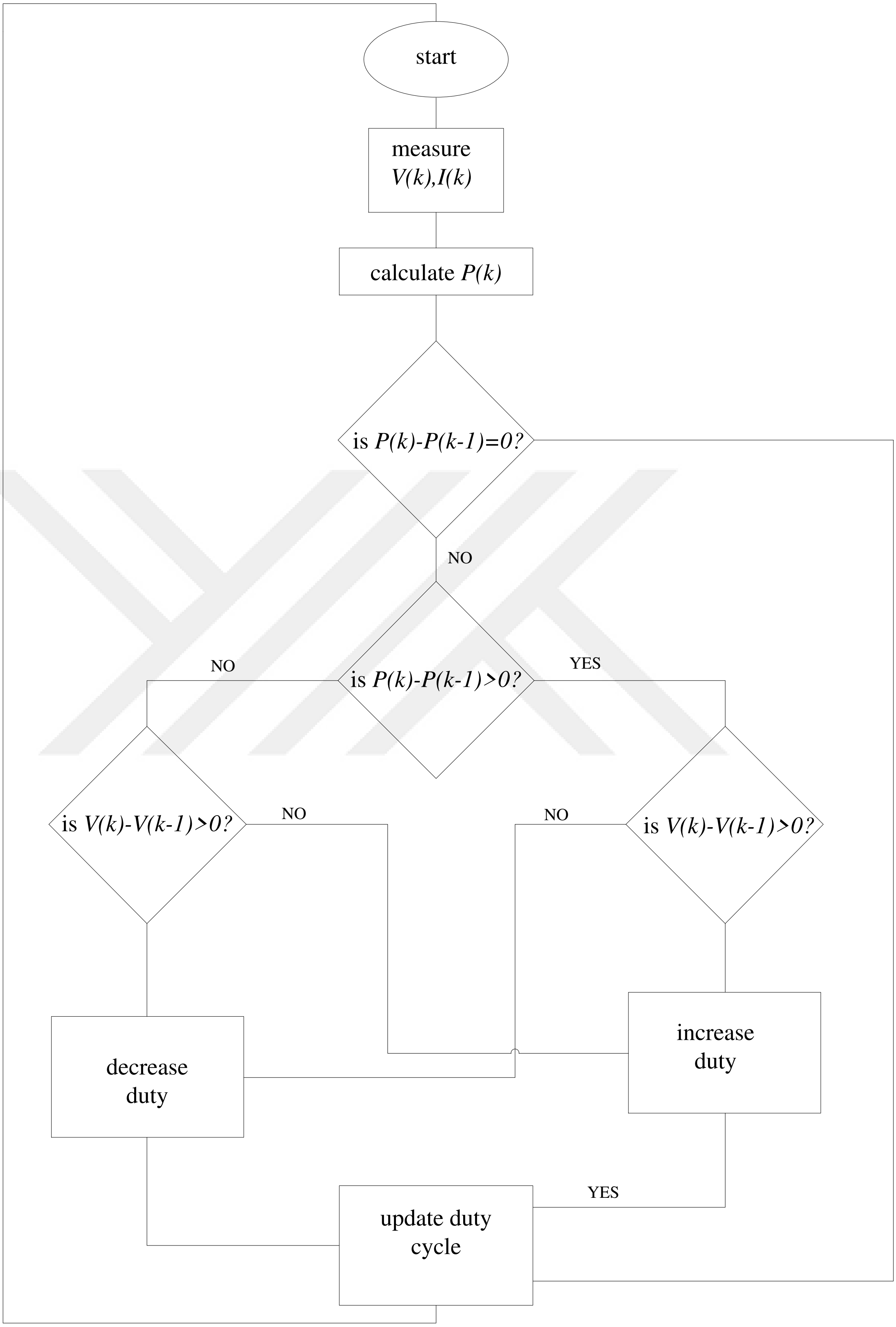

Figure 2.9 Flowchart of a P&O algorithm of MPPT [19].

The measurement taken initially is of $V(K)$ and $I(K)$, the power output $P(k) = V(K) \times I(K)$, following this, the perturbation is applied on the voltage, then, new power $P(k + 1)$ is calculated, if $P(k + 1) - P(k) < 0$, then, a change of perturbation direction is required i.e. voltage is reduced, else, perturbation continues in the forward direction [19] i.e. the maximum power is ahead and the voltage is increased etc.

2.6.1.2 Incremental Conductance (IC)

In incremental conductance (IC), the slope of the current with respect to the voltage is utilized and compared to the instantaneous conductance of the PV cell/array. Mathematically, IC can be represented as follows;

$$\frac{dI}{dV} = -\frac{I}{V}$$

By definition, $\frac{dI}{dV}$ is known as the IC, while $-\frac{I}{V}$ is the negative instantaneous conductance of the cell/array. One good advantage of the IC over P&O algorithm is that; IC has the ability of knowing beforehand direction in which the voltage should be increased. For the MPP to be reached, first, the slope of the current with respect to the voltage is observed;

If, $\frac{dI}{dV} > -\frac{I}{V}$ then, the voltage is increased, else, if $\frac{dI}{dV} < -\frac{I}{V}$ the voltage is decreased. The designed controller therefore maintains this operating point pending on the observation of a change in the IC before another command is given for the change of operating point [19].

2.6.1.3 Parasitic Capacitance (PC)

The fact that the solar cell is modeled as a P-N Junction and from which the junction has a PC made it a well suited way for drawing a MPPT algorithm in tracking the maximum power of the cell by looking at the energy stored in the parasitic junction. The Parasitic Capacitance algorithm has similarity with the Incremental algorithm or one can safely say it is a modified version of the IC. This is modeled by adding the parasitic capacitance term to the well-known solar model.

2.6.1.4 Constant Current Constant Voltage Algorithm (CC-CV)

These two algorithms utilized the fact that the solar PV cell has a constant ratio between the voltages at maximum power and the open circuit voltage. And the current ratio of the two ratios are both less than 1. The constant current however has some difficulty in implementation because, the I_{sc}measurement is very difficult more so if it is to be implemented on satellites since in applications like satellites, there is a power demand at all times. The constant voltage algorithm also requires a temporary deactivation of the supply line for measurement of the cell's open-circuit voltage, so, power generation would be lost during the period. The constant voltage algorithm uses the value of the voltage to control the duty ratio of the converter in order to track the MP.

2.6.2 Comparison of MPPT Algorithms

In [19, 25-26], a table of various types of MPPT algorithm with their associated efficiencies have been presented and reproduced here for reference purposes in Table2.2.It is interesting to know that the algorithms discussed above have been grouped and named as "hill climbing" algorithms because of the perturbation on the PV characteristics curve. The less complex an algorithm, the less power consumed for the MPPT operation. The P&O algorithm seems to be the most simplest of all even as it has some inefficiencies when the perturbation period is not optimally chosen.

Table 2.2 Comparison of different MPPT algorithms [19, 25-26].

Parameter	P&O	Incremental Conductance	Open-Circuit Method	Short-Circuit Current method
System efficiency	High	High	Medium	Medium
Accuracy	Medium	High	Low	Medium
Computation	Low	High	Low	Low
Complexity	Low	High	Low	Low
Speed	High	Medium	Low	Low

2.7 Power Conditioning and Distribution Sub-Units

The power conditioning sub unit is connected as a series block of DC-DC converters with the solar cells, to function as a conditioning unit for the input power to the loads (regulate voltage and current) to standard voltage levels of say, 3.3, 5.0, 7.0 12 V etc. for the satellite bus and charge the batteries. The battery charging and discharging functions are achieved through the use of these DC-DC converters normally embedded with MPPT as Battery Charge Regulators BCR.

The generated power from the solar cells or the battery which has been conditioned to standard voltages of normally 3.3V or, 5.0V, as it is generally accepted for CubeSat because it is a low power system; the regulated voltages are distributed to the loads, which includes the primary payload(s), the platforms etc. The distribution subunit is a DC-DC converter based of either buck, boost or a combination of the two - known as buck-boost converter. The converters may or may not provide direct control of the current flowing to the loads, sometimes point of load switches are considered for such – especially if a point-of-load regulator is used.

DC-DC converters exist in several modes and types, apart from the switched based inductive converter, linear voltage regulators and charge pumps also exist and each type has its own characteristics factors influencing the choice of a particular converter includes but not limited to; (a) range of voltage conversion, (b) efficiency of power conversion, and (c) quantity and sizes of components involved – the footprints [19].

DC-DC converters are classified as either - Isolated or Non-isolated. The Isolated converters employ the use of transformers, in our application - for CubeSat, there are constrains that would not allow the use of these kinds of converters – Mass and Volume. Examples of these are; Forward and Fly back converters. The Non-isolated types of converters are the Buck, Boost, Buck-Boost, Single Ended Primary Inductance Converter (SEPIC), Cuk converters and the charge pumps. Further classification is, some DC-DC converters are Linear or Switched-Mode. The Linear types use resistors networks while the Switched-Mode uses switches – MOSFET, IGBTs etc.

2.7.1 Linear Voltage Regulator

DC-DC converter can be realized by the use of series resistors forming voltage dividers, or some form of combination of these with Op-Amp to form linear regulators. Linear regulators and voltage dividers are a permanent source of voltage drops and heat, hence, the efficiencies of these are very small and therefore, not suitable for so many battery powered applications like CubeSat because of the very low efficiencies and heat generation associated with these kind of voltage regulators as expressed in [19 and 23]. A typical implementation of a Linear Voltage Regulator is shown in Figure 2.10 as found in [23].

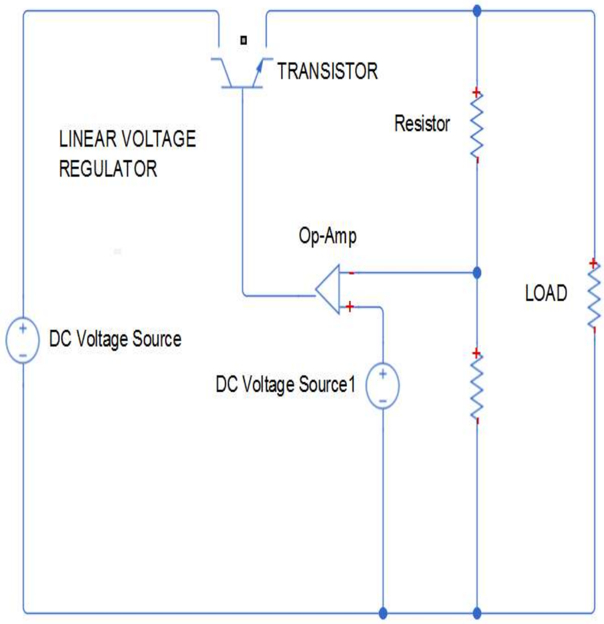

Figure 2.8 A typical circuit diagram of a linear voltage regulator [23]

2.7.2 Switched-Mode Power DC-DC Converter

Like their name implies, Switched-Mode DC-DC converters extensively utilize active switches and of course some storage elements like inductors and capacitors for the voltage conversion. Improved efficiencies of conversion more than obtained in Linear Voltage Regulators, much less heat generation because of almost ideal case of 0 voltage drops across the switches have made the choice of these kind of converters very suitable for many applications where relatively stable voltages or currents at the inputs or outputs of such converters are of serious concerns. Again, because of the possible selection of very high frequency in switching, the resulting inductors and capacitors for the circuits would be smaller and hence space is conserved – smaller footprints. The Switched-Mode converters enables us to realize Buck, Boost, and Buck-Boost conversion and charge pumps through the manipulation of what is called Duty Cycle Ratio that are not possible with the Linear Voltage Regulators that only allow for realizing buck conversion.

2.7.2.1 Buck Converter

A Buck converter does exactly what its name suggest – transforming a higher DC voltage of certain magnitude to a lower DC voltage of another magnitude at efficiencies of between 70 to 95 % [19,23]. A network of switch, diode inclusive, an inductor and a capacitor are sufficient to describe an ideal buck converter, the inductor and the capacitor are acting as a low pass filter for removing high frequency switching components in the output voltage [19].

The switches implemented could be IGBTs, MOSFETs, diodes, BJTs, and Thyristor etc. a typical buck converter schematic is shown in Figure 2.11 where a switch is connected in series with the voltage source, and the diode shown could be replaced by another switch say MOSFET, and hence, another special buck converter called synchronous buck converter is realized. as explained above, the inductor and capacitor are in low pass mode and the inductor stores energy when the switch is closed, the diode in this case is reversed biased and hence in blocking-mode, then, the stored energy in the inductor is discharged to the load; the ac component is passed through the capacitor after opening the switch – controlled by the duty cycle. The duty cycle ratio is obtained through implementing say a pulse width modulation (PWM) at high frequency for opening and closing the switches. i.e.

$$D = \frac{t_{on}}{T_{sw}} \tag{2.1}$$

Where, t_{on} is the period when the switch is ON and T_{sw} is the period of switching between ON and OFF times in a feedback loop. The PWM allows for the control and regulation of the output. D lies between 0 and 1, and the switching frequency F_{sw} lies normally between 1 KHz to 1MHz depending on the speed of the type of switch used as reported in [24]. The output voltage of the buck converter V_{out} is

$$V_{out} = D \times V_{in}. \tag{2.2}$$

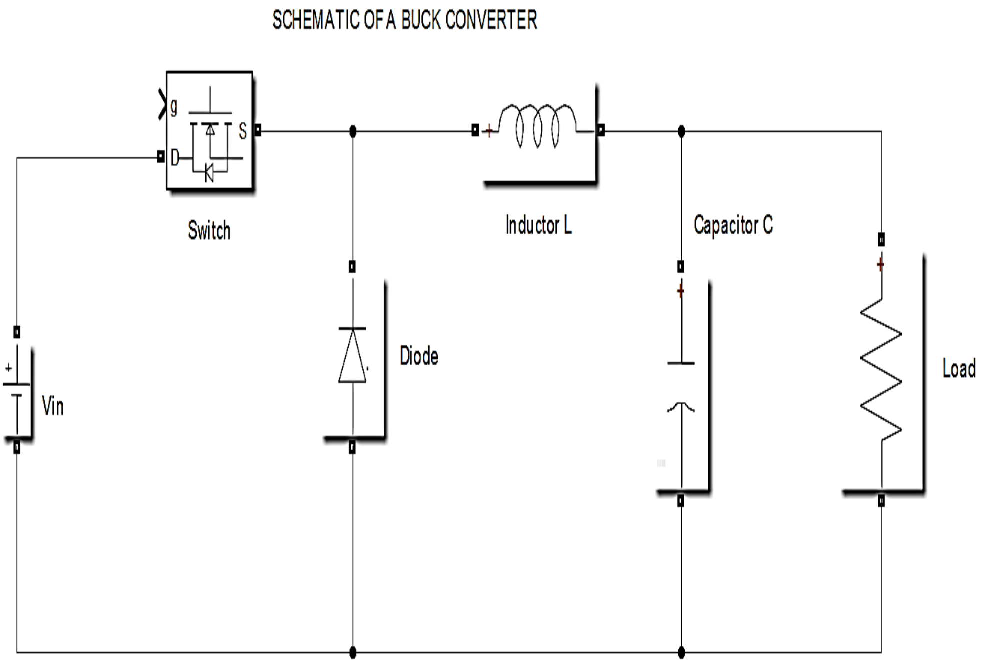

Figure2.9 Buck converter schematic diagram [23].

2.7.2.2 Boost Converter

The boost converter as its name implies, is employed in situations where the input DC voltage is to be boosted to an output DC voltage of higher magnitude. This type of converter is sometimes referred to as indirect energy transfer converter that first of all stores the energy in the inductor during ON period while only the capacitor is supplying power to the load, and releases it during the OFF period of the switching process [23]. One of the inherent problems in the boost converter is its conversion delay during a sudden rise in power demand at the output. This converter is normally

in low-input ripple topology operation in continuous conduction mode CCM because the inductor is connected in series with the source and because of its opposition to fast current variations. Just like the buck converter, the main components are switches (MOSFETs, diode) an inductor, a diode and an output capacitor. During the ON period, the input voltage appears across the inductor immediately, the inductor current reaches a peak of its value, since the switch is almost a short circuit to the ground, the diode is almost in a blocking mode, so no current flows through it. The output capacitor and the load on the other hand, are "disconnected" or floating. On switching OFF of the switch, the stored energy in the inductor forces a current through the series diode in to the capacitor and the load. The OFF time provides that the voltage is increased beyond the input voltage.
The dc transfer function for this operation mode is from the duty cycle-

$$D = \frac{V_{out} - V_{in}}{V_{in}}. \qquad (2.3)$$

The boost converter has a pulsating output; hence, it has been described as "noisy". Figure 2.12 shows a typical schematic diagram of a boost converter [23].

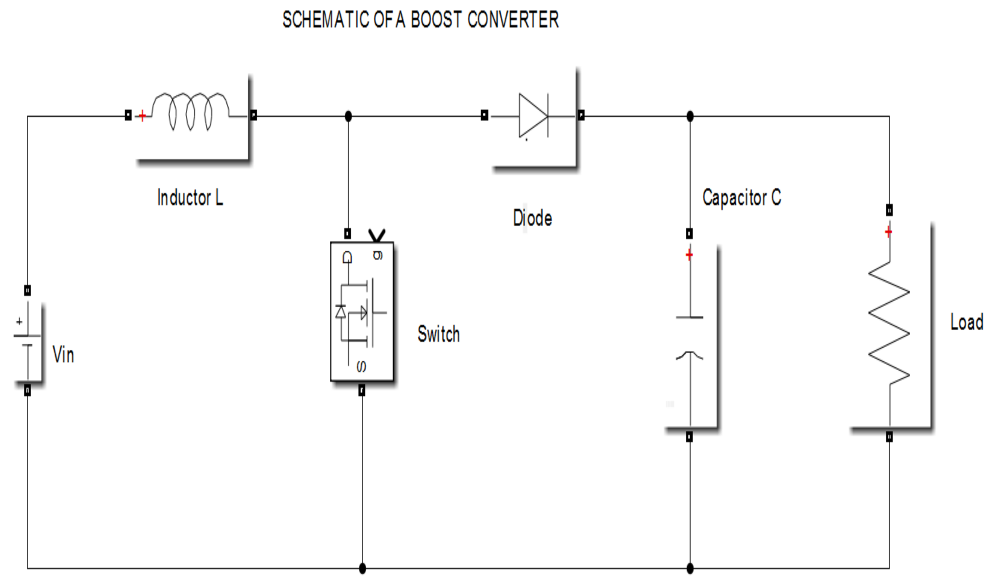

Figure 2.10 Boost converter schematic diagram [23]

The following points help completely describe in words the boost converter behaviour and characteristics in CCM operation;

i. Its output voltage is greater than its input voltage
ii. The load current has no influence on its conversion ratio but the ratio cannot go beyond 4 or 5 in the CCM operation, conversely, the conversion ratio depends on the load current in discontinuous conduction mode DCM
iii. Varying the duty ratio D enables control of the output voltage
iv. There are losses associated with the diodes reverse recovery charge
v. Control of the switching is easy because of the common ground it is connected to
vi. The converter cannot be protected from short circuit because the input and the output voltages have a direct path through the Inductor and the diode during the OFF period of the switch
vii. Average input current is the same as average Inductor current

2.7.2.3 Buck-Boost Converter

The buck-boost converter is simply a hybrid of the buck and the boost converter. It only operates in buck mode when the desired output voltage is less than the input voltage and it boosts otherwise. The buck-boost converter topology is slightly like the buck converter because of the structure of the switch placement in the circuit – in series with the source, and partly like the boost converter if not for the flipped diode connection – implying negative output voltage, and the inductor is now connected to the common ground as shown in Figure 2.13. We can deduce from the figure that it is much the same like the other converters discussed above in terms of the number and types of components used to realize it – two switches (say a MOSFET, and a diode), a capacitor and an inductor.

The buck-boost converter also has direct energy transfer topology and has some disadvantages of poor input and output current profile and a switch type constrain that makes it more complex and more or less expensive when compared to the other two options of either buck or the boost converter types. The switch has to be a P-type MOSFET, or if a bipolar transistor a PNP or an N-Channel NPN, and it did not stop there, it needs a buffer circuit to be generating a floating gate voltage signal.

The operation of the buck-boost converter is analyzed as follows; during the ON period of the switch, the input voltage is entirely "seen" by the inductor if the components are assumed to be ideal, and, the diode is reversed biased. The capacitor in the ON duration supplies the load. When the switch is OFF, the inductor voltage reverses and the diode conducts thereby discharging the inductor and supplying the load and charging the capacitor. The average inductive voltage over the full switching cycle is 0 and the transfer function is shown in equation (2.3) where$D$ is the duty cycle [23].

$$\frac{V_o}{V_{in}} = \frac{-D}{1-D}. \tag{2.4}$$

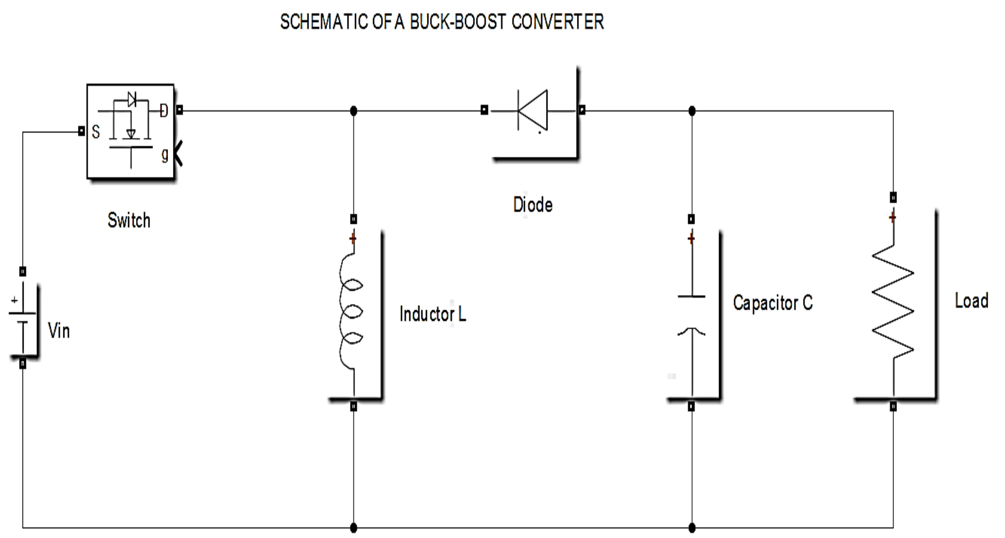

Figure 2.11 Buck-boost converter schematic [23].

2.7.2.4 The SEPIC Converter

A single ended primary inductance converter SEPIC is another type of buck-boost converter that is able to maintain an output voltage lower or higher than the input voltage and most commercial EPS manufacturers use this DC-DC converter topology in their designs. CydeSpace EPS is based on this topology [46]. The SEPIC comprises of four energy storage elements – two capacitors and two inductors, the other elements are two switches. One advantage of a SEPIC is, it has very low ripple profile and the output is not inverted. However, the SEPIC is very difficult to control because it has a fourth order transfer function [25 - 27].Figure 2.14shows a schematic of a SEPIC [27, 35-37].

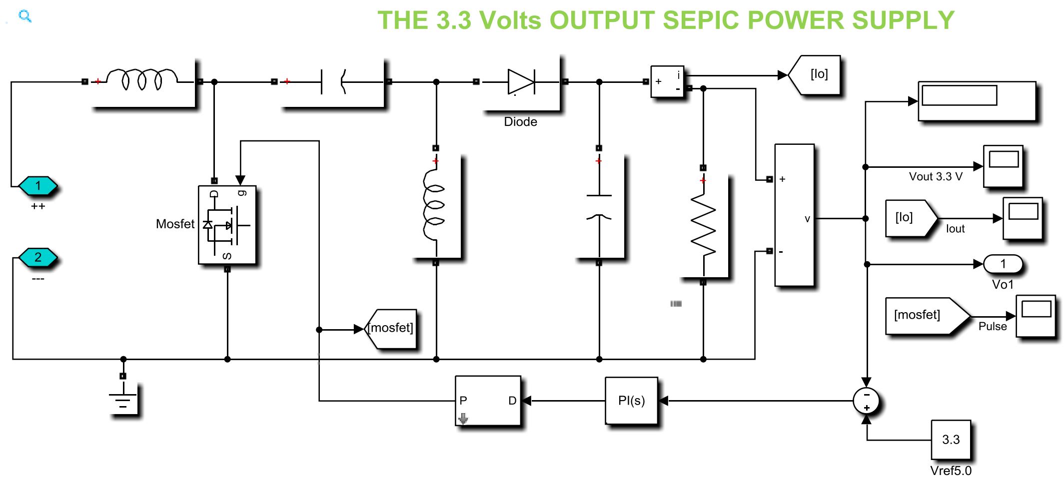

Figure 2.12 A Schematic of a SEPIC [27, 35-37].

2.7.3 Input and Output Filtering

One of the major problems of switch-mode power supply DC-DC converters is the noise inherent in their outputs as found in the literature clearly from the measured outputs of these converters. In the CubeSat application for example, all the subsystems would be supplied by these converters, i.e. the same power lines supplying all the loads in most cases. Electro-magnetic interference EMI is one of the problems where DC-DC converters are connected because the inputs or the outputs have ripples that can affect other subsystem’s operations, hence, an input and output filtering network should be employed to minimize such noise. The use of input/output filtering network would improve the EMI and the electro-magnetic compatibility EMC profiles of the converters. In this work however, a SEPIC topology is used and it has very low ripple as stated in section 2.7.2.4 above especially when coupled inductors are used. So, no filtering network was designed. The section of input filtering was brought here for reference and completeness.

2.7.4 Converter Control Modes

The converters are employed to regulate voltage to a specific fixed level in most cases, some of the converters are connected to variable loads, and the load current have influence on the outputs of most of the converters. There is therefore the need for controlling these converters to maintain the output at fixed levels. In CubeSat power system, we are designing for various subsystems loads that require fixed voltages – 5.0V and 3.3V are typical.

The most common control modes used for the converters found in the literature are; Voltage-Mode and Current-Mode Controls. The control modes are basically doing the same work since they rely virtually on the condition of the output to control the duty ratio. The voltage-mode control uses the output voltage directly and a reference voltage to control the duty cycle in a closed loop, while, the current-mode control requires to sense the inductor current in an inner loop in conjunction with the output voltage to control the duty ratio. The voltage mode of control is simpler to implement with a few components, and the other control type is more complex.

The DC-DC converter control in either voltage or current mode requires a model of the converter to be obtained before any reasonable controller design can be achieved. We may be interested in knowing how the variations in the input voltage, the nature of the load currents, the duty ratio etc. affects the output voltage that we want to stabilize. The switching process and the time-varying nature of PWM however, pose some challenges. Engineers have however found some suitable techniques for obtaining the dynamical models of the small signal perturbations around the steady state points of the converters. Small signal analysis through what is called state-space circuit averaging techniques have been used in obtaining the models of the dynamic nature of the DC-DC converters for appropriate controller design as seen in the literature. We are going to implement the SSA technique for modeling the converters for control purposes.

CHAPTER III

PROBLEM FORMULATION AND METHODOLOGY

3.1 The Conceptual Mission

The overall aim is to design an EPS for a 1U CubeSat that can adequately supply power to all the mission loads. The power is to be generated using solar cells that are to be mounted on the body of the CubeSat, a Lithium-ion battery is to be used for power storage for onward use during eclipse and during high power demand operations. The orbit selected for the conceptual mission is LEO at around 500 km for agricultural/environmental monitoring, and atmospheric research purposes or any other academic purpose by University Students, in-flight testing of solar cells and other technology demonstrations etc. The CubeSat is conceived therefore for remote sensing, so, the payload is a camera. The satellite is expected to have a sun-synchronous orbit.

Simple missions like this could be conceived to demonstrate the usefulness of space technology in enhancing agriculture and environmental monitoring capabilities, and give students and researchers opportunities for further development. This work envisages that there could be low budget for university projects, and hence, a simple approach to be taken is by attempting to select commercial off the shelf (COTS) components for the EPS without compromising efficiency and reliability.Table 3.1 gives a summary of the selected mission parameters for the thesis work.

Table 3.1 Mission orbit parameters.

The Orbit Parameters			
Parameters	**Value**	**Unit**	**Remarks**
Orbit type	Sun-synchronous	N/A	This orbit ensures that a satellite makes its passes over a location at the same local time every day. This is important for especially remote sensing satellites.
Orbit altitude $(H_{mission})$	500	Km	This is the orbital height with respect to Earth; chosen.
Inclination i	98	º (degrees)	Measure of the angle of inclination of the path of the CubeSat with respect to the Equatorial plane.
Orbit Period	94.6	Minutes	Time required for the CubeSat to complete one orbit round the Earth at the altitude chosen
Period in Sunlight	58.9	Minutes	Duration in Sunlight
Period in eclipse	35.737	Minutes	Time duration in shadow of the earth
Solar irradiation	1367	W/m^2	Average solar flux received from the sun in space
Albedo	410	W/m^2	The reflected energy from the earth
Infrared shine	240	W/m^2	

3.2. The Power Budget: PV Cells and Battery Selection

Normally, the power requirements of the various loads of the CubeSat ought to be known by the power system design team before proceeding to the next item in the line –Power Budget. However, since this work is based on a Conceptual mission, the power consumption information of the subsystems is best estimated by looking at similar CubeSat projects and other suppliers documents. A typical power budget in tabular form is shown in Table 3.2 giving the power requirements of a CubeSat platforms and their varying duty cycle and operation modes.

ClydeSpace for example, have given us a simple, yet concise guide on how to go about this, especially when such information are not yet clear to us [47]. We must ensure that the power produced by the solar cells during an orbit, is higher than or equal to the power consumed in that orbit so as not to eventually discharge the battery completely which means a failure of the mission. As a rule of thumb, 60% of Power produced by a panel is suggested for a 4 facet satellite (X/Y sides) for the Orbit's average power available, in this work, AzurSpace solar cells and panels which are COTS components were selected for the design. The AG30C space solar cell from AzurSpace is a 30% efficiency class cells and the datasheet information was extracted and presented in Table 3.3, while the cell is shown in Figure 3.1. Another cell that may be considered is the XTJ Triangular Advanced Solar Cell TASC from Spectrolab whose space heritage and smaller size including efficiency is tempting for employment in especially the two possible faces of the CubeSat that may be occupied by other components. The relevant datasheet parameters were also extracted and presented in Table 3.4.

Table 3.2 Power budget

<table>
<tr><th>Subsystem</th><th>Power in mW</th><th>Duty Cycle Safe Mode in %</th><th>Duty Cycle Payload Operation in %</th><th>Recovery Mode Operation in %</th><th>Power Over Orbit in mW</th><th>Remarks</th></tr>
<tr><td>On-Board Data Handling</td><td>200</td><td>100</td><td>100%</td><td>100%</td><td>200</td><td>Always (ON)</td></tr>
<tr><td>(COMMS)</td><td>550</td><td>20</td><td>20%</td><td>20%</td><td>110</td><td></td></tr>
<tr><td>EPS</td><td>36</td><td>100</td><td>100%</td><td>100%</td><td>36</td><td>(always ON)</td></tr>
<tr><td>(ADCS)</td><td>65</td><td>100</td><td>100%</td><td>100%</td><td>65</td><td>always ON in all modes)</td></tr>
<tr><td>Payload</td><td>800</td><td>30</td><td>30%</td><td>0%</td><td>240</td><td>Operating power of the payload including warm up</td></tr>
<tr><td>Total</td><td>851</td><td></td><td></td><td></td><td></td><td>power consumption during eclipse</td></tr>
<tr><td rowspan="2">Total</td><td>1651</td><td>651</td><td>651</td><td>411</td><td>651</td><td>Required Array Orbit power for different modes of operation</td></tr>
<tr><td colspan="3">1651 mW</td><td colspan="3">Orbit Peak Power Required = (payload operation mode) + power required for battery heating and other small sensors.</td></tr>
</table>

Table 3.3 Electrical and mechanical characteristics of 3G30C-advanced solar cell from AZURSPACE

Electrical and mechanical characteristics of 3G30C advanced solar cell from AZURSPACE	
Parameter	**Value**
Part name	3G30C Advanced
Technology/Base Material	Triple Junction GaInP/GaAs/Ge on Ge Substrate
Efficiency η	30%
Cell Area	30.18 cm^2
Average Open Circuit Voltage V_{oc}	2.7V @ BOL
Average Short Circuit Current I_{sc}	0.5202A@ BOL
Voltage at Maximum Power V_{mpp}	2.411V
Current at Maximum Power I_{mpp}	0.5044A @BOL
Average Weight	< 86 mg/cm^2
Temperature Gradients	
Open Circuit Voltage $\Delta V_{oc}/\Delta T\uparrow$	-6.2 mV/
Short Circuit Current $\Delta I_{sc}/\Delta T\uparrow$	0.36 mA/
Voltage at max. Power $\Delta V_{mpp}/\Delta T\uparrow$	-6.7mV/
Current at max. Power $\Delta I_{mpp}/\Delta T\uparrow$	0.24mA/
Spectrum: AMO WRC 1367 W/m^2; T = 28 ^{0}C. @ Fluence of 1MeV (ecm^2)	

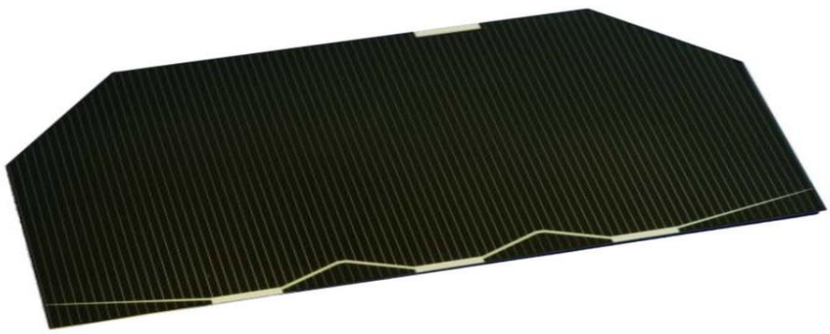

Figure 3.1 AZURSPACE solar cell [8]

Table 3.4 Electrical and mechanical characteristics of NeXT triple-junction solar cells from Spectrolab Inc. California

Electrical and Mechanical Characteristics of NeXT Triple-Junction Solar Cell XTJ from Spectrolab Inc. California	
Parameter	**Value**
Part name	NeXT Triple Junction Cells XTJ
Technology/Base Material	Ultra Triple Junction GaAs i.e. GaInP/GaAs/Ge
Efficiency η @ max. power	29.8 %
Cell Area	26 cm^2
Open Circuit Voltage V_{oc}	2.633 V @ BOL
Short Circuit Current I_{sc}	17.76 mA/cm^2 @ BOL
Voltage at Maximum Power V_{mpp}	2.348 V
Current at Maximum Power I_{mpp}	17.02 mA/cm^2 @BOL
Average Weight	< 84 mg/cm^2
Temperature Gradients	
Open Circuit Voltage $\Delta V_{oc}/\Delta T\uparrow$	-5.8 mV/ @BOL
Short Circuit Current $\Delta I_{sc}/\Delta T\uparrow$	11.6 mA/ @BOL
Voltage at max. Power $\Delta V_{mpp}/\Delta T\uparrow$	-6.5mV/ @BOL
Current at max. Power $\Delta I_{mpp}/\Delta T\uparrow$	6.6μA/cm^2/ @BOL

3.2.1 Battery Selection

There are several Lithium technology battery manufacturers and suppliers like VARTA, KOKAM, ABSL and Vendors like ClydeSpace ISIS, Pumpkin, Endurosat and CubeSat Shop etc. whose products have been tested and are in flight on several CubeSats and other satellites. Table 3.5below provides an overview of the COTS batteries in the market from these manufactures. Three models from these suppliers were selected for the data extraction and evaluation.

This unit stores the excess power for usage during eclipse and peak power operations period like during Payload operation and communication periods during a particular orbit of the CubeSat. From the literature review, Lithium-ion based batteries are very popular since they have heritage in Space and we have not found any evidence of failure due to using Lithium-ion battery in the literature. Lithium-ion/Polymer batteries have been described as being the best for CubeSat power applications [8].

From the conceptual power budget, the eclipse power consumption would not be more than 0.5Wh. Therefore, the battery capacity can be calculated from the depth of discharge, typically, a DOD from 15% to 30% is okay. For the purpose of this design, 20% DOD is selected as used in [19] and also suggested in [20]. The expected power consumption is about 851mW in eclipse period, but 900 mW is assumed here to take cognizance of possible losses. With a DOD of 20%, it implies that any battery having the capacity of 2.68Wh would be sufficient. For reliability and redundancy, two batteries can be implemented in parallel and Table 3.5 gives us a picture of which ones to choose.

Table 3.5 List and parameters of batteries considered

Manufacturer	**VARTA AG**	**KOKAM**	**PANASONIC**
Technology	Lithium Polymer	Lithium Polymer	Lithium Ion
Model	1/LPP 503759 8HH PCM W	SLPB526495	NCR18650
Nominal Voltage (V)	3.7	3.7	3.6
Nominal Capacity (Ah)	1320mAh rated 5.2 WH With PCM	3.3	2750mAh min. 2900mAh typical
Max. Charge Voltage	4.2 V (±50mV)		4.2 V (±50mV)
Max. discharge Current	2000 ma		1C @ 2.5V cut-off
Max. charging Current	1980 ma		0.7C @ 4.2 V 55mA
Charging temperature range	0^0C - to - +45^0C		
Discharge temperature range	-20^0C -to- +60^0C		
Maximum continues discharge current	1320mAh	2 Ah	
Energy density (Wh/Kg)	226	182	214
Weight (grams)	23	67	46.5
Dimensions [W],[L],[T] (mm)		[64.5] [95.5] [5.4]	Cylindrical 18.5mm radius, 65.3mm height
AC-IR (mΩ)		15	

3.3 Power Supply and Battery Charging Converter Selection

The converter selected for the power supply design is based on SEPIC topology because of its heritage in power supply design for CubeSats and other battery powered devices like laptops, pacemakers etc. It also has numerous advantages as mentioned in the literature [27, 35]. It has basically four energy storage elements which are two inductors and two capacitors. The two inductors can be wound on the same core in opposite directions, hence, ripple currents generated by the inductors cancel out.

Consequently, the battery charge regulator (BCR) is also SEPIC topology based and is connected to the output of the solar panels and used for charging the batteries and supplying power to the loads through the converters. The BCR to be implemented is supposed to be an MPPT based system so as to maximize the efficiency of the power generation unit by adjusting the voltage and currents of the solar panels. Microcontrollers can be implemented to do the MPPT, and, there are dedicated ICs used for such which have shown good efficiencies and have been employed in so many designs of EPS [19].

CHAPTER IV

PRELIMINARY SUBSYSTEMS DESIGN

4 Introduction

The preliminary system design enables us to design the overall EPS. We have performed the trade-off as to which solar cell to use and what converter types to and topology to adopt. The solar cell type we selected is a triple-junction solar cell. The converters topology is SEPIC and the charger is CC-CV MPPT.Thedesign of the voltage regulation/conditioning converters (3.3 V and 5.0 V) was also accomplished. Figure 4.1 shows a block diagram of the CubeSat EPS with the main components in block diagram as adapted from [17].

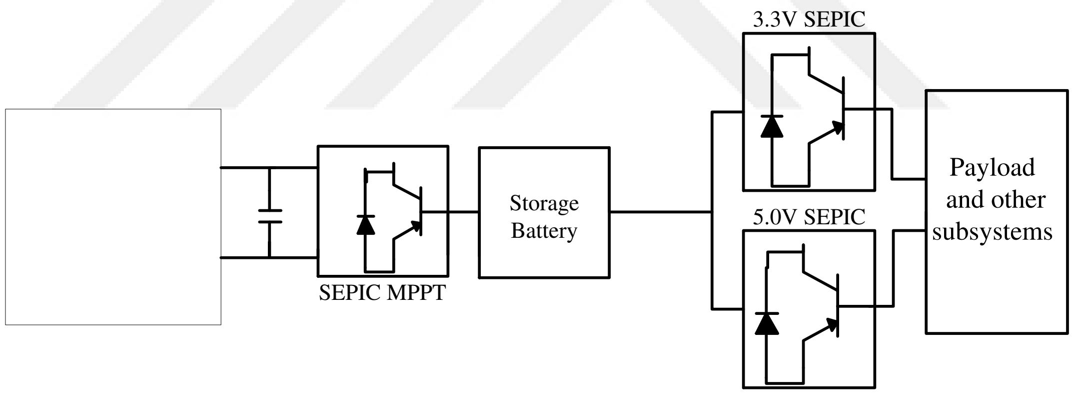

Figure 4.1 EPS block diagram of basic subsystem

4.1 Power Generation

The power generation as discussed before, is from solar energy using PV cells. The PV cells chosen are; AzurSpace solar cell 30% class, which is a Triple Junction GaAs technology. This was chosen because of the heritage in the space industry, the company says it has a record number of 1.5 Million of its solar cells in space and no failure recorded [48]; i.e. so many satellites have flown to space with this type of cells from AzurSpace because of their reliability. Table3.3 in Chapter III contains the technical specifications of the cell as extracted from the data sheet.

Our budget thus for the AzurSpace cells as shown in equation (4.1) means;

$$0.6 \times V_{mpp} \times I_{mpp} = 0.6 \times 4.822 \times 0.5044 = 1.459W. \quad (4.1)$$

With2 cells in series and voltage of 2.411V per cell. This is a very good figure typical of most 1U CubeSat in Space [22].
The Spectrolab's cells as shown in equation (4.2) would yield;

$$0.6 \times V_{mpp} \times I_{mpp} = 0.6 \times 4.696 \times 0.4425 = 1.2466W. \quad (4.2)$$

From Table 3.3 in Chapter III, connecting two of the cells in series would yield an open circuit Voltage of 5.4 Volt and voltage at maximum power of 4.822 volt at solar irradiance of 1367 W/m^2. The current at both maximum power and short circuit would remain the same because of the series connection, the short-circuit current for the AzurSpace cell is shown in equation (4.3).

$$I_{sc} = 520.2mA, \quad (4.3)$$

While, equation (4.4) shows the current at maximum power point.

$$I_{mpp} = 504.4\ mA \quad (4.4)$$

.

Since the CubeSat has six (6) sides, all the six sides could be covered by the solar cells on a panel of 2 cells in series except the top and bottom faces where some of the equipment like antenna will be mounted on top side, and, because to avoid cells mismatch, we should use same type of cells on the bottom and the top faces. Therefore, a much smaller panel has been selected in order to make use of the remaining space after the antenna and say the camera have been mounted on it for both the top and the bottom facets like it was done in KufaSat project [17] as shown in Figure 4.2 below. The other solar cell (but not taken for evaluation in this thesis, brought here for reference purpose only) is the Triangular advanced Solar Cell TASC from Spectrolab and the extract from the data sheet is shown in Table 3.4.

Spectrolab has delivered more than 2.6 million cells in Space generating power up to or more than 820 KW for various space assets in orbit [49].

To evaluate the performance of the cells, a mathematical model of the PV cells was constructed. The model was implemented in a computer simulation environment. The simulation results were evaluated and presented in this thesis.

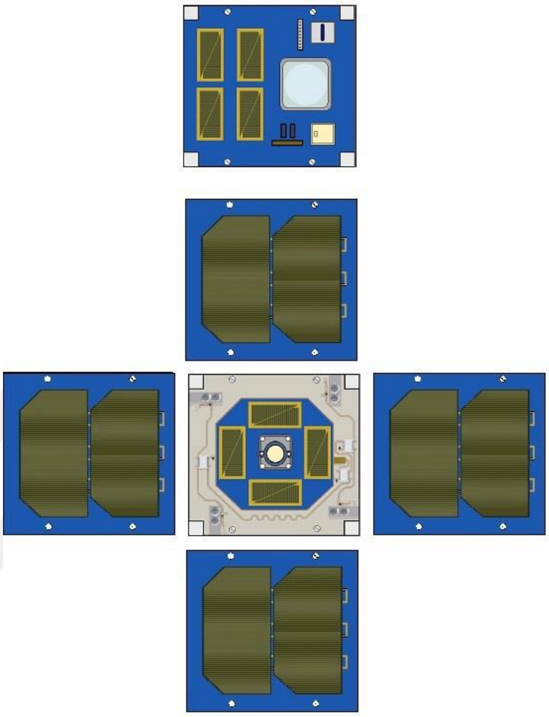

Figure 4.2 KufaSat solar panel design [17]

Table 4.1 above shows the solar cells connection topology, Sides +X and –X connected in together in parallel, while sides +Y and –Y are also connected together in parallel so that at any particular time, at least one of the sides is providing power when exposed to the solar radiation and the sides that may be facing the Earth too could provide a bonus power from Earth Infrared radiation or the Albedo. The output of each pairs of sides is connected to a BCR for providing power to the CubeSat bus and charging the battery as in Figure 4.2.

Table 4.1 The solar cells connection topology considered in this thesis

Side	No. of PV Cells	V_{mpp}	I_{mpp}	P_{mpp}
+X	2	4.822	0.5044	2.432
-X	2	4.822	0.5044	2.432
+Y	2	4.822	0.5044	2.432
-Y	2	4.822	0.5044	2.432
-Z	2	4.822	0.544	2.432
+Z	2	4.822	0.544	2.432

4.1.1 Triple-Junction PV Cell Modeling

The EPS designs of most of 1U CubeSats are using a panel of two cells in series, and, these are attached to the four or all the six faces of the satellite [17]. In this work, the same architecture is employed. The solar cell have been modeled and simulated in order to evaluate the performance of the cells and the panel under consideration.

Researchers in [28 - 30] have extensively dealt with modeling of a multi-junction solar cells and their characterization for conversion efficiency under various environmental conditions of temperature and irradiance. They characterize a solar cell in the form of equivalent circuit having a light dependent current source in anti-parallel with two elements - a diode and another parasitic element tagged as R_P for shunt resistance to account for losses due to manufacturing and assembly errors, charge transport etc. Another parasitic element $R_S$connected in series with these is responsible for power losses due to current flow in the contacts. Figure4.3 shows a single diode equivalent circuit representation of a triple-junction solar cell. The single diode model has been said to be sufficient to model the cell according to [28].Two diode models also exist and the model has been studied in [29]. The cell was manufactured in such a way that three different cells of varying band gap energies were stacked in series for better photon conversion in to electricity, with the cell having the largest band gap on top of the three sub-cells. The cell modeled is

GaInP/GaAs/Ge AZURSPACE having efficiency of 30% as illustrated in Table 3.3 of Chapter III. So, just like Figure 4.3, the cell was modeled as a series of three sub-cells with same current passing through and in voltage additive topology i.e. summing the voltages of the sub-cells to get the total voltage of the cell.

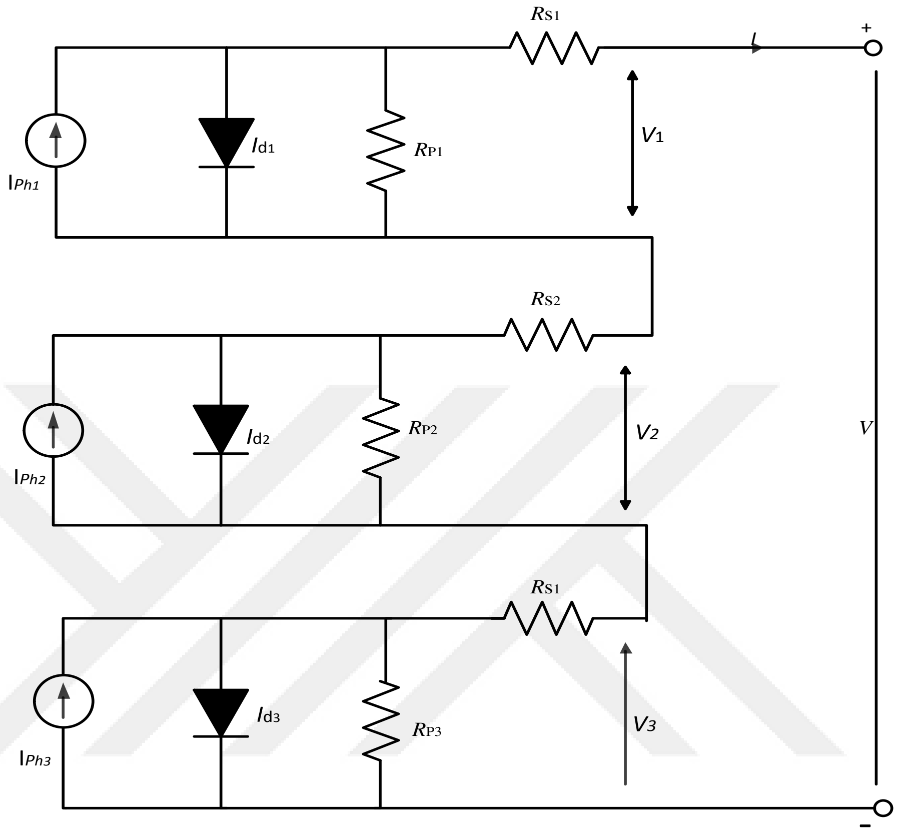

Figure 4.3 Equivalent circuit model of a triple-junction solar cell in one-diode configuration

The following equations (4.5 to 4.16) describe effectively the mathematical model of the triple-junction solar cell according to [28, 29, 38, 41].

$$I = I_{ph,i} - I_{s,i}\left[e^{\left(\frac{V+I.A.R_{s,i}}{n.V_t}\right)} - 1\right] - \frac{V + I.A.R_{s,i}}{A.R_{p,i}} \quad (4.5)$$

$$I_{ph} = \left[I_{sc} + k_i\left(T_c - T_{ref}\right)\right].\frac{G}{G_{ref}} \quad (4.6)$$

$$I_{si} = I_{oi} = I_{rs}.T_c^{\left(\frac{3+\gamma i}{2}\right)}.e^{\frac{-q.E_{gi(T_c)}}{n.k.T_c}} \tag{4.7}$$

$$E_{gi(T_c)} = E_{gi(0)} - \frac{\alpha_i T_c^{\ 2}}{T_c + \beta} \tag{4.8}$$

$$V_t = \frac{N_s.k.T_c}{q} \tag{4.9}$$

Inserting equation (4.7) in to equation (4.5) and rearranging the resulting equation by neglecting $R_{p,i}$since it is a very large value yields the cell voltage equation (4.10);

$$V_i = \frac{n_i.k.T_c}{q}.\ln\left(\frac{I_{sc,i}}{I_{o.i}} + 1\right) - I.A.R_{s,i} \tag{4.10}$$

The total cell voltage is;

$$V = \sum_{i=1}^{3} V_i \tag{4.11}$$

Equation (4.12) is obtained by inserting all the variables for equation (4.11) known as the total cell voltage equation as follows;

$$V = \frac{k.T_c}{q}.\left[n_1.\ln\left(\frac{I_{sc,1}}{I_{o,1}} + 1\right) + n_2.\ln\left(\frac{I_{sc,2}}{I_{o,2}} + 1\right) + n_3.\ln\left(\frac{I_{sc,3}}{I_{o,3}} + 1\right)\right] - I.A.R_s \tag{4.12}$$

Equation (4.13) is the series resistance equation of the cell;

$$R_s = \sum_{i=1}^{3} Rs_i \tag{4.13}$$

The total open-circuit voltage of the cell is shown in equation (4.14);

$$V_{oc} = \frac{k.T_c}{q}.\left[n_1.\ln\left(\frac{I_{sc,1}}{I_{o,1}}+1\right)+ n_2.\ln\left(\frac{I_{sc,2}}{I_{o,2}}+1\right)+n_3.\ln\left(\frac{I_{sc,3}}{I_{o,3}}+1\right)\right] \quad (4.14)$$

Equation (4.15) is the fill factor equation FF, whereas, in equation (4.16), the efficiency equation is presented.

$$FF = \frac{V_{mpp}.I_{mpp}}{V_{oc}.I_{sc}} \quad (4.15)$$

$$\eta = efficiency = \frac{1}{P_{in}}.\sum_i \left(V_{oc,i}I_{sc,i}.FF\right).100 \quad (4.16)$$

Where, I is the cell current in ampere, $I_{ph,i}$ is the photo-generated current of the cell, $I_{sc,i}$ is the short-circuit current of the cell at the reference temperature given in the datasheet, $I_{s,i} = I_{o,i}$ is known as the diode's reverse saturation current, R_s is the series resistance, R_p represents the parallel or shunt resistance,V_{oc} is the open-circuit voltage of the cell,n_i the ideality factor of the semiconductor material used in constructing the cell normally between 1 and 2. V_t is the thermal voltage representing the temperature dependency of the cell, $q = 1.602e^{-19}C$ a constant value known as the charge of an electron. $\gamma_i = 2$ is another constant of ideality of the cell, $k = 1.38\exp(-23)J/K$ known as Boltzmann's constant, β_i and α_i aretemperature fitting parameters of the cell, $I_{rs} = k_i$ is the recombination current of the diode usually measured through experiment.$E_{gi(0)}$ is the band gap energy of the cell given at $T = 0K$ in eV.The values of the parameters necessary to implement the model using equation (4.5-4.16) obtained from [28, 32-34, 38, 41-43] are presented in Table 4.2.

Table 4.2 List of model parameters implemented some adapted from [28 - 34]

Parameter	Value	Parameter	Value	Parameter	Value
$E_{g1(0)}$	$1.79\ eV$	γ_1	1.81	n_1	1.89
$E_{g2(0)}$	$1.39eV$	γ_2	1.86	n_2	1.59
$E_{g3(0)}$	$0.68\ eV$	γ_3	1.44	n_3	1.43
K_{i1}	$0.0253mA/℃$	α_1	$7.5e^{-4}$	K_1	$1.86e^{-9}$A
K_{i2}	$0.0005mA/$	α_2	$5.405e^{-4}$	K_2	$2.195e^{-7}$A
K_{i3}	$0.0098mA/℃$	α_3	$4.7774e^{-4}$	K_3	$10.5e^{-9}$A
K_{v1}	$-6.93mV/℃$	R_{S1}	0.023Ω	T_{ref}	$298.15K$
K_{v2}	$-6.2mV/℃$	R_{s2}	0.0012Ω	G_{ref}	$1367W/m^2$
K_{v3}	$-5.6mV/℃$	R_{s3}	0.0008Ω	I_{mpp}	$504.4mA$
β_1	372	R_{p1}	$16M\Omega$	V_{mpp}	$2411mV$
β_2	204	R_{p2}	$4.5M\Omega$	V_{oc}	$2700mV$
β_3	235	R_{p3}	$540K\Omega$	I_{sc}	$520.2mA$

The overall implementation for a module of 2 cells in series is shown in Figure 4.4. While, the blocks showing the calculations of the model equations are presented in Figures4.5, 4.6, and 4.7. The simulation results are presented and discussed in Chapter V.

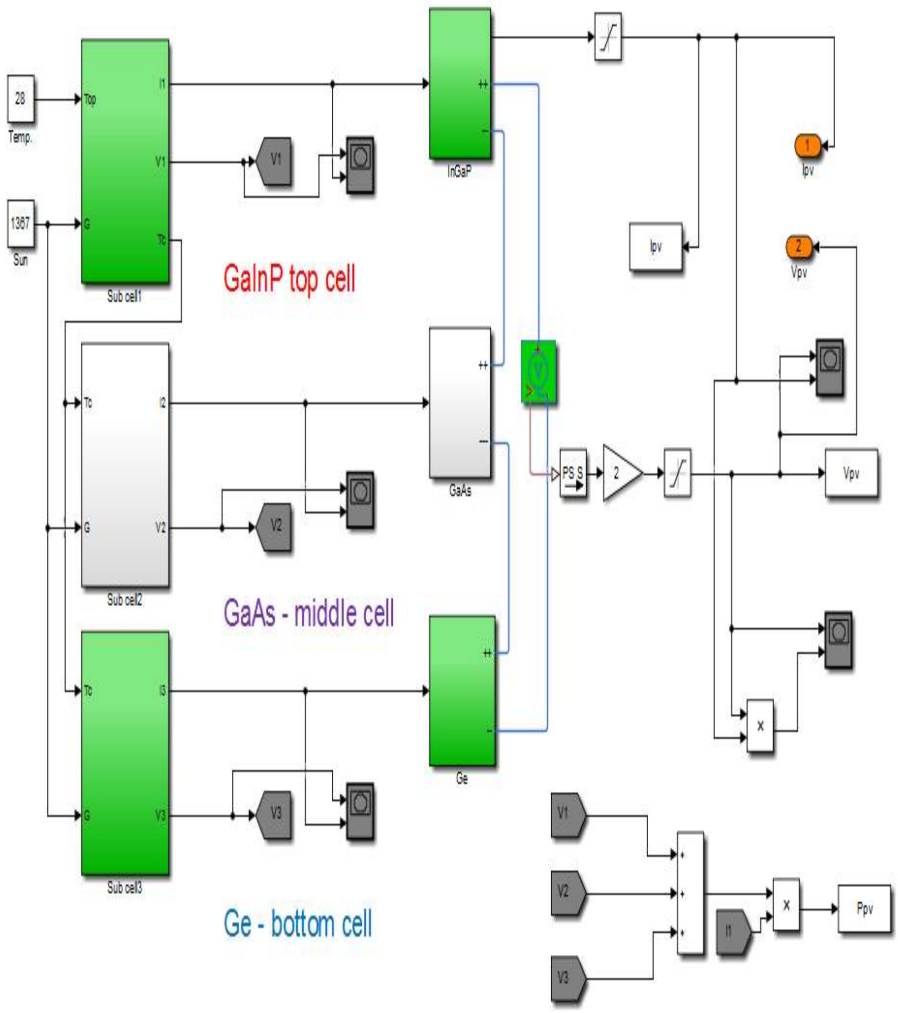

Figure 4.4 Model of the triple-junction solar module of 2 cells in series

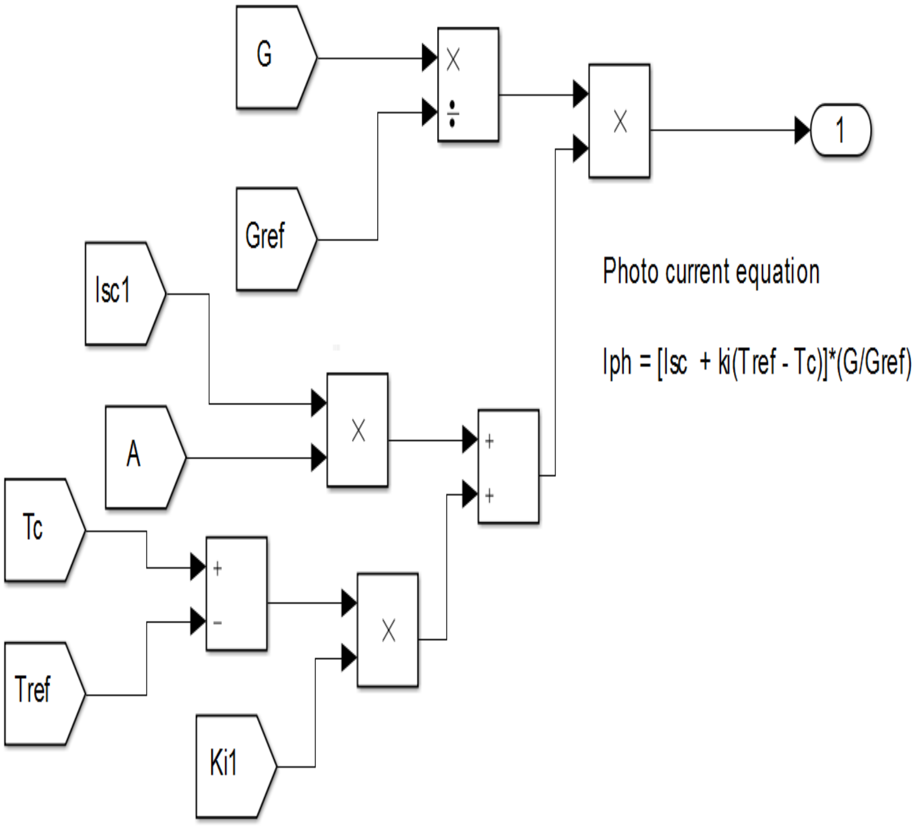

Figure 4.5 Photo-current equation$I_{ph,i}$

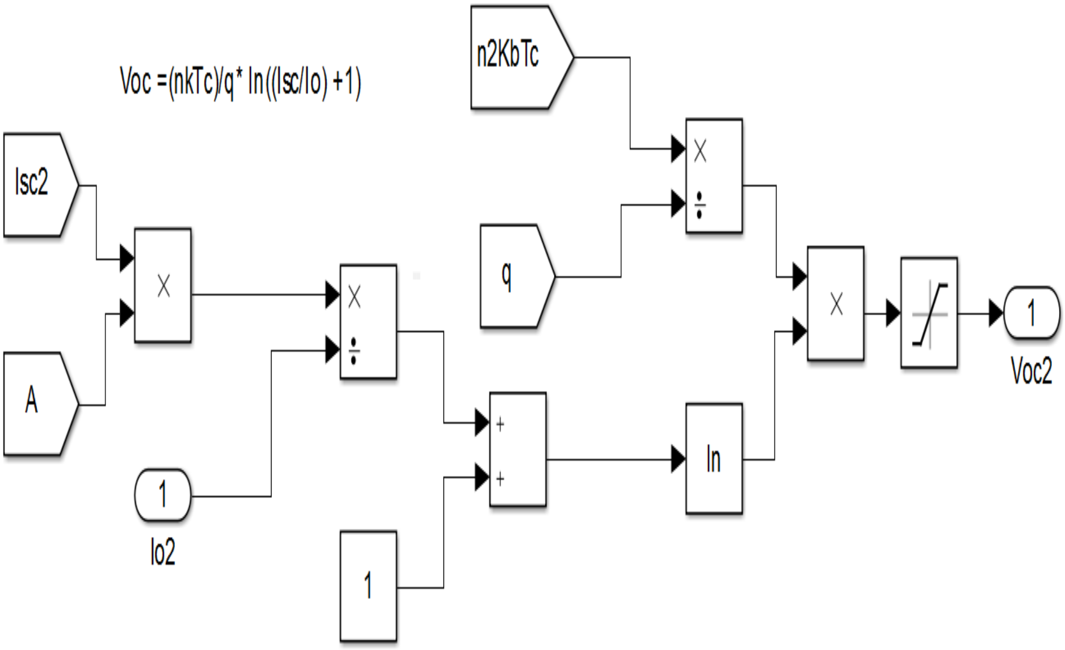

Figure 4.6 Open-circuit voltage equation $V_{oc,i}$

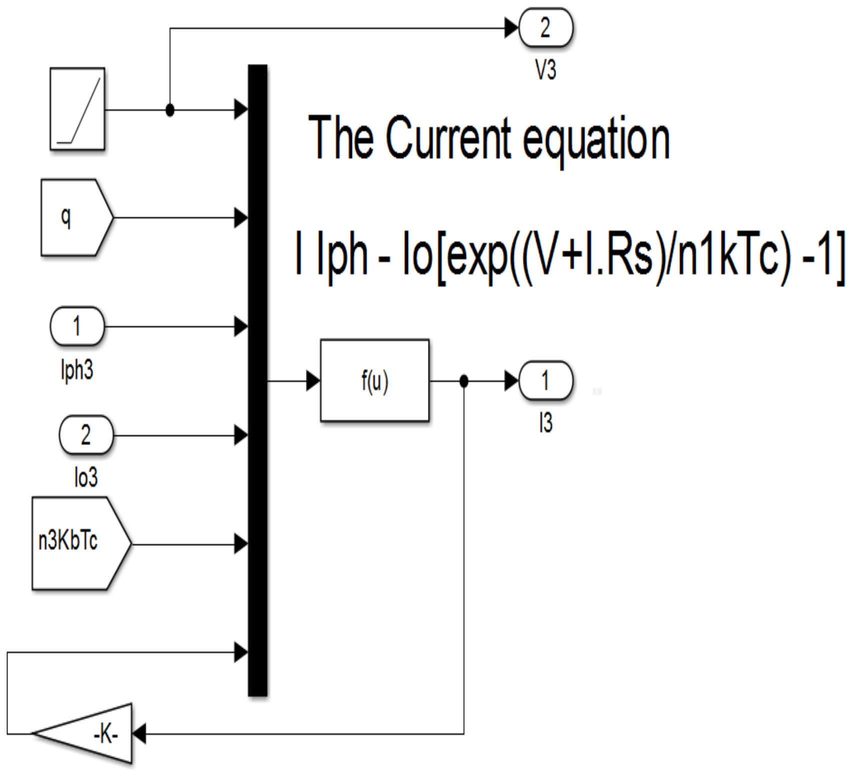

Figure 4.7 The output current equationI_{pv}

4.2 SEPIC Analysis,Modeling and Design

The (SEPIC) is a very popular converter topology because of its very good (EMI) profile since its input current is non-pulsating thereby eliminating the needs for filtering circuits, and, the output voltage is not inverted – i.e. same as the input. Another advantage of using SEPIC is that a simple switch gate drive can be used because the switch is tied to the ground of the circuit. That is, since it has same ground node for the input and output, complexity in the gate drive circuit design is reduced. Though the SEPIC to be used here is a non-isolated one, the circuit topology has a series capacitor that makes it capable of "true shut down" i.e., it can isolate the output from the input in case of a short- circuit. SEPIC is very suitable for battery powered applications and it has footprints in devices like laptop, CubeSat etc.[25 - 27]. Figure 4.8 shows a schematic of a SEPIC showing all the active and passive elements of the converters used for the design of the 3.3V and 5.0V supplies for the subsystems.

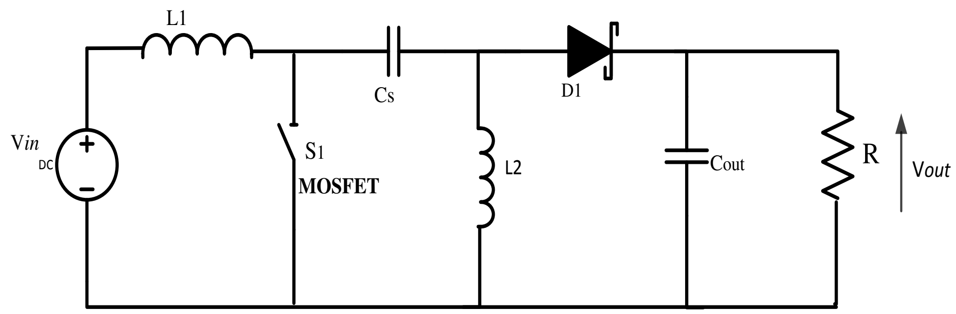

Figure 4.8 Schematic diagram of a SEPIC

The SEPIC has two operational states being controlled by the duty cycle "D".The transfer relationship between the input and the output of an ideal SEPIC as shown in equation (4.17) is given by:

$$\frac{V_o}{V_{in}} = \frac{d}{1-d} \tag{4.17}$$

Here, "d" is the duty cycle containing large and small signal as seen in [35]
It is modeled using state-space equations in CCM where the inductor current i_{l1} never falls to zero.The equations of the model for switching periods $dT_s$and $(1-d)T_s$ are obtained. The equations are for the two modes of operations -dT_s when S_1, is on and $(1-d)T_s$when the switch $S_1$is off. Figure 4.9shows the ON state of the SEPIC, while Figure4.10 shows the OFF state.

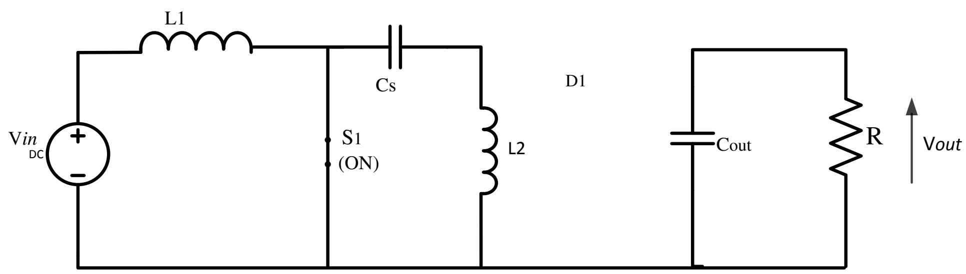

Figure 4.9 SEPIC in ON state

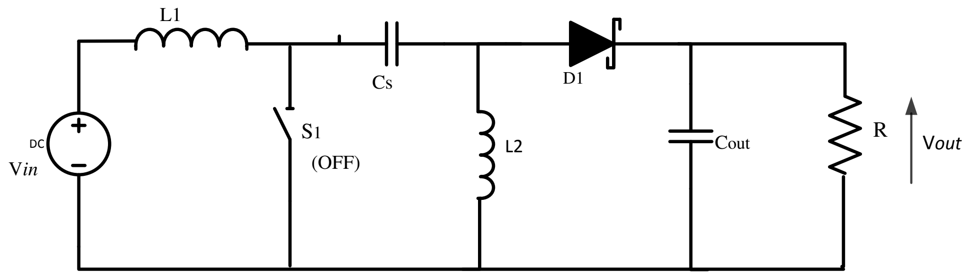

Figure 4.10 SEPIC in OFF state

The two operations modes of the SEPIC are analysed as thus;
In order to conduct a simplified analysis of the SEPIC, the following assumptions are made, i.e. a PWM steady state operation in CCM is assumed, the switch is turned off, and capacitor C_1had been charged to the input voltage $V_{in}$and has zero ripple voltage. Furthermore, capacitor equivalent series resistance ESR and inductor equivalent series inductance ESL are assumed to have little impact on the converter dynamics and therefore neglected. Similarly, the switch is also assumed to be ideal and voltage drop is zero

When the SEPIC switch S_1 is on as shown in Figure4.9, at this period of $d \times T_s$, the inductor L_1 is storing energy from the input voltage source and L_2 is charged from the series capacitorC_1. The diode is reversed biased, therefore not conducting. We should note that, in this period, both L_1 and L_2 are disconnected from the load. Consequently, the output capacitor C_2 is left to supply the load current. The voltage across the inductor L_1 is V_{in}, the average voltage on C_1 is $V_{in} = v_{c1}$.SinceC_1 is connected in parallel withL_2, L_2 sees a voltage of $-v_{c1}$.

For the period $(1-d)T_s$, i.e. when S_1 is off as shown in Figure4.10, the inductor currents$i_{l1}$and i_{l2}do not change momentarily but continues to flow through C_1 and the diode to the load. The output voltage V_{out} is impressed on L_1 making $V_{L1} = V_{out}$. At this point, the switch is blocking a voltage of $V_{in} + V_{out}$ because C_1 had been charged to V_{in} during the on period.
If $i_{l1}$and i_{l2} are the inductor currents for both L_1 and L_2, and v_{c1} and v_{c2} are the voltages across C_1 and C_2, these are defined as state variables describing the states of the converter for use in state-space equation. The state equations are;

for $0 < t < dT_s$operation mode:

$$\frac{di_{l1}}{dt} = -\frac{i_{l1}}{L_1} + \frac{V_{in}}{L_1}$$

$$\frac{dv_{c1}}{dt} = \frac{v_{c1}}{C_1}$$

$$\frac{di_{l2}}{dt} = -\frac{v_{c1}}{L_2} - \frac{i_{l2}}{L_2} \tag{4.18}$$

$$\frac{dv_{c2}}{dt} = -\frac{v_{c2}}{RC_2}$$

For the $0 < t < (1-d)T_s$ mode of operation:

$$\frac{di_{l1}}{dt} = -\frac{i_{l1}}{L_1} - \frac{v_{c1}}{L_1} - \frac{v_{c2}}{L_1}$$

$$\frac{dv_{c1}}{dt} = \frac{i_{l1}}{C_1}$$

$$\frac{di_{l2}}{dt} = -\frac{i_{l2}}{L_2} - \frac{v_{c2}}{L_2} \tag{4.19}$$

$$\frac{dv_{c2}}{dt} = -\frac{i_{l1}}{C_2} - \frac{i_{l2}}{C_2} - \frac{v_{c2}}{RC_2}$$

Equations (4.18) and (4.19) are the state equations describing the two operation modes of the ideal SEPIC shown in Figure4.9 and Figure4.10 [27, 35-37].

State-space averaging technique allows us to linearise the obtained equations of the SEPIC for both the on and off states.
The state-space equations are shown in their general form in equation (4.20).

$$[\dot{\boldsymbol{x}}] = [\boldsymbol{A}][\boldsymbol{x}] + [\boldsymbol{B}][\boldsymbol{u}]$$
$$[\boldsymbol{y}] = [\boldsymbol{C}][\boldsymbol{x}] + [\boldsymbol{D}][\boldsymbol{u}] \tag{4.20}$$

Equation (4.20) is a state-space equation containing matrices$\dot{\boldsymbol{x}}$,$\boldsymbol{A}$, **B**, $\boldsymbol{C}$, $\boldsymbol{D}$, and$\boldsymbol{y}$. Matrix $\boldsymbol{A}$is known as the system matrix of the state variables. It determines how the current states $\boldsymbol{x}$ affects the change in state $\dot{\boldsymbol{x}}$. The **B** matrix is known as control matrix describing the relationship between the current inputs and the state change. The $\boldsymbol{C}$matrix is known as the output matrix which determines the relationship between the states of the system $\boldsymbol{x}$and the output $\boldsymbol{y}$. Matrix $\boldsymbol{D}$is known as the feed-forward matrix that can make the system's input to have direct effect on the output$\boldsymbol{y}$.$\boldsymbol{u}$isthe input vector [50]. A detailed explanation of SSA technique can be found in [51].
When $\boldsymbol{A_1}$, $\boldsymbol{B_1}$, $\boldsymbol{C_1}$,$\boldsymbol{D_1}$, and$\boldsymbol{A_2}$, $\boldsymbol{B_2}$, $\boldsymbol{C_2}$, $\boldsymbol{D_2}$ **a**re the matrices describing the operation modesdT_s and $(1-d)T_s$. The SSA equations are defined in equation (4.21).

$$[\dot{\boldsymbol{x}}] = \big[[\boldsymbol{A_1}.d] + [\boldsymbol{A_2}.(1-d)]\big][\boldsymbol{x}] + \big[[\boldsymbol{B_1}.d] + [\boldsymbol{B_2}.(1-d)]\big][\boldsymbol{u}]$$
$$[\boldsymbol{y}] = \big[[\boldsymbol{C_1}.d] + [\boldsymbol{C_2}.(1-d)]\big][\boldsymbol{x}] + \big[[\boldsymbol{D_1}.d] + [\boldsymbol{D_2}.(1-d)]\big][\boldsymbol{u}] \tag{4.21}$$

The state-space equations of the converter for both the on and off state are shown in equation (4.22) and equation (4.23) respectively.

$$A_1 = \begin{bmatrix} \frac{-1}{L_1} & 0 & 0 & 0 \\ 0 & 0 & \frac{1}{C_1} & 0 \\ 0 & \frac{-1}{L_2} & \frac{-1}{L_2} & 0 \\ 0 & 0 & 0 & \frac{-1}{RC_2} \end{bmatrix}, [B_1] = \begin{bmatrix} \frac{1}{L_1} \\ 0 \\ 0 \\ 0 \end{bmatrix}, [C_1] = [0 \quad 0 \quad 0 \quad 1], [D_1] = [0] \tag{4.22}$$

$$A_2 = \begin{bmatrix} \frac{-1}{L_1} & \frac{-1}{L_1} & 0 & \frac{-1}{L_1} \\ \frac{1}{C_1} & 0 & 0 & 0 \\ 0 & 0 & \frac{-1}{L_2} & \frac{1}{L_2} \\ \frac{-1}{C_2} & 0 & \frac{-1}{C_2} & \frac{-1}{RC_2} \end{bmatrix}, [B_1] = \begin{bmatrix} \frac{1}{L_1} \\ 0 \\ 0 \\ 0 \end{bmatrix}, [C_1] = [0 \quad 0 \quad 0 \quad 1], [D_1] = [0] \tag{4.23}$$

In order to apply the state-space averaging technique SSA to our model, we average the SEPIC state equations by multiplying them with the operation periods dT_s and $(1-d)T_s$. The duty cycle weighed-averaged model known as the averaged large signal model ALSM was obtained by inserting equations (4.22 and 4.23) in to equation (4.21) and presented in equation (4.24) and equation (4.25).

$$\begin{bmatrix} \dot{i_{l1}} \\ v_{c1} \\ i_{l2} \\ v_{c2} \end{bmatrix} = \begin{bmatrix} \frac{1}{L_1} & \frac{d-1}{L_1} & 0 & \frac{d-1}{L_1} \\ \frac{1-d}{C_1} & 0 & \frac{d}{C_1} & 0 \\ 0 & \frac{-d}{L_2} & \frac{-1}{L_2} & \frac{1-d}{L_2} \\ \frac{1-d}{C_2} & 0 & \frac{d-1}{C_2} & \frac{-1}{RC_2} \end{bmatrix} . \begin{bmatrix} i_{l1} \\ v_{c1} \\ i_{l2} \\ v_{c2} \end{bmatrix} + \begin{bmatrix} \frac{1}{L_1} \\ 0 \\ 0 \\ 0 \end{bmatrix} . [v_{in}] \tag{4.24}$$

$$[v_o] = [0 \quad 0 \quad 0 \quad 1] \begin{bmatrix} i_{l1} \\ v_{c1} \\ i_{l2} \\ v_{c2} \end{bmatrix} + [0][v_{in}] \tag{4.25}$$

Note here that; $\dot{\boldsymbol{x}} = \begin{bmatrix} \dot{i_{l1}} \\ v_{c1} \\ i_{l2} \\ v_{c2} \end{bmatrix}$ representing the rate of change in state,

$[\boldsymbol{x}] = \begin{bmatrix} i_{l1} \\ v_{c1} \\ i_{l2} \\ v_{c2} \end{bmatrix}$ represents the state variables. $\boldsymbol{y}$the output= v_o.

The feed-forward matrix$[\boldsymbol{D}] = 0$ and will be neglected for remainder of this analysis.

To obtain the steady-state and the small-signal models of the converter, the derivative terms in equation (4.24) are set to zero, all other variables are set to steady-state values, therefore;

$$\dot{x} = 0,$$
$$i_{l1} = I_{l1},$$
$$v_{c1} = V_{c1},$$
$$i_{l2} = I_{l2},$$
$$v_{c2} = V_{c2},$$
$$d = D,$$
$$v_{in} = V_{in},$$
$$v_o = V_o.$$

The steady-state model is presented in equations (4.26 and 4.27)

$$\begin{bmatrix} 0 \\ 0 \\ 0 \\ 0 \end{bmatrix} = \begin{bmatrix} \frac{1}{L_1} & \frac{D-1}{L_1} & 0 & \frac{D-1}{L_1} \\ \frac{1-D}{C_1} & 0 & \frac{D}{C_1} & 0 \\ 0 & \frac{-D}{L_2} & \frac{-1}{L_2} & \frac{1-D}{L_2} \\ \frac{1-D}{C_2} & 0 & \frac{D-1}{C_2} & \frac{-1}{RC_2} \end{bmatrix} \cdot \begin{bmatrix} I_{l1} \\ V_{c1} \\ I_{l2} \\ V_{c2} \end{bmatrix} + \begin{bmatrix} \frac{1}{L_1} \\ 0 \\ 0 \\ 0 \end{bmatrix} . [V_{in}] \tag{4.26}$$

$$[V_o] = [0 \quad 0 \quad 0 \quad 1]\begin{bmatrix} I_{l1} \\ V_{c1} \\ I_{l2} \\ V_{c2} \end{bmatrix} \tag{4.27}$$

The small signal model of the converter is obtained using the ALSM of equations (4.24 and 4.25) by applying a perturbation around the steady-state variables of the model where;

$$\dot{x} = \dot{X} + \dot{\hat{x}}$$

$$d = D + \hat{d}$$

$$v_o = V_o + \hat{v}_o,$$

$$v_{in} = V_{in} + \hat{v}_{in}$$

these are inserted into equation (4.24 -4.25) as shown in equations (4.28 and 4.29). The small signal model is extracted from equations (4.28 and 4.29) by multiplying the steady-state parts and the disturbance around the steady-state. These are separated into steady-state and small signal parts after neglecting non-dominant terms from the multiplication results.

$$\dot{\begin{bmatrix} I_{l1} + \imath_{l1} \\ V_{c1} + v_{c1} \\ I_{l2} + \imath_{l2} \\ V_{c2} + v_{c2} \end{bmatrix}} = \begin{bmatrix} \frac{1}{L_1} & \frac{D-1+\hat{d}}{L_1} & 0 & \frac{D-1+\hat{d}}{L_1} \\ \frac{1-D-\hat{d}}{C_1} & 0 & \frac{D+\hat{d}}{C_1} & 0 \\ 0 & \frac{-D-\hat{d}}{L_2} & \frac{-1}{L_2} & \frac{1-D-\hat{d}}{L_2} \\ \frac{1-D-\hat{d}}{C_2} & 0 & \frac{D-1+\hat{d}}{C_2} & \frac{-1}{RC_2} \end{bmatrix} . \begin{bmatrix} I_{l1} + \hat{\imath}_{l1} \\ V_{c1+}\hat{v}_{c1} \\ I_{l2} + \hat{\imath}_{l2} \\ V_{c2+}\hat{v}_{c2} \end{bmatrix} + \begin{bmatrix} \frac{1}{L_1} \\ 0 \\ 0 \\ 0 \end{bmatrix} . [V_{in} + \hat{v}_{in}] \tag{4.28}$$

$$[V_o + \hat{v}_o] = [0 \quad 0 \quad 0 \quad 1]\begin{bmatrix} I_{l1} + i_{l1} \\ V_{c1} + v_{c1} \\ I_{l2} + i_{l2} \\ V_{c2} + v_{c2} \end{bmatrix} \tag{4.29}$$

The extracted complete small signal part is presented in equations (4.30 and 4.31). However, an output current term $\hat{\imath}_z$was added in the model, this may be useful for current control.

$$\begin{bmatrix} \dot{\hat{\imath}}_{l1} \\ \hat{v}_{c1} \\ \hat{\imath}_{l2} \\ \hat{v}_{c2} \end{bmatrix} = \begin{bmatrix} \frac{1}{L_1} & \frac{D-1}{L_1} & 0 & \frac{D-1}{L_1} \\ \frac{1-D}{C_1} & 0 & \frac{D+\hat{d}}{C_1} & 0 \\ 0 & \frac{-D}{L_2} & \frac{-1}{L_2} & \frac{1-D}{L_2} \\ \frac{1-D}{C_2} & 0 & \frac{D-1+\hat{d}}{C_2} & \frac{-1}{RC_2} \end{bmatrix} \cdot \begin{bmatrix} \hat{\imath}_{l1} \\ \hat{v}_{c1} \\ \hat{\imath}_{l2} \\ \hat{v}_{c2} \end{bmatrix} + \begin{bmatrix} \frac{i_{l1}+v_{c2}}{L_1} & \frac{1}{L_1} & 0 \\ \frac{i_{l2}+i_{l1}}{C_1} & 0 & 0 \\ \frac{-v_{c1}-v_{c2}}{L_2} & 0 & 0 \\ \frac{i_{l2}-i_{l1}}{C_2} & 0 & \frac{-1}{C_2} \end{bmatrix} \cdot \begin{bmatrix} \hat{d} \\ \hat{v}_{in} \\ \hat{\imath}_z \end{bmatrix} \tag{4.30}$$

$$[\hat{v}_o] = [0 \quad 0 \quad 0 \quad 1] \begin{bmatrix} i_{l1} \\ v_{c1} \\ i_{l2} \\ v_{c2} \end{bmatrix} \tag{4.31}$$

From equations (4.26 and 4.27), we can obtain line-to-output transfer function of our plant:

$$\frac{V_o}{V_{in}} \tag{4.32}$$

While, equation (4.30 and 4.31) would produce three transfer functions for the control-to-output:

$$\frac{\hat{v}_o}{\hat{d}} \tag{4.33}$$

Evaluated at $\hat{v}_{in} = \hat{\imath}_z = 0$

Small signal line-to-output:

$$\frac{\hat{v}_o}{\hat{v}_{in}} \tag{4.34}$$

Evaluated at $\hat{d} = \hat{\imath}_z = 0$

Small signal output impedance:

$$\frac{\hat{v}_o}{\hat{\imath}_z} \tag{4.35}$$

Evaluated @ $\hat{d} = \hat{v}_{in} = 0$. Equations (4.30-4.35) were used for the controller design.

4.2.1 SEPIC Converter Power Stage Design

There are several methods of design calculations for the SEPIC. However, the design guides given by Texas Instruments in [36 -37] is adopted for this thesis work. The design equations are presented in this section. The converters so designed are to have the following output specifications; 3.3 and 5.0 Volts, with output currents of 2.5 and 2.0 A respectively. The switching frequency selected was 1MHz to allow for choosing smaller components in the design [27, 36-37].A schottky diode was also selected for use because of the low forward voltage drop of the diode. The input voltage range of the converters is from 3.0 to 4.2 volts because the power source is a battery whose cut-off voltage is around (2.7 to 3)V and maximum voltage of 4.2V.While the other requirements are shown in Table 4.3.

4.2.1.1 Duty Cycle Calculation:

The duty cycle is calculated according to the maximum and minimum input voltages to the converters. The input source in this case is a battery having a maximum cut-off voltage of 2.7V and a maximum operating voltage of 4.2. In this design, we limit the minimum input voltage to 3.0V and the maximum voltage to 4.2V. Equations (4.36 - 4.37) are the formulas for calculating the maximum and minimum duty cycles respectively [36-37].

$$D_{max} = \frac{V_{out} + V_d}{V_{in,min} + V_{out} + V_d} \tag{4.36}$$

$$D_{min} = \frac{V_{out} + V_d}{V_{in,max} + V_{out} + V_d} \tag{4.37}$$

4.2.1.2. Inductor Sizing and Selection:

A very good design principle for inductor sizing was given in [36-37]. 40% peak-to-peak ripple current was advised as sufficient, however, in this thesis, 20% current ripple is accepted because we want to ensure minimisation of ripples in the design. For equal value coupled inductors, the ripple current flowing is given by equation (4.38):

$$\Delta I_L = I_{out} \times \frac{V_{out}}{V_{in,min}} \times 20\% \tag{4.38}$$

The inductors values can be calculated from equation (4.39) as follows [36];where, F_{sw} is the switching frequency D_{max} is given as the duty cycle occurring at the minimum input voltage V_{in}.

$$L_1 = L_2 = \frac{V_{in,min} \times D_{max}}{2 \times \Delta I_L \times F_{sw}} \tag{4.39}$$

In order for the inductors not to saturate, the peak current in the inductor should not exceed the values in equations (4.40 and 4.41).

$$I_{L1,peak} = I_{out} \times \left(\frac{V_{out} + V_d}{V_{in,min}}\right) \times [1 + 20\%] \tag{4.40}$$

$$I_{L2,peak} = I_{out} \times [1 + 20\%] \tag{4.41}$$

The inductor sizing for the SEPIC in this was guided by equations (4.38-4.41). Any inductor meeting this requirement is okay for our design. For the inductors values calculated for both the 3.3 and 5.0 v, refer to Table4.3.

4.2.1.3 MOSFET Selection

The MOSFET is the active switch in the converter and care is required in selecting it for a better performance. The MOSFET should be able to handle the peak currents from both inductors in the circuit. The maximum voltage across the drain to source of the switch is $V_{out} + V_{in,max}$. The rated drain-source voltage of the MOSFET to be used should be greater than $V_{out} + V_{in,max}$ in the circuit.This is because, during operation period of $(1-d)T_s$, the switch sees a voltage of $V_{in} + V_{out}$ on the inductor $L_1$and the capacitor C_1. The switch capable of blocking $V_{in} + V_{out}$as presented in equation (4.42) is required.

$$V_{in} + V_{out} \tag{4.42}$$

The peak currents to be handled by the switch in our converter is as shown in equation (4.43):

$$I_{Q1,peak} = I_{L1,peak} + I_{L2,peak} \tag{4.43}$$

We have already assumed ideal switching, so, voltage drop and power loss are not considered in this design owing to the fact that it's a very low voltage power supply. However, it must be able to handle the maximum root-mean square RMS current to flow in it as shown in equation (4.44).

$$I_{Q,rms} = I_{out} \times \sqrt{\frac{(V_{out} + V_{in,min} + V_d)(V_{out} + V_d)}{V^2{}_{in,min}}} \tag{4.44}$$

Any MOSFET switch capable of handling the voltages and currents as specified by equations (4.42 - 4.43) is sufficient for our design. We selected the switch based on our specifications of the 3.3V and 5.0V SEPIC.

4.2.1.4. Coupling Capacitor Design C_1

The capacitor C_1 as shown in figure 4.8 is known as coupling capacitor. The capacitor must be selected according to the high RMS currents relative to the output of the converter [36]. This C_1 capacitance enables the SEPIC to be rated good for low power applications because the RMS current passing through the coupling capacitor is very small especially the ceramic capacitors [36]. The voltage rating of the coupling capacitor C_1 must be greater than the maximum input voltage of the converter. In this thesis, the maximum input voltage is 4.2V. Therefore, the voltage rating is shown in equation (4.45).

$$C_1 > 4.2V \tag{4.45}$$

The RMS current to flow in the coupling capacitor is given by equation (4.46), whereas the capacitor's peak-to-peak ripple voltage with ESR neglected is shown in equation (4.47) as explained in [36-37].

$$I_{C1,rms} = I_{out} \times \sqrt{\frac{V_{out} + V_d}{V_{in,min}}} \tag{4.46}$$

$$\Delta V_{C1} = \frac{I_{out} \times D_{max}}{C_1 \times F_{sw}} \tag{4.47}$$

Equations (4.45-4.47) guided our design and sizing of the coupling capacitor for the two SEPIC in this thesis. Refer to Table4.3 for the calculated and selected values of the capacitor.

4.2.1.5. Output Capacitor Design$\mathbf{C_2/C_{out}}$

The output capacitor $\boldsymbol{C_2/C_{out}}$is responsible for supplying the load during the switch operation modes of $d \times T_s$, i.e. the on state of the SEPIC. As a result, the output capacitor sees a very large ripple current. Therefore, we must select a capacitor capable of handling these ripple currents. The capacitor RMS current equation (4.48) as shown is very important.

$I_{Cout,rms} = I_{C1,rms}$,

$$I_{Cout(rms)} = I_{out} \times \sqrt{\frac{V_{out} + V_d}{V_{in,min}}} \tag{4.48}$$

Since we have interest in reducing output voltage ripple, we chose to limit the peak-to-peak ripple voltage to around2% in the design. If required, ESR should be calculated using equation (4.49). However, we have not considered the ESR in this thesis for simplicity.

$$ESR_{out,} \leq \frac{V_{ripple} \times V_d \times V_{out}}{I_{L1,peak} + I_{L2,peak}} \tag{4.49}$$

The output capacitor is calculated using equation (4.50). The ripple voltage chosen is $V_{ripple} = 0.02V$.

$$C_{out} \geq \frac{I_{out} \times D_{max}}{V_{ripple} \times V_d \times F_{sw}} \tag{4.50}$$

The design of the $3.3V$ *and* $5.0V$ converters was achieved using the design equations(4.36 - 4.50) above and are presented in Table 4.3.

4.2.1.6.Diode Selection

For the output diode, the diode selected is a Schottkty diode of very low forward voltage drop of 3.0V [27, 35-36]. It must be able to withstand the peak current and the reverse voltage. The peak current of the diode is equal to the peak current of the switch equation (4.43). The output diode must be able to stand minimum peak reverse voltage equal to the sum of maximum input voltage and the maximum output voltage as in equation (4.51).The diode's current is equal to the output current [35].

$$V_{RD} \geq V_{in,max} + V_{out,max} \tag{4.51}$$

Table 4.3 SEPIC designed values

Components/Variables	3.3V Converter Parameters	5.0V Converter Parameters
$L_1 = L_2$	$3.3\mu H, 4\,.7\mu H$	$3.0\mu H, 4.7\mu H$
C_1	$10\mu F$	$10\mu F$
C_2	$> 68\mu F$	$> 42\mu F$
V_d	$0.3\ V$	$0.3\ V$
V_{out}	$3.3\ V$	$5.0\ V$
$V_{in,min}$	$3.0\ V$	$3.0\ V$
$V_{in,max}$	$4.2\ V$	$4.2\ V$
D_{max}	0.545	0.638
D_{min}	0.461	0.557

ΔV_{c1}	13.6%	12.7%
I_{out}	$2.5\ A$	$2.0\ A.$
$V_{out,min}$	$3.29\ V$	$4.89\ V$
$V_{out,max}$	$3.34\ V$	$5.05V$

4.2.2 SEPIC Controller Design

The controllers for the $3.3V$ and the $5.0V$ converters were designed from the state-space model equations. Proportional-Integral PI controllers were chosen for this design. However, it is noteworthy that, both the plant and the controller models transfer functions are of fourth order. Control design for fourth order systems is very difficult to implement. The plants transfer functions for the two converters of $3.3V$ and $5.0V$ respectively are shown in equations (4.52 -4.53).

$$G_{3.3V} = \frac{1.79 \times 10^9 s^2 + 3.892 \times 10^{14} s + 1.712 \times 10^{19}}{s^4 + 4.34 \times 10^5 s^3 + 6.029 \times 10^{10} s^2 + 2.833 \times 10^{15} s + 2.179 \times 10^{19}} \quad (4.52)$$

$$G_{5.0V} = \frac{9.404 \times 10^8 s^2 + 2.001 \times 10^{14} s + 1.117 \times 10^{19}}{s^4 + 4.255 \times 10^5 s^3 + 5.688 \times 10^{10} s^2 + 2.471 \times 10^{15} s + 8.844 \times 10^{18}} \quad (4.53)$$

The control-to-output transfer functions of the converter in fourth order and reduced second order are shown in equations (4.54- 4.57) for the two converters respectively.

$$G_{dv,3.3V} = \frac{4.853\times10^4 s^3+4.693\times10^{10} s^2+8.313\times10^{15} s+3.91\times10^{20}}{s^4+4.255\times10^5 s^3+5.802\times10^{10} s^2+2.714\times10^{15} s+2.088\times10^{19}} \quad (4.54).$$

$$G_{dvr,3.3V} = \frac{4.768\times10^4 s+3.761\times10^{10}}{s^2+2.205\times10^5 s+2.009\times10^9} \quad (4.55)$$

$$G_{dv,5.0V} = \frac{5.302\times10^4 s^3+4.044\times10^{10} s^2+6.775\times10^{15} s+3.118\times10^{20}}{s^4+4.255\times10^5 s^3+5.688\times10^{10} s^2+2.471\times10^{15} s+8.844\times10^{18}} \quad (4.56)$$

$$G_{dvr,5.0V} = \frac{5.243\times10^4 s+3.001\times10^{10}}{s^2+2.207\times10^5 s+8.516\times10^8} \quad (4.57)$$

Figure 4.11 is a block diagram implementation of the SEPIC and the PI controller showing the reference and the output voltage. It is a feedback controller system. This is how the two converters were implemented.

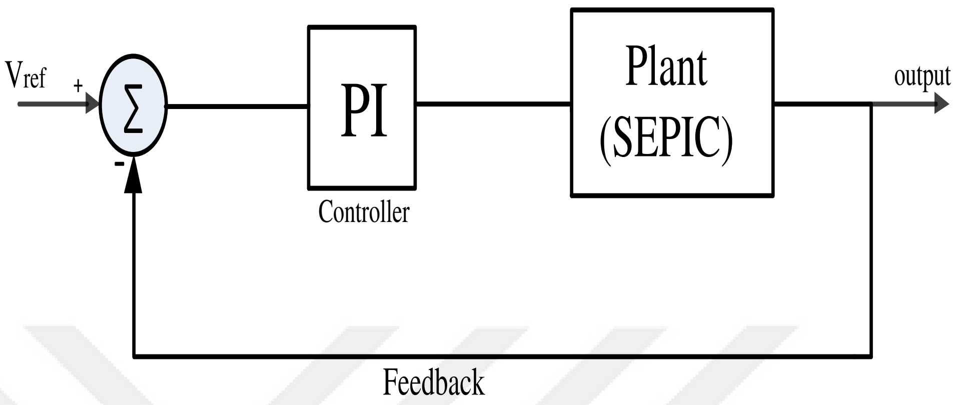

Figure 4.11 A block diagram implementation of the converter and the PI controller

4.3 Design Summary

In this chapter, a preliminary design of all the subsusystems have been presented. A layout of the EPS was presented in block diagram. The design of the solar cell/panel for the EPS has been well spelt out. The triple-junction solar cell selected was 3G3OC of 30% conversion efficiency from AzurSpace. The cell was modeled and simulated using equivalent circuit method. The converters chosen in chapter III which is SEPIC topology was presented, analysed, modeled and designed. State-space averaging technique was employed in the analysis and modeling of the SEPIC. Design calculations was conducted to obtain the values and ratings of the passive and active components of the converters. From the modeling, PI controllers were designed for both the (3.3 and 5.0)V converters. The simulation studies and results have been presented in chapter V.

CHAPTER V

SIMULATION STUDIES

5 Introduction

The selected triple-junction solar cell and the designed SEPIC converters were modeled and simulated in a computer simulation environment. The solar cell model shows a very good promise because it only has very minute errors. Temperature effects on the cell voltage, current and the band gap energy were investigated. Similarly, the converters have produced very excellent results with the PI controllers. The results of the simulations are presented and analysed in this chapter.

5.1 Triple-Junction PV Cell Simulation Results

The triple-junction solar cell modeled and simulated in this thesis work is a high efficiency 3G30C solar cell manufactured by AzurSpace [48]. The cell datasheet parameters were listed in Tables 3.3 and Table 4.2. The cell was subdivided into three series connected sub cells. These sub cells have different profiles of voltages and currents. The summation of the three individual voltages of the sub-cells equals that of the single solar cell. In Figure 5.1, we can see clearly that the GaAs sub-cell has the highest voltage followed by the GaInP sub-cell and lastly the Ge sub-cell. However, the currents remain the same because we assumed that the sub-cells are latticed matched to allow same amount of current flow through them even though Germanium has a better current property.

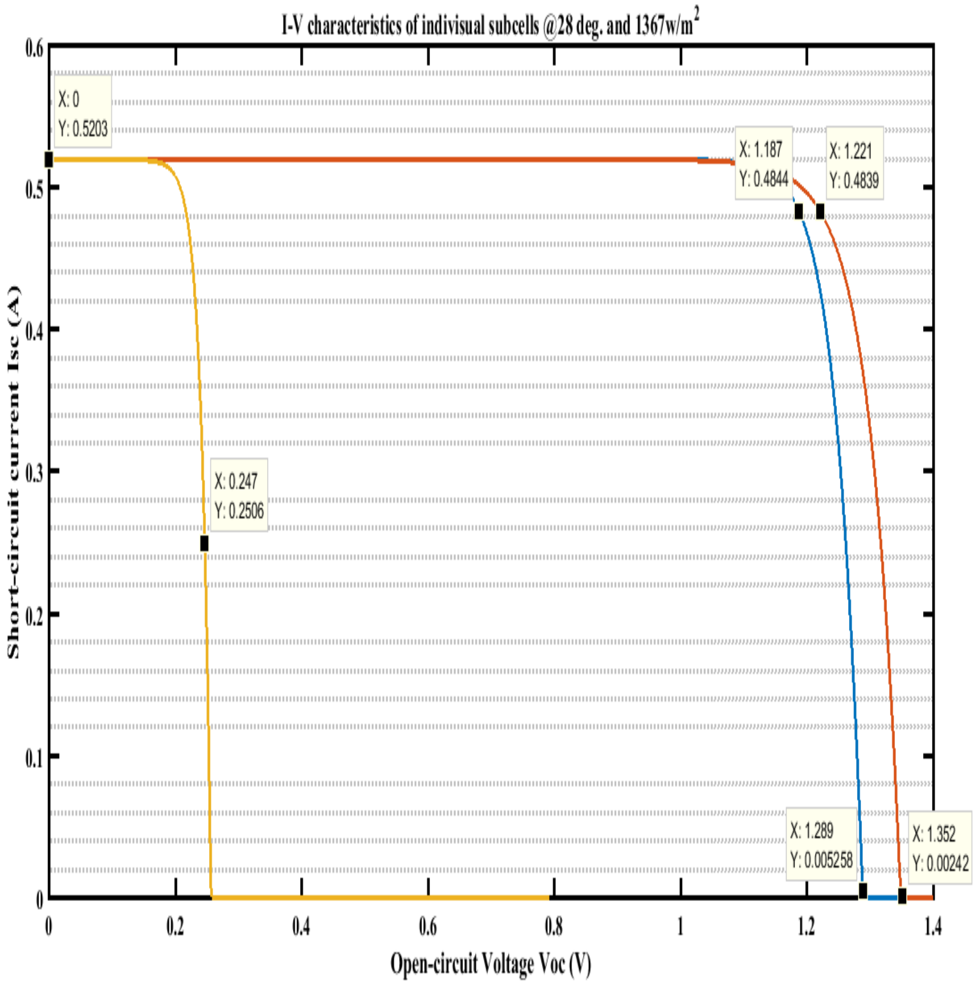

Figure 5.1 I-V curves of the individual sub-cells

Figure 5.2 is an I-V curve of the simulated cells under the standard test conditions as given in the datasheet of the manufacturers. The P-V characteristics curve of the cell is shown in Figure 5.3. The simulation was conducted in order to evaluate the performance of the cell as given in the datasheet so that we can design our systems confidently using the cells to power the CubeSat.

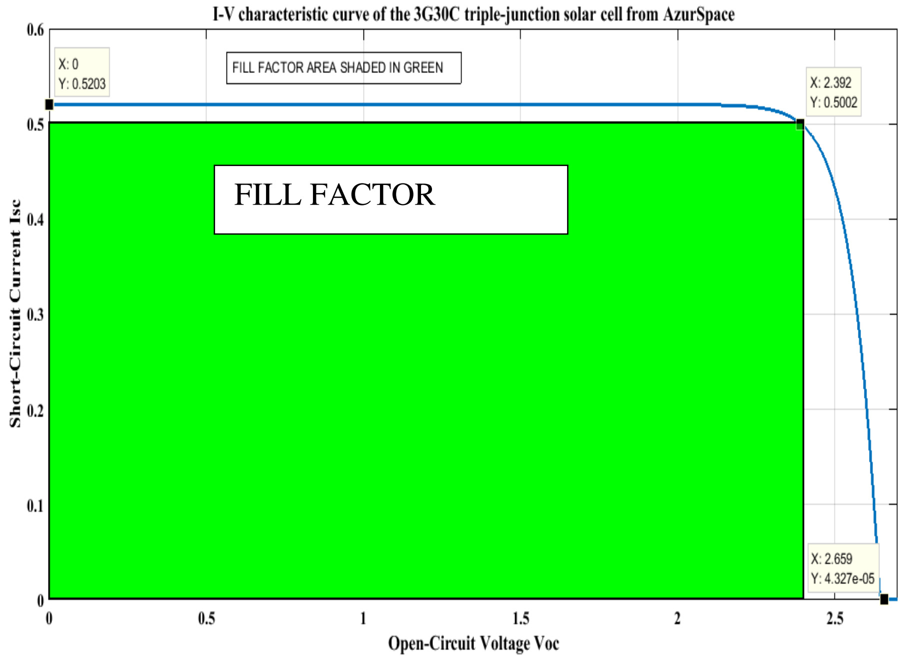

Figure 5.2 I-V characteristics curve of the triple-junction cell 3G30C from AZURSPACE

Table 5.1 gives a summary of the datasheet and simulated values of the cell. A comparison is made so that we can confidently say the model accurately mimics the selected solar cell. The simulated values are taken from Figure 5.1 and Figure 5.2. Differences observed between the simulated and quoted values are noted. These could be attributed to the calibration of the adopted parameter values. The values of the parameters used were taken from researches under AM1.5 - terrestrial cells under 25°C instead of AM0 – at 28°C for space. Percentage errors from Table 5.1 shows how good the model follows the actual characteristics of the solar cell.

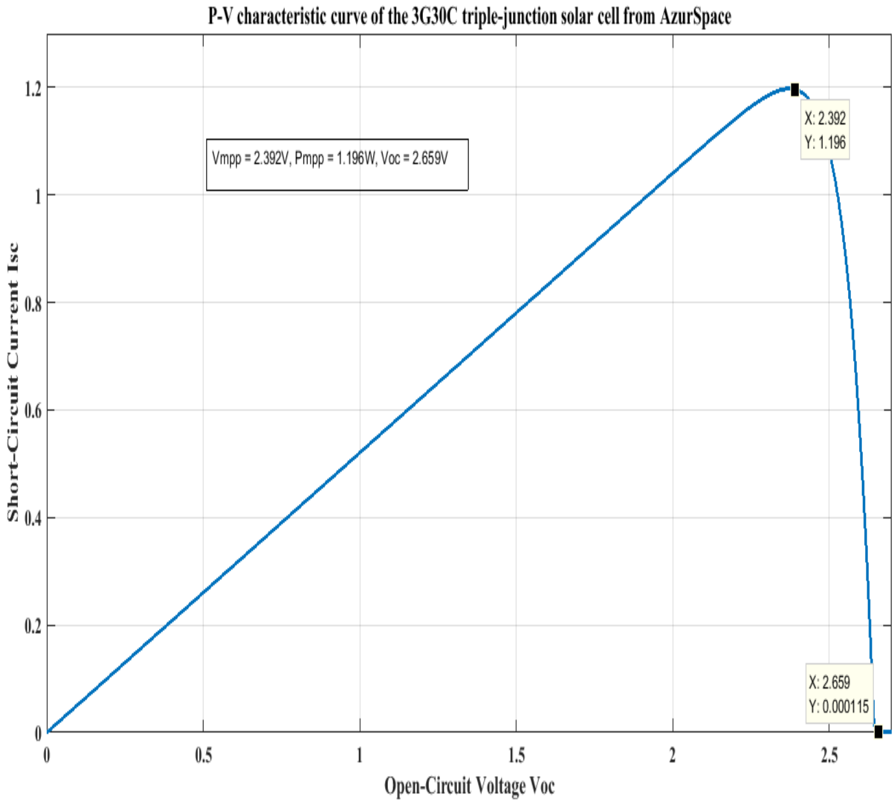

Figure 5.3 P-V characteristics curve of 3G30C triple-junction solar cell from AZURSPACE

Table 5.1 Comparison of datasheet values and simulation results

Parameters	Simulated values	Datasheet values	Percentage Error
$I_{mpp}(mA)$	500.2	504.4	0.8%
$V_{mpp}(mV)$	2392	2411	0.7%
$P_{mpp}(W)$	1.196	1.216	1.644%
$V_{oc}(mV)$	2659	2700	1.518%
$I_{sc}(mA)$	520.3	520.2	0.019%

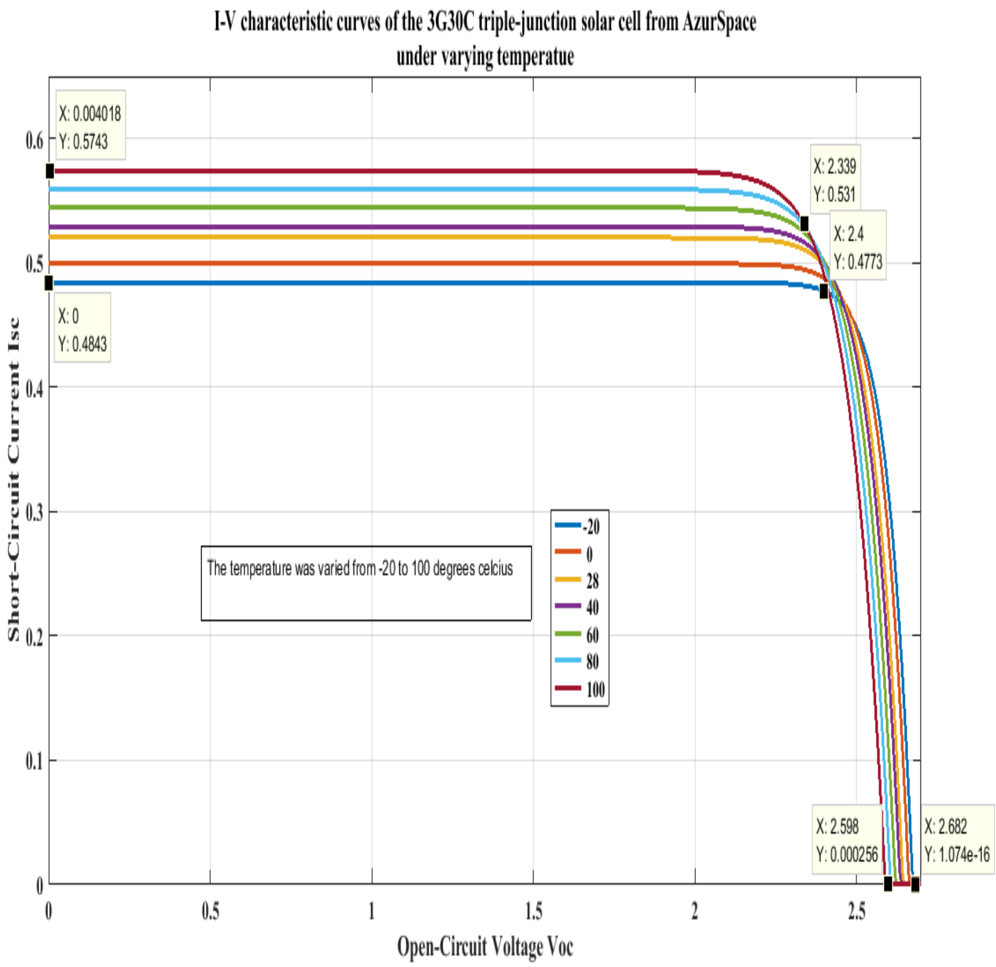

Figure 5.4 I-V characteristics curves of the solar cell under varying temperature

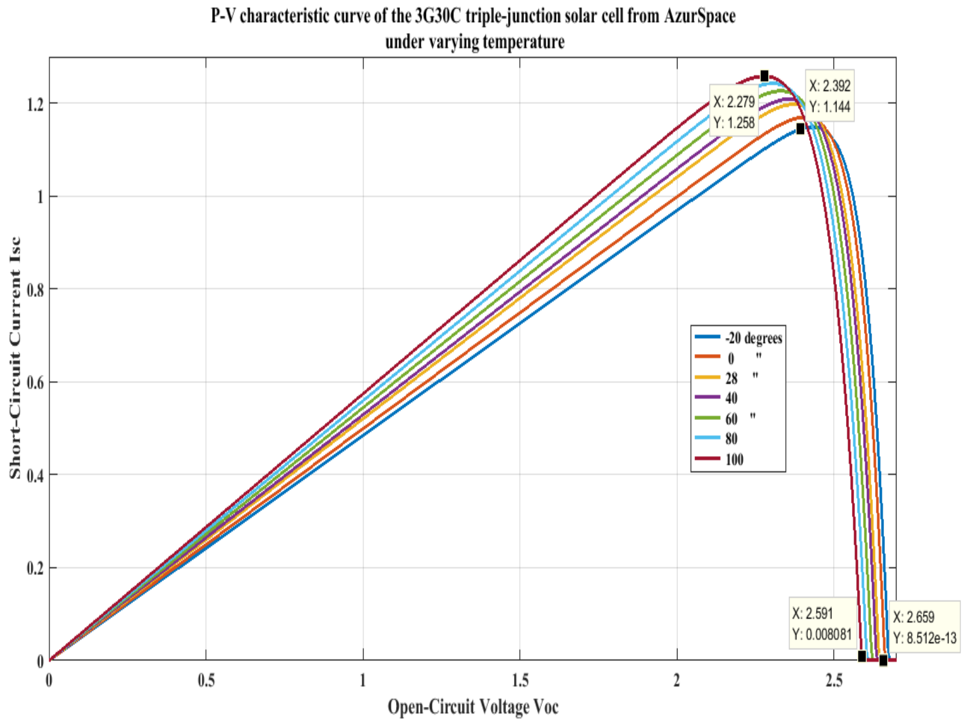

Figure 5.5 P-V characteristics curves of the solar cell under varying temperatures

5.1.1 Temperature Effects on the Solar Cell

Figure 5.4 and 5.5 show I-V and P-V characteristics curves of the triple-junction solar cells under varying temperatures and fixed irradiance, this is necessary because, the EPS is to orbit space and the temperature in space where satellites operate may vary. From the Figures (5.4 and 5.5), we can clearly see the effect of temperature change on the open-circuit voltage, but, the effect on the current is somewhat regulated by a factor k_i known as the short-circuit temperature coefficient, this value is usually very small, however, the temperature effect is still there on the current from the I-V curve. We can vividly see that as the temperature varies from $-20°\text{C}$ *to* $100°\text{C}$, I_{sc}variesfrom(0.483 *to* 0.5743)A. The open-circuit voltage V_{oc} varies from (2.598 *to* 2.682) V. Increase in temperature has major impact on the open-circuit voltage. As seen from the Figure (5.5), as the temperature increases, the open-circuit voltage decreases also.

One of the three consequences of the temperature change on the solar cell is the change in the band gap energy, this is rightly so because the model has a band gap equation dependent on the operating temperature and other materials constants. β *and* α are semiconductor material constants for temperature effect on the band gap energy of a solar cell. The band gap has an inverse relationship with the operating temperature as stated in [28 - 29, 38]. The band gap energy has effect on the open-circuit voltage of the cell.

Table 5.2 shows how the band gap energy decreases with increase in temperature in all the three sub-cells of the triple-junction solar cells, and hence, the open-circuit voltage too decreases.

Equation (5.1) is the band gap energy equation of the triple-junction solar cell model. The band gap energy of the cell $E_{gi(T_c)}$ is a function of the square of the operating temperature of the solar cell ${T_c}^2$. $E_{gi(0)}$ is the band gap energy at 0 Kelvin. Equation (5.1) clearly shows how the band gap can reduce with increasing operating temperature [11, 28-29].

$$E_{gi(T_c)} = E_{gi(0)} - \frac{\alpha_i {T_c}^2}{T_c + \beta} \tag{5.1}$$

The band gap equation above shows how temperature change can clearly affect its value, thereby corroborating the values listed in Table 5.2. In the simulation, varying the temperature from $(-20$ to $100)$℃ resulted in a band gap energy change of 0.0821eV in the GaInP sub-cell, 0.0546eV in the GaAs sub-cell and 0.0455eV in the Ge sub-cell. We should note that the higher the band gap energy, the higher the conversion efficiency of the solar cell. Methods for improving the conversion efficiency through the band gap engineering have been suggested in [38].

Table 5.2 Temperature effect on band gap energy in eV

Temperature in ℃	$E_g(eV)$ **GaInP**	$E_g(eV)$ **GaAs**	$E_g(eV)$ **Ge**
−20	1.7132	1.3143	0.6174
0	1.7033	1.3055	0.6100
20	1.6932	1.2966	0.6024
25	1.6906	1.2944	0.6005
28	1.6890	1.2930	0.5993
40	1.6827	1.2876	0.5947
60	1.6720	1.2784	0.5868
80	1.6611	1.2691	0.5788
100	1.6499	1.2597	0.5708

5.1.2 Effect of Irradiance on the Solar Cell

The irradiance is about the most important environmental factor affecting the performance of the solar cell, this is because according to the model of the cell, it is a current generator and the current equation is a function of the irradiance. The irradiance under which the 3G30C solar cell was tested according to the datasheet is $1367 W/m^2$ AM0 [48].

During the simulation study, the irradiance was varied from $(200\ to\ 1367)\ W/m^2$ in a step of $200 W/m^2$ and at a constant temperature of 28°C. Figures 5.6 and 5.7validate the statement above that the short-circuit current is most affected by the change in irradiance rather than the open-circuit voltage. From the figures, we can also observe the changing profiles of maximum power points of the simulated solar cell. The current at maximum power I_{mpp} vary from (0.5002 to 0.06343) A as seen in Figure 5.6. While, in Figure 5.7, we observe the variation of maximum power P_{mpp} from (1.196 to 0.1553) W. The results in Figures 5.6 and 5.7 clearly agree and validate the photo-dependent current equation of solar photovoltaic model as a function of the irradiance. The photo-current equation (5.2) is reproduced below for easy reference. The variable G in equation (5.2) represents the solar irradiance, decreasing it decreases the photocurrent.

$$I_{ph} = \left[I_{sc} + k_i\left(T_c - T_{ref}\right)\right].\frac{G}{G_{ref}} \tag{5.2}$$

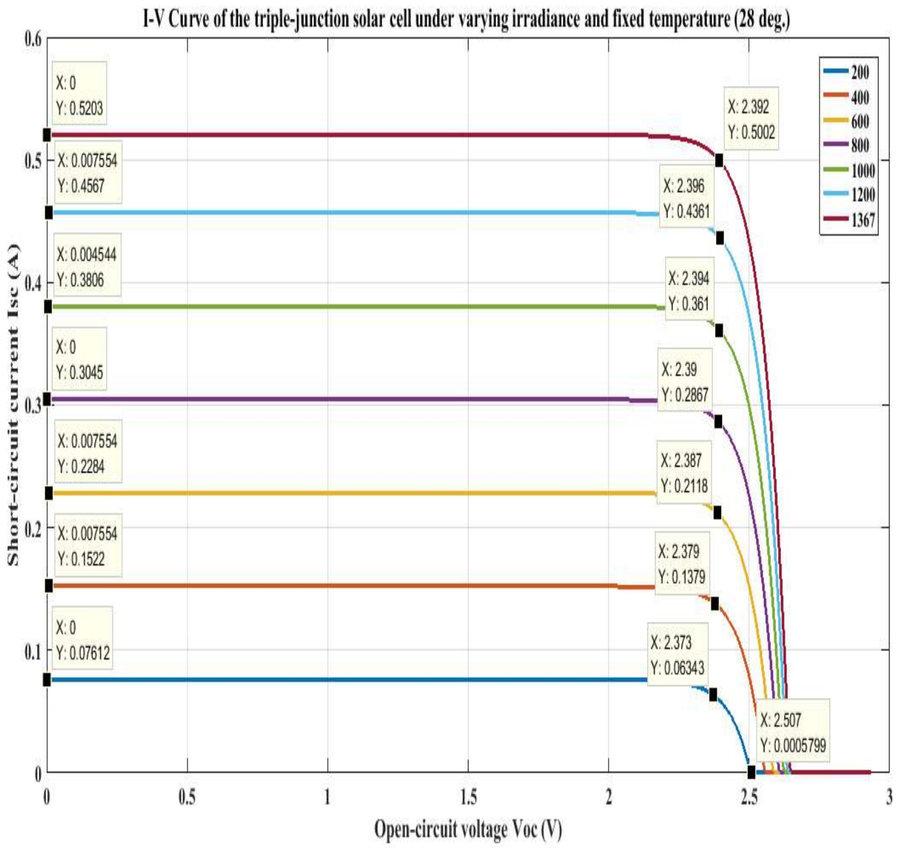

Figure 5.6 I-V characteristics curves of solar cell under varying irradiance and fixed temperature (28 Deg.)

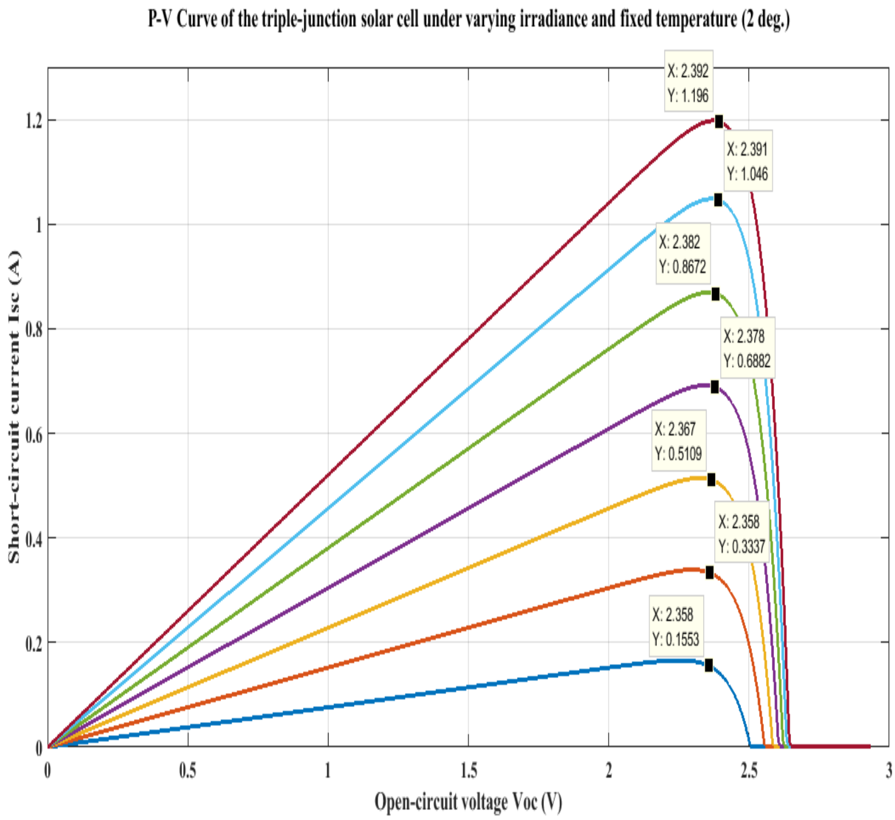

Figure 5.7 P-V characteristics curves of solar cell under varying irradiance and fixed Temperature (28 Deg.)

5.1.3 Fill Factor FF

The solar cell has a measure of quality as shown in the model from equation (4.15), this is called the fill factor (FF). It is the ratio of the product of the maximum power profiles to that of the open/short-circuit of the cell. Equation (4.15) is reproduced here for ease of reference as equation (5.3)

$$FF = \frac{V_{mpp}.I_{mpp}}{V_{oc}.I_{sc}} \tag{5.3}$$

The area shaded green in Figure 5.2 is the fill factor, and it shows the cell quality

$$FF_{simulated} = \frac{2.392 \times 0.5002}{2.7 \times 0.5202} = 0.8519$$

$$FF_{calculated} = \frac{2.4 \times 0.5044}{2.7 \times 0.5202} = 0.8658$$

The percentage error between the simulated and the theoretical fill factor is just 1.6, so, we can say the model is accurate within the limits of error.

5.1.4 Profiles of the PV Panel

The panel is a combination of two cells in series, each cell has an open-circuit voltage of$2.7V$, which makes the panel having a V_{oc} of 5.4V and an $I_{sc}\ of\ 0.5202\ A$ Figure 5.8 and Figure 5.9 are the I-V and P-V curves of the panel showing all the details of the expected performance. The FF is the area of the portion shaded in green colour in Figure 5.2 and 5.8respectively, this gives the maximum power point of 2.392W and a voltage at maximum power of 4.783 V.

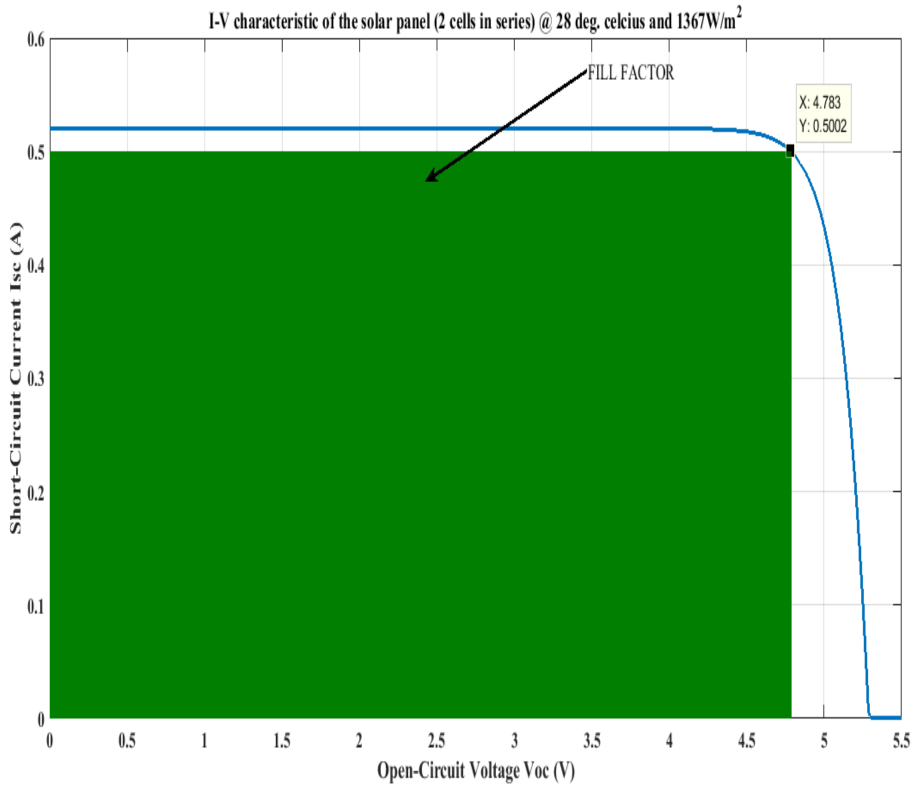

Figure 5.8 I-V characteristics of the simulated solar panel

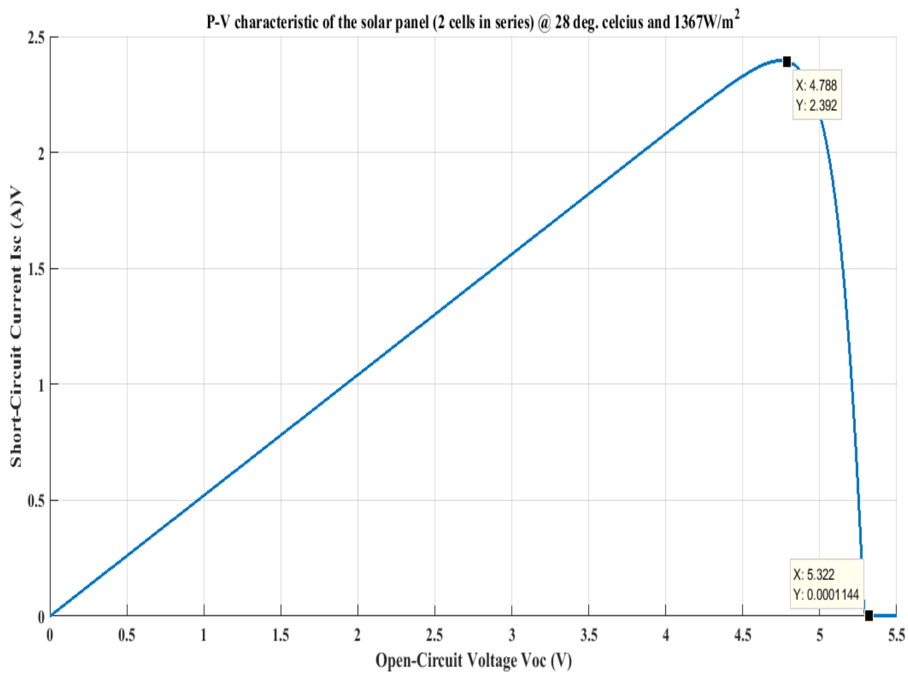

Figure 5.9 P-V characteristics of the simulated solar panel

5.2. SEPIC Simulation Results

The converters have been implemented on a computer simulation environment, and, the results were found to be quite satisfactory. Figures (5.10 -to- 5.11) present the output voltage and current curves of the 3.3 and 5.0 V converters respectively. The results are all within the limits specified in Table 4.3 of Chapter IV.

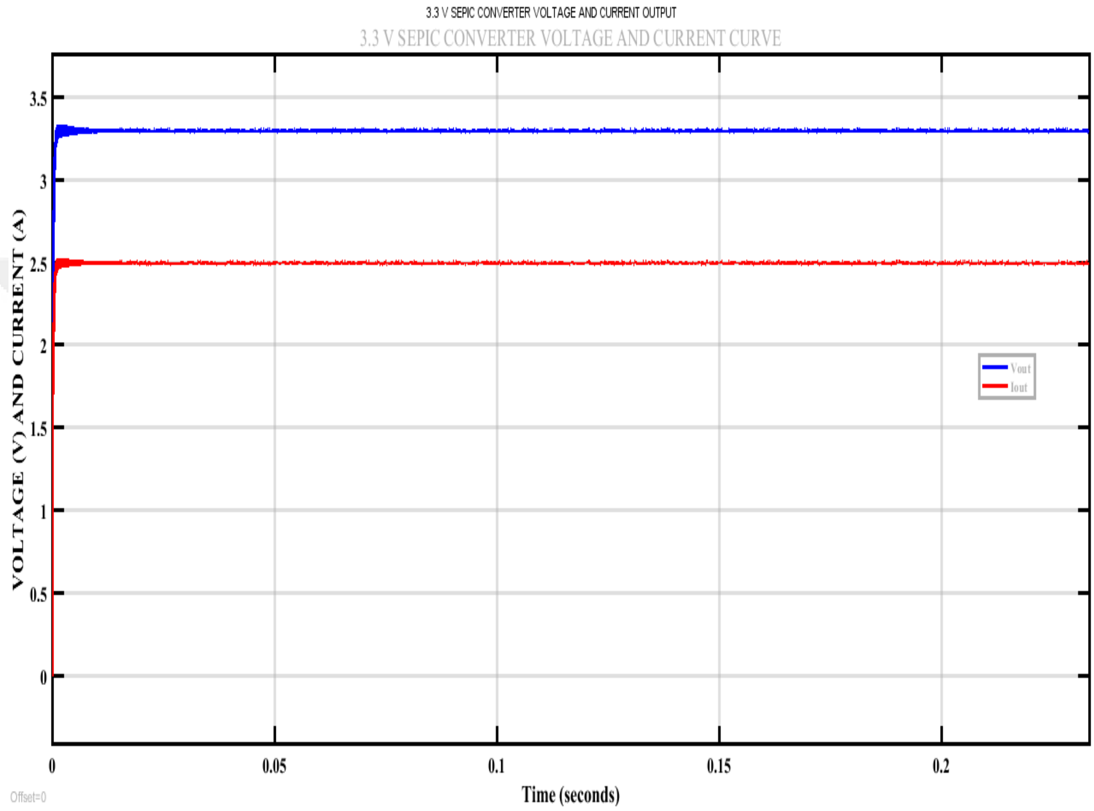

Figure 5.10 The voltage and current curves of the 3.3V SEPIC

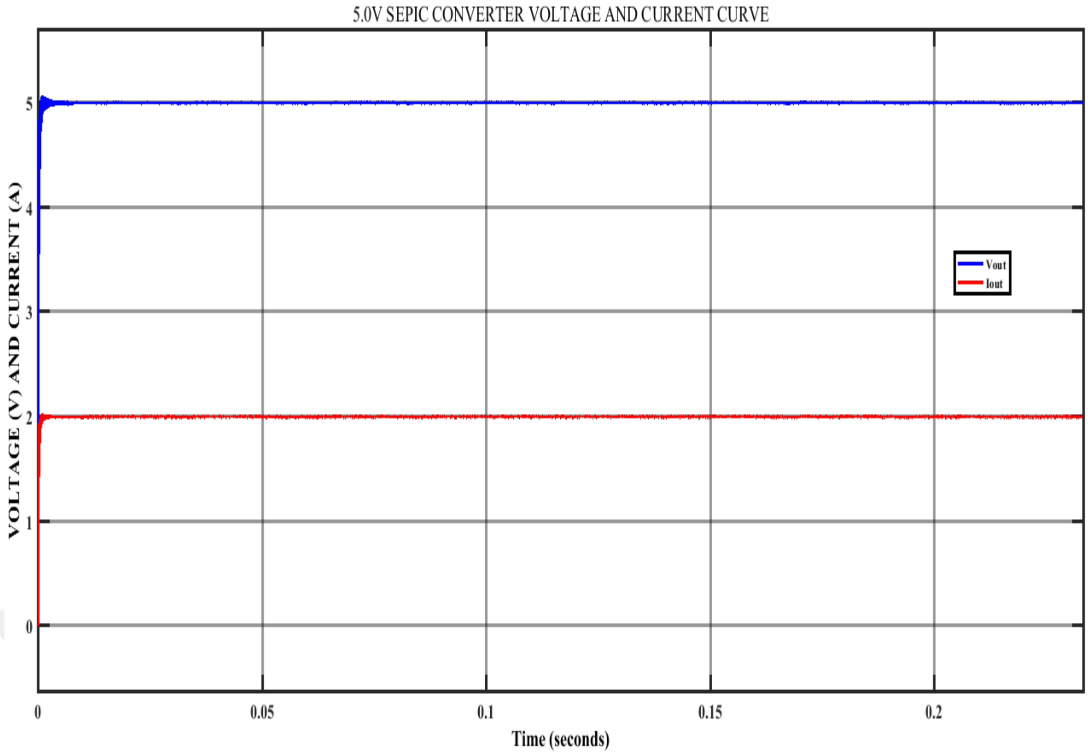

Figure 5.11 The output voltage and current curves of the 5.0V SEPIC

Designing a controller for a fourth-order system is a very difficult task as earlier stated in section 4.2.2 [27, 35], more so if a PI controller is to be implemented, therefore, a suitable way of reducing the models to second-order was employed with the help of computer. The step response of the original fourth-order and the reduced second-order models were compared. The reduced order models were able to represent the original models successfully. Figure 5.12 shows the step response of the systems – both the original and the reduced system of the 3.3V converter for comparison purposes and analysis.

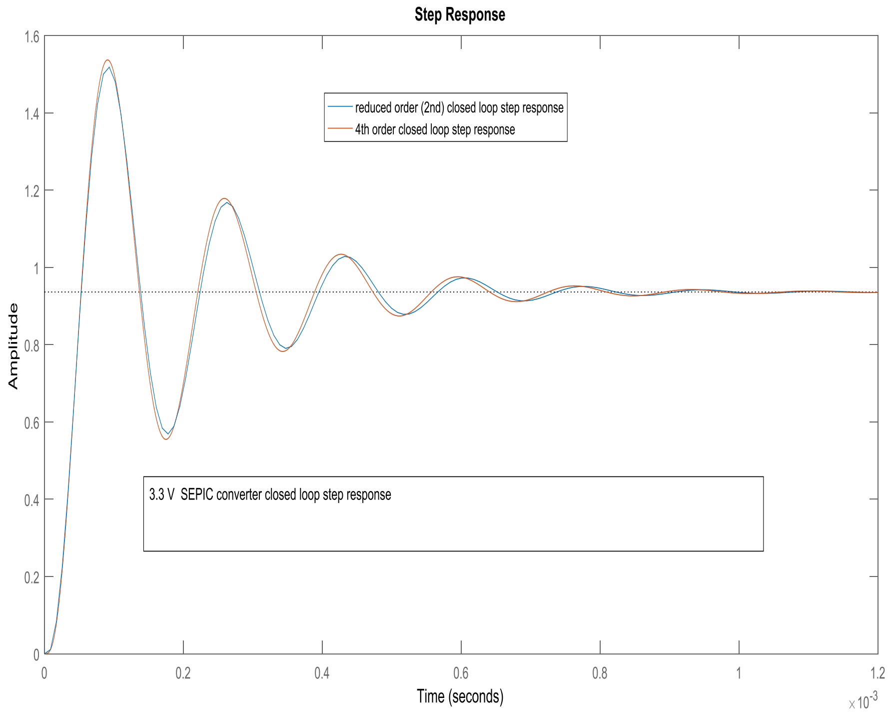

Figure 5.12 Closed loop original and reduced order step response of the 3.3V SEPIC

Equation (5.4) ($C_{3.3V}$) is the closed-loop converter transfer function of the 3.3V converter.

$$C_{3.3V} = \frac{2.45 \times 10^{8} s^{3} + 5.37 \times 10^{13} s^{2} + 2.63 \times 10^{18} s + 1.482}{s^{5} + 4.255 \times 10^{5} s^{4} + 5.827 \times 10^{10} s^{3} + 2.767 \times 10^{15} s^{2} + 2.351 \times 1} \quad (5.4)$$

However, a fine tuning has been made to obtain the best sets of the PI controller coefficients, where:

$$P = 0.139798984777943$$

$$I = 903.402279923993$$

These coefficients are best for the two converters. The new step response using the above PI coefficients is shown in Figure 5.13.

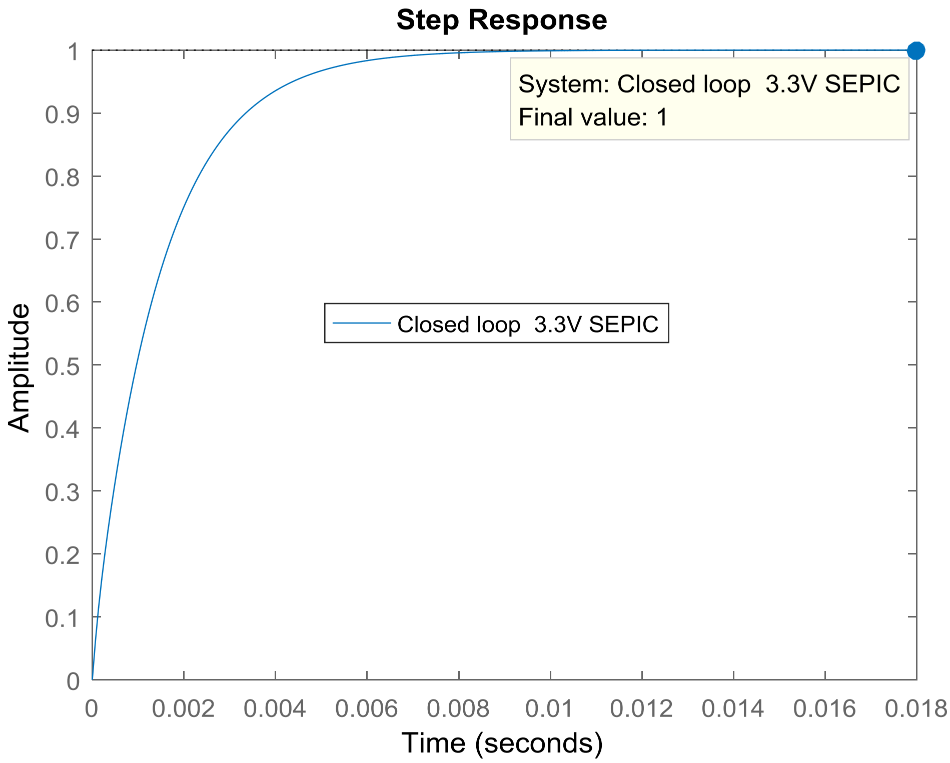

Figure 5.13 Closed-loop step response of the 3.3V SEPIC

For the 5.0V SEPIC, Figures (5.14) and (5.15) show the step response for both the calculated and the tuned PI controller. The closed-loop transfer function $C_{5.0V}$ for the 5.0V converter is shown in equation (5.5). The comparison between the closed-loop fourth and the reduced order system is shown in Figure (5.16) and clearly it was having lots of oscillations and therefore discarded and the fine-tuned coefficients accepted and used for the controllers.

$$C_{5.0V} = \frac{1.315 \times 10^{8} s^{3} + 2.882 \times 10^{13} s^{2} + 1.742 \times 10^{18} s + 1.009 \times}{s^{5} + 4.255 \times 10^{5} s^{4} + 5.701 \times 10^{10} s^{3} + 2.5 \times 10^{15} s^{2} + 1.059 \times 10^{19} s} \quad (5.5)$$

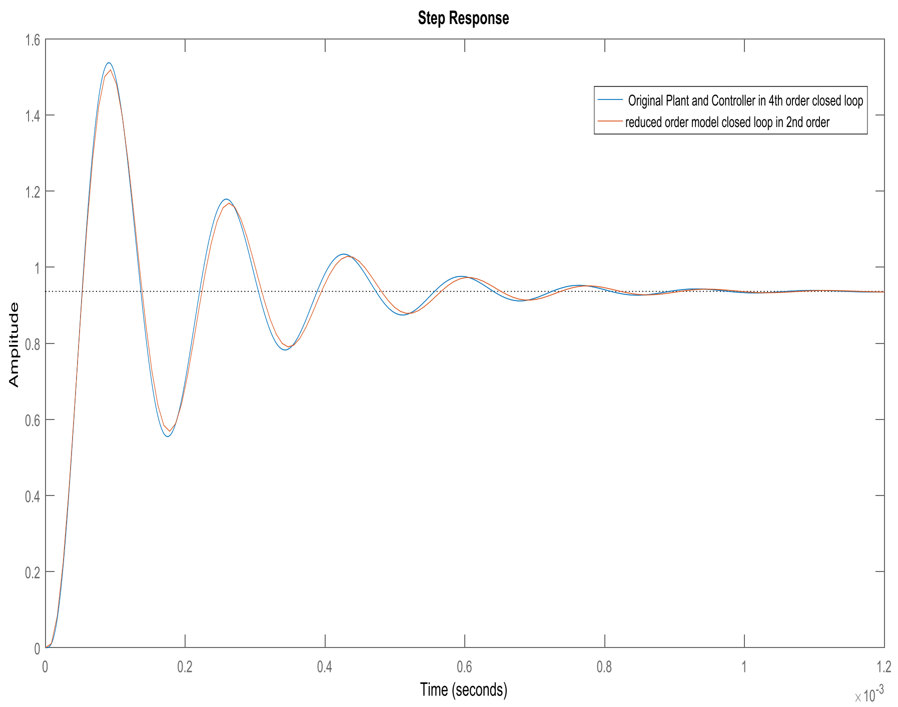

Figure 5.14 Tuned Step Response of the Closed Loop 5.0V Converter

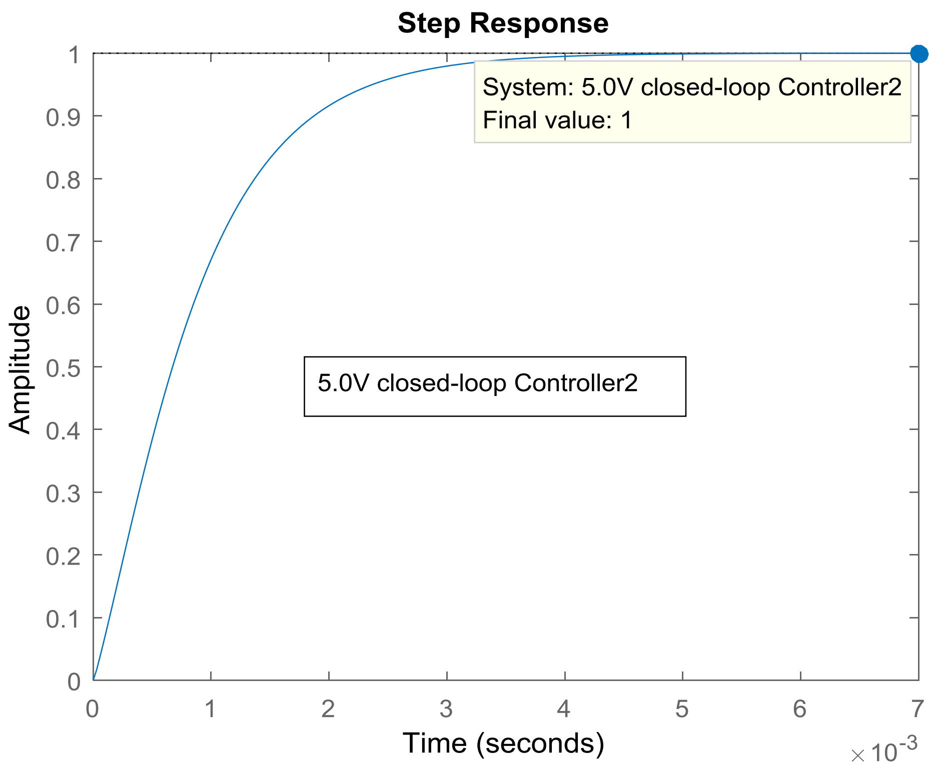

Figure 5.15 Step response of closed-loop 5.0V converter.

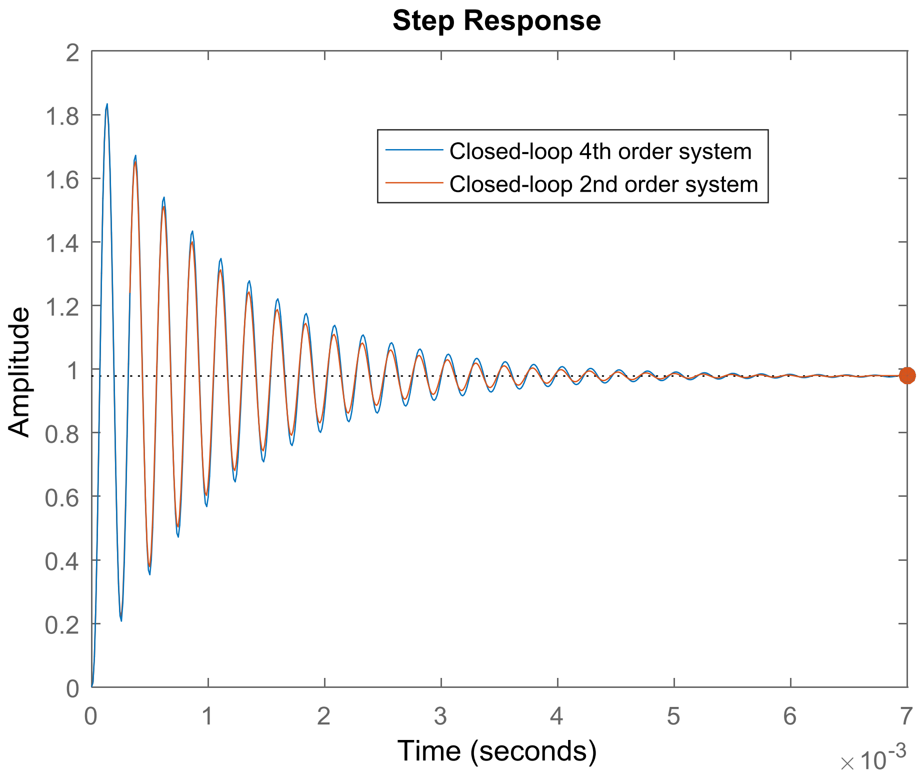

Figure 5.16 Closed-loop response for the 4th order and the 2nd order system of the 5.0V SEPIC

Further, ripples in the output voltages and currents of the(3.3 and 5.0)V were examined. Where, the zoom out of the 3.3V converter voltage is shown in Figure (5.17) and that of the current is presented in Figure (5.18).From the three profile curves of the 3.3 V converter, we can see that the controller does well in controlling the plant. The ripples in both the voltage and current are very small and within limits specified earlier. The voltage ripple is around 1.2% while that of the current is less than 1%.The output voltage variation is $(3.294\ to\ 3.306)$ V and the current varies from $(2.495\ to\ 2.504)$ A.

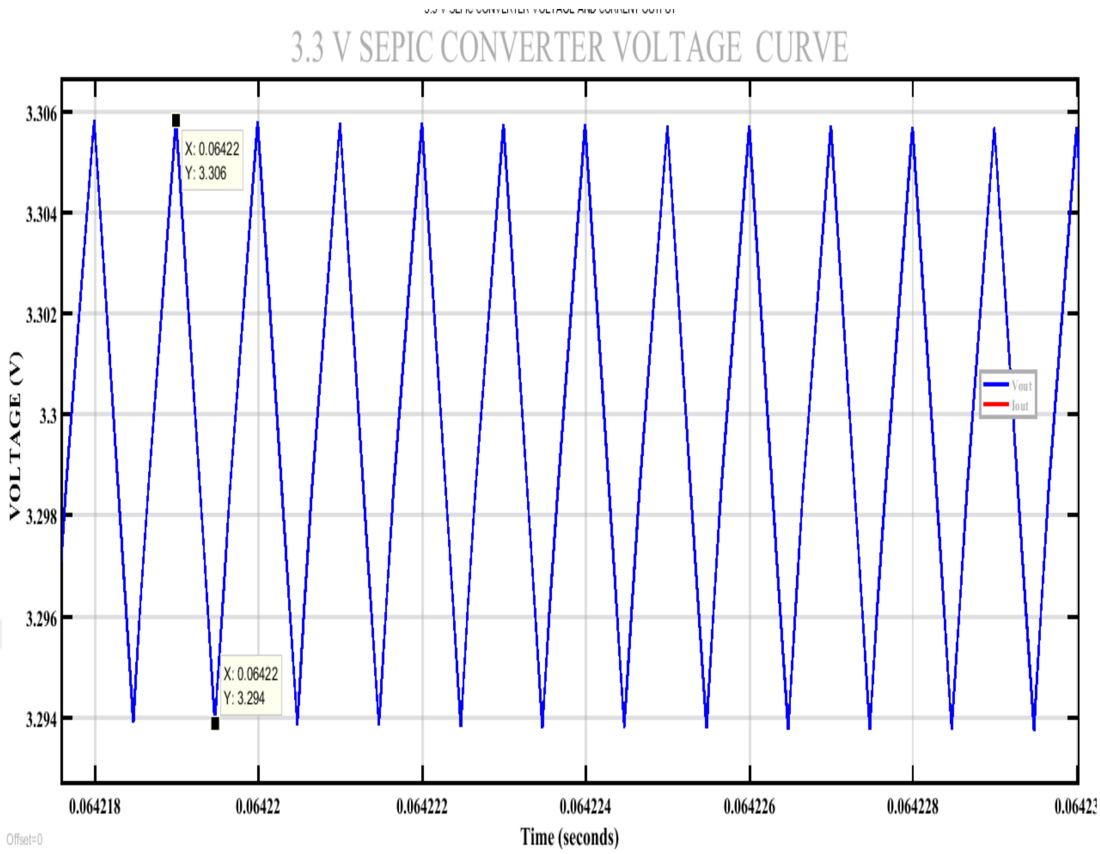

Figure 5.17 The output voltage zoom out of the 3.3V SEPIC.

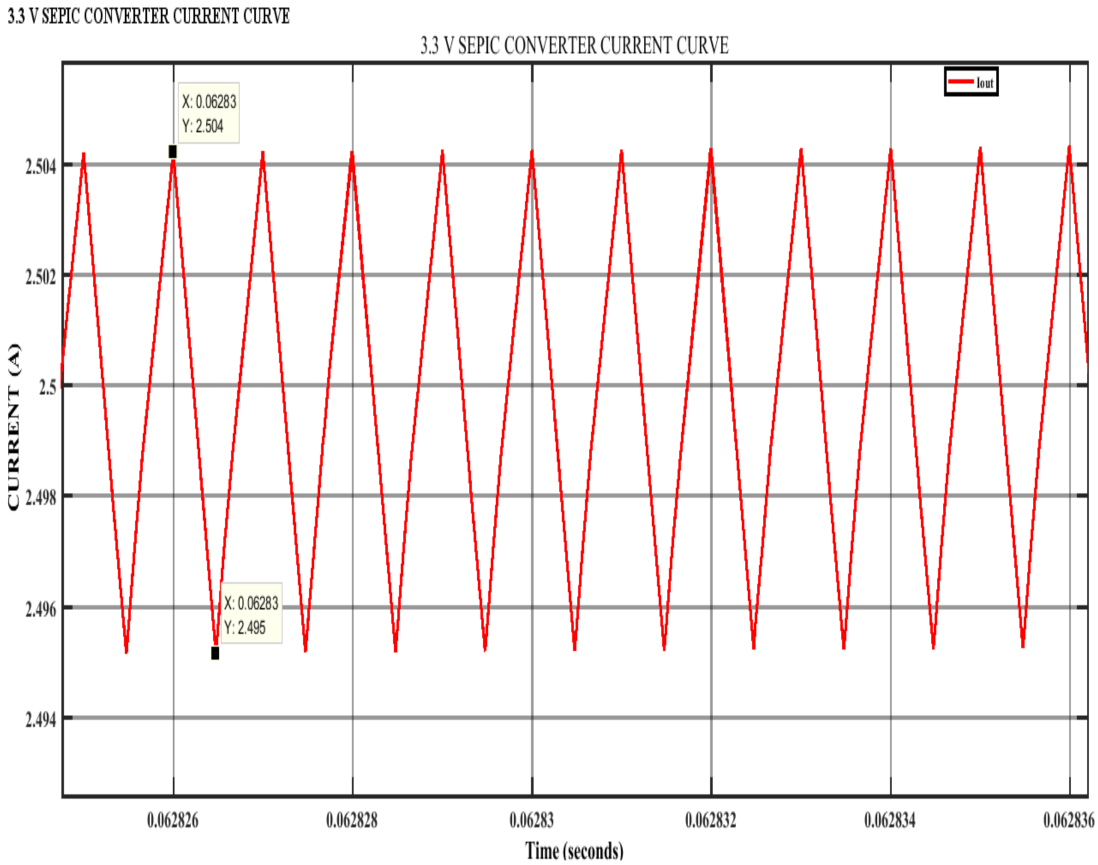

Figure 5.18 The output current zoom out of the 3.3V SEPIC

The 5.0V converter curves are similarly presented in Figure5.19and Figure5.20, like the other 3.3V, the 5.0V converter also shows good behaviour of output voltage and current. The output voltage Vo varies from $(4.994\ to\ 5.006)V$ as shown in Figure5.19 while, the current is varying from $(1.998\ to\ 2.002)\ A$ as can be read from Figure5.20.

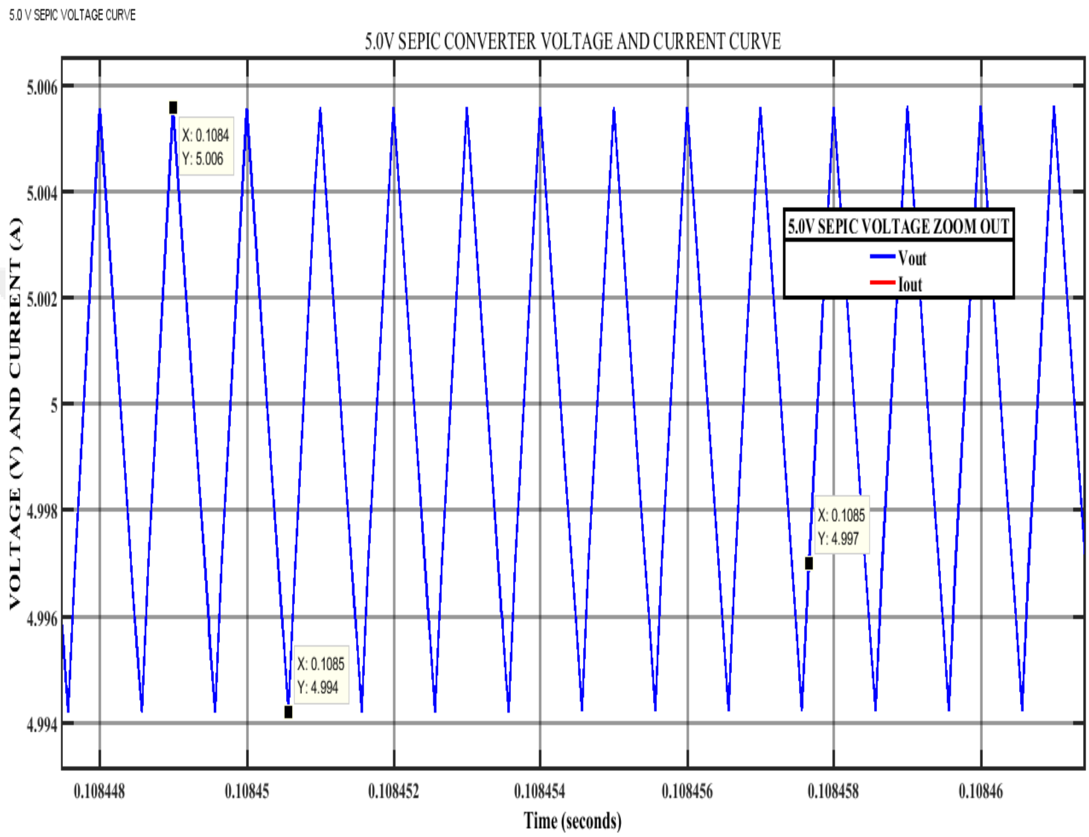

Figure 5.19 Zoom out of the output voltage of the 5.0V SEPIC

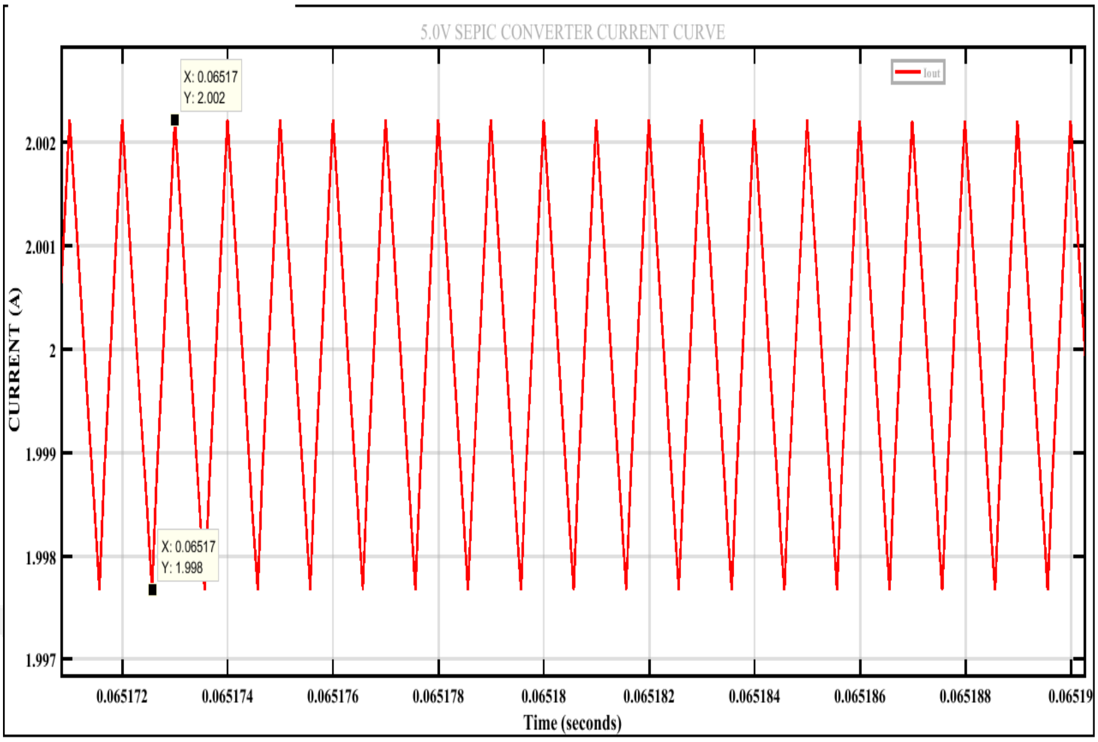

Figure 5.20 Zoom out of the output current curve of the 5.0V SEPIC

The characteristics voltage and current outputs of the two converters are quite encouraging, as a result, a comparison of these is made with the output voltage profiles of the COTS EPS characteristics readily available in the market being supplied by two famous satellite kits Manufacturers – GOMspace of Denmark and Endurosat of Ecuador in Table 5.3 as shown.

Table 5.3 Comparison of converter voltage output with those of manufacturers

Voltage (V)	Designed Converter	ENDUROSAT	GOMspace
3.3	$3.294\ to\ 3.306$	$3.3 - -3.45$	$3.29 - -3.45$
5.0	$4.994\ to\ 5.006$	$4.88 - 5.15$	$4.89 - -5.05$

The comparison in Table 5.3 gives us confidence to accept the result of our converters modeling, controller design and simulation. However, it is worthy of note that, the converter design were made with ideal components, therefore, we cannot draw final conclusions of their superiority over others. Further studies and analysis have to be made.

CHAPTER VI

CONCLUSION

6 Introduction

In this Chapter, a summary of the work undertaken in this thesis is presented. This is followed by recommendations based on the experiences and the lessons learnt during the course of the work and preparations of the report. A conclusion about the whole thesis is drawn and a brief comment is made on the future works to be carried in regards to achieving better results and mastering of the subject matter with an objective of becoming professional in the field of Power Electronics and Design of Power Systems for Satellites and other portable devices.

6.1 Summary

A preliminary design of an Electrical Power Subsystem (EPS) for a 1U CubeSat was conducted in this thesis work. The functionalities and requirements of the EPS were clearly spelt out from the onset. The design was performed after a fairly but thorough literature review of the methods, the difficulties involved, information available especially on the technologies pertaining to satellites subsystems when it comes to the power supply design etc. The review led to the discovery of the how electrical power is being generated on-board a satellite through the use of solar photovoltaic cells which are distinctively different in terms of the technology of manufacture and the efficiency from the ones seen commonly on our roof tops. The photovoltaic cells are of the triple-junction types. The generated power is being stored on-board by a storage system basically a battery of the lithium technology. The battery or batteries are being charged by a network of semiconductor devices mostly of the Switched-Mode called SMPS and in conjunction with MPPT algorithm to extract the maximum power from the solar cells.

Mathematical modeling of the basic elements of the EPS was made and the design parameters were also obtained. A computer simulation was made in order to confirm some of the characteristics of these elements as stated on their respective datasheets and to design controllers for the converters chosen.

The solar photovoltaic cells chosen in this thesis work are from AzurSpace - Space grade solar cells manufactures in Germany, lithium-ion battery is the one selected and implemented in the simulation. The converter topology used is SEPIC.

The results of the solar cell simulation have confirmed the performance of the cell selected and therefore successful. The converters design and simulation produced very good results and confirm the theory of the SEPIC. Network of switches was employed for simulating the MPPT algorithm which was a P&O and was found to be successful. PI controllers were designed and implemented for the converters. All the results obtained were in presented and analyzed using tables, figures, and equations in this report.

However, is important to note that the EPS so designed was from a preliminary study, therefore, it is quite skeletal and not conclusive in terms of all the peripherals that may be required to produce an engineering model, this would be achieved in future, hopefully soon.

6.2 Recommendation

There were a lot of lessons and experiences learnt while performing this study, the following were drawn on the ways to design the EPS for a CubeSat mission that would lead to producing an engineering model and prototype ready for production.

1. The requirement of the mission must be understood and allowance has to be made for adjustments if need for some inevitable changes arise.
2. Performance evaluation of all the components to be selected to certify that the selected components would give the results expected as claimed by the manufacturer.
3. Triple-junctions solar cells are not modeled like the conventional single-junctions cells, but, they are stack of three (3) sub cells having different contributions to the voltage profile and photo-conversions, care must be taken in modeling the cells to avoid errors from coming in.

4. Most of the constant parameters of the triple junction's solar cell model are temperature dependent, therefore, accurate tests have to be conducted to determine them or numerically intensive computations have to be carried out in order to obtain these values which may not be accurate. In the literature, different researches have presented varying values for the same parameters, so one must take care to select the ones that can give near accurate results.

5. When SEPIC topology is being considered for the converter design, it should be noted that the transfer function yields fourth order equation which is a non-minimum phase system and its controller design is very difficult.

6. For accuracy of the MPPT, there are other ICs presented in the literature that can be considered based on the outlined requirements.

6.3 Conclusion

This thesis work we have been able to model and design the major components of a 1U CubeSat power supply subsystem. Mathematical models were obtained and presented, simulations were carried out and the results were studied and discussed. A triple-junction solar cell was selected, mathematically modeled and simulated. The results were validated from by comparing with the datasheet values. State-space averaging technique was used in modeling SEPIC for the purpose of analysis and controller design in this work, the converters are the 3.3V, 2.5 A and 5.0V, 2.0 power supplies for 1U CubeSat loads.

3.3 V and 5.0 V SEPIC were analysed, modeled and simulated and the results have been well within the limits expected. The output voltages of the converters were compared to the reported similar converters by leading manufacturers of such power supplies and the designed converters outputs are excellent.

6.4 Future Work

1. Completion of this power subsystem design of CubeSat including all sensors, switches and protection circuitry etc. up to engineering model system and to produce and test the prototype.

2. Analytical modeling, testing and simulation of multi-junction solar photovoltaic cells with a view to improving existing models, performance

evaluation and analytical extraction of the cell parameters not given on the datasheets by manufactures.

3. Modeling and evaluation of DC-DC switched-mode power converters using state-space averaging and other techniques for improved controller designs.
4. Modeling and simulation for performance evaluation of lithium technology based cells/batteries.
5. Apply the knowledge learnt from above for electrical vehicle modeling and simulation.

REFERENCES

[1] Sellers, J.J., Astore, W.J., Giffen, R.B. and Larson, W.J., (2000).*Understanding Space: an Introduction to Astronautics*. 3rd edition. New York: McGraw Hill.
[2] Craig S. Clark, Alejandro Lopez. Mazarias, “Power System Challenges for Small Satellite Missions” Clyde Space Ltd., 6.01 Kelvin Campus, West of Scotland Science Park, Glasgow G20 0SP Scotland.
[3] Sun, C.S. and Juang, J.C., (2012). Design and Implementation of a Microsatellite Electric Power Subsystem. *Journal of Aeronautics, Astronautics and Aviation. Series A*.**44**(2),67-73.
[4] Cal Poly, S.L.O., (2009). CubeSat Design Specification Rev. 12.*The CubeSat Program*..California: California State Polytechnic University.
[5] Jacobsen, L.E., (2012).*Electrical Power System of the NTNU Test Satellite: Design of the EPS*(Master's thesis, Institutt for elektronikk og telekommunikasjon).
[6] Skyttemyr, K.O., (2013).*Design and Implementation of the Electrical Power System for the CubeSTAR Satellite*(Master's thesis).
[7] Ramamurthy, A., (2009). Flexible Digital Electrical Power System Design and Modeling for Small Satellites.
[8] Thirion, P., (2009). Design and Implementation of On-board Electrical Power Supply of Student Nanosatellite oufti-1 of University of Liège. Master's thesis, University of Liège, Liège.
[9] Pelakauskas, M., (2011). ESTCube-1 Satellite Electrical Power System Battery Subsystem Design and Testing. *Unpublished Master’s Thesis, University of Tartu, Tartu, Estonia*.
[10] Pozo, K. F. (2012). CubeCat-1: Implementation, testing, and integration of the communication subsystem. *UniversitatPolitècnica de Catalunya, thesis*.
[11] Di Piazza, M.C. and Vitale, G., (2012).Photovoltaic Sources: Modeling and Emulation. *Green Energy and Technology* London: Springer Science & Business Media.
[12] Jiang, Z., Dougal, R.A. and Liu, S., (2003). Application of VTB in Design and Testing of Satellite Electrical Power Systems. *Journal of Power Sources*. ***122***(1), 95-108.
[13] Bailey, S. and Raffaelle, R., (2005). Space Solar Cells and Arrays. *Handbook of photovoltaic Science and Engineering*, New York: John Wiley and Sons Ltd,413-448.
[14] Stanton, W., Schulz, P., Wise, J. and King, B., (2014), Intelligent Power Management System for a Nanosatellite. *New Mexico Tech Satellite Report*, New Mexico Tech. University.
[15] Asif, S. (2008). Evolutionary computation based multi-objective design search and optimization of spacecraft electrical power subsystems (Doctoral dissertation, University of Glasgow).
[16] Dey, B. K., Khan, I., Mandal, N., & Bhattacharjee, A. (2016). Mathematical Modeling and Characteristic Analysis of Solar PV Cell. *Information Technology, Electronics and Mobile Communication Conference (IEMCON)*.1-5.

[17] Mahdi, M. C.,Jaafer, J. S., and Dr. Shehab, A.,(2014) Design and Implementation of an Effective Electrical Power System for Nano-Satellite *International Journal of Scientific & Engineering Research.* ***5****(5)* 2229-5518

[18] Capel, A. (2001). Mathematical model for the representation of the electrical behaviour of a lithium cell. In *Power Electronics Specialists Conference.* **4**, 1976-1981.

[19] Hemmo, J. (2013). Suomalaisten nanosatelliittien tehonsyöttöjärjestelmät.

[20] Patel, M.R., 2004. *Spacecraft power systems*. Boca Raton 1st edition Boca Raton, Florida: CRC press.

[21] Lazar, R. D., Bucelea, V., Loidl, A., Formanek, L., & Chlubna, T. (2002). *Optimized Design of Power Supply for CubeSat at Aalborg University* (Doctoral dissertation, Institute of Energy Technology, Aalborg Univ., Aalborg, Denmark).

[22] Jenkins, R. D. (2010). NPS-SCAT: Systems Engineering and payload subsystem design, integration, and testing of NPS first CubeSat (Doctoral dissertation, Monterey, California. Naval Postgraduate School).

[23] Christophe P. Basso: Switch-Mode Power Supplies, Second Edition. Simulations and Practical Designs of Non-isolated Converters, Chapter (McGraw-Hill Professional, 2014), Access Engineering

[24] Erickson, R. W. (2001). DC–DC power converters. *Wiley encyclopedia of electrical and electronics engineering*. New York: John Wiley and Sons Ltd.

[25] Priya, S. P., Radhika, A., & Vinothini, T. D. (2012). MPPT and SEPIC Based Controller Development for Energy Utilisation in CubeSats. *India Conference (INDICON), Annual IEEE* 143-148.

[26] Waghulde, D., Kapgate, N., Pisal, S., Papal, S., Gajare, T., Rathod, B., ... & Phanse, A. (2016). Simulation, Design and Implementation of Various MPPT Systems for Micro Cube-Satellite Application. *Computational Intelligence on Power, Energy and Controls with their Impact on Humanity (CIPECH), Second International Innovative Applications.* 80-84.

[27] Li, N. (2012). *Digital control strategies for DC/DC SEPIC converters towards integration* (Doctoral dissertation, Lyon, INSA).

[28] Segev, G., Mittelman, G. and Kribus, A., (2012). Equivalent Circuit Models for Triple-Junction Concentrator Solar Cells. *Solar Energy Materials and Solar Cells.****98***, 57-65.

[29] Laurent, A. (2016). Modelling and analysis of multi-junction photovoltaic cells using MATLAB/Simulink for the improvement of conversion efficiency. University of Southern Queensland.

[30] Thakur, M., & Singh, B. (2015). A MATLAB/Simulink Modal of Triple-Junction Solar Cell and MPPT Based on Incremental Conductance Algorithm for PV System. *International Journal of Engineering Research and Applications.****5***(9), 92-95.

[31] Nishioka, K., Takamoto, T., Agui, T., Kaneiwa, M., Uraoka, Y. and Fuyuki, T., (2004). Evaluation of InGaP/InGaAs/Ge triple-junction solar cell under concentrated light by simulation program with integrated circuit emphasis. *Japanese Journal of Applied Physics*. ***43***(3), 882.

[32] Babar, M., Rizvi, A.A., Al-Ammar, E.A. and Malik, N.H., (2014). Analytical model of multi-junction solar cell. *Arabian Journal for Science and Engineering.****39*** (1), 547-555.

[33] Cotfas, D.T., Cotfas, P.A. and Machidon, O.M., April (2018). Study of Temperature Coefficients for Parameters of Photovoltaic Cells. Hindawi *International Journal of Photoenergy*.

[34] Catelani, M., Ciani, L., Kazimierczuk, M.K. and Reatti, A., (2016). MATLAB PV solar concentrator performance prediction based on triple junction solar cell model. *Measurement. **88***, 310-317.
[35] Padhi, B.K. and Narain, A., (2013). Controller design for SEPIC converter using model order reduction. *International Journal of Electrical, Electronics and Data Communication*. ***1***(3), 19-24.
[36] Zhang, D., (2006). AN-1484 Designing a SEPIC Converter. *Texas Instruments*. Dallas:
[37] Jeff, F., (2016). Designing DC–DC Converters Based on SEPIC Topology. *Analog Instrumentation Journal.* Dallas: *Texas Instruments. Web. **12***.
[38] Abdulrahman Babiker Hussain, Abdelrahman S. Abdalla, Abdellahi Sidi Mukhtar, M. Elamin, R. Alammari & A. Iqbal (2017) Modeling and simulation of single- and triple-junction solar cells using MATLAB/SIMULINK, International Journal of Ambient Energy.**38**:6,613-621,DOI: 10.1080/01430750.2016.1181567
[39] ENDUROSAT CubeSat Structure. Available at: https://www.endurosat.com/products/#power-modules. Accessed 15.08.2018
[40] GOMspace Structure Available at: https://gomspace.com/Shop/subsystems/power-supplies/nanopower- p31u.aspx. Accessed 15.08.2018.
[41] A. H. Didaand M. Bekhti, (2017) Study, Modeling and Simulation of Electrical Characteristics of Space Satellite Solar Cells. *IEEE 6th International Conference on Renewable Energy Research and Applications (ICRERA)* San Diego, CA, 983-987. doi:10,1109/ICRERA.2017.819205
[42] Gerald Siefer, AW Belt (2014)Analysis of Temperature Coefficients for III-V Multi-Junction Concentrator Cells *Progress in Photovoltaic Research and Applications.**22*** (5), 515-525.
[43] Yuya Sakurada, Yasuyuki Ota, and Kensuke Nishioka April (2011) Simulation of Temperature Characteristics of InGaP/InGaAs/Ge Triple-junction Solar Cell Under Concentrated Light, *Japanese Journal of Applied physics*.**50** 4S.
[44]PUMPKIN Structure. Available at: http://www.pumpkinspace.com/store/p30/Chassis_Walls.html. Accessed 15.08.2018.
[45] Jha, A.R., (2009). *Solar Cell Technology and Applications*. New York: Auerbach publications.
[46] ClydeSpace EPS. Available at: https://www.clyde.space/products/18-3rd-generation-1U-EPS Accessed 25.08.2018.
[47] Clark, C. and Logan, R., (2011). Power Budgets for Mission Success. *CubeSat Workshop*. London: ClydeSpace UK.
[48] 3G30C Advanced Solar Cell 29.5%. Available at: http://www.azurspace.com/index.php/en/products/products-space/space- solar-cells. Accessed 25.08.2018.
[49] NeXt Triple-Junction Solar Cell XTJ. Available at: https://www.spectrolab.com/photovoltaics.html Accessed 25.08.2018
[50] Zadeh, L. and Desoer, C., (2008). *Linear system theory: the state space approach*. Mineola, New York: Courier Dover Publications.
[51] Eng, V., Pinsopon, U. and Bunlaksananusorn, C., (2009), May. Modeling of a SEPIC converter operating in continuous conduction mode. *Electrical Engineering/Electronics, Computer, Telecommunications and Information Technology, 2009. ECTI-CON. 6th International Conference.***1**, 136-139. IEEE.